RECUEIL 2020

DES ACTIVITES DU THEME

« ARCHIVES ET CLIMAT »

GLACCIOS

OCEANIS

GEOTRAC

PALEOCEAN

CLIMAG

MISSIONS

St Paul et Amsterdam- Mesures isotopiques

Cattani, O., Landais, A., Vimeux, F.

Mission de terrain, 2019

Programme IPEV ADELISE St Paul et Amsterdam

Du 8 novembre 2019 au 02 janvier 2020, O. CATTANI a participé aux rotations OP3, OP4 des rotations de ravitaillement des îles australes à bord du navire scientifique Marion Dufresne des TAAF (Territoires Australes et Antarctiques Françaises) afin de rejoindre l'île d'Amsterdam, située au centre de l'océan indien par 37°50'S.

Ce projet du LSCE, soutenu par l'IPEV (Institut polaire français Paul-Emile Victor) a pour but de mesurer en continu les rapports isotopiques atmosphériques de la vapeur d'eau au sein de l'océan indien sur le site de prélèvement de Pointe B. de l'île d'Amsterdam (Figure 1), afin de déterminer les effets éventuels régionaux de l'Antarctique (sites appareillés de Concordia et de D.D.U.) et de l'île de la Réunion (site appareillé du Maido). O. CATTANI a eu 3 semaines pour mener à bien l'installation complète de l'instrument (Figure 2) ainsi que tous les tests de stabilité et calibration permettant de valider les futures mesures qui sont envoyées quotidiennement au LSCE pour analyse. Un V.S.C. (Volontaire au Service Civique) formé sur site s'occupera de l'instrument et notamment de sa maintenance pendant son hivernage jusqu'à fin décembre 2020.

Fig. 1. Le site de Pointe B. sur l'île d'Amsterdam.

Fig. 2 : Vue de l'installation de l'instrument de mesure de la composition isotopique de la vapeur d'eau dans le bâtiment scientifique de prélèvement d'air de Pointe B.

Campagne AMOR-SB5 : Trois nouveautés pour les mesures dans les sédiments

Bombled, B., Rabouille C., Lapham L.

Novembre 2020

En Novembre 2020 l'équipe OCEANIS a effectué une campagne, à bord du Bateau GGIX de la société XBlue, à l'embouchure du Rhône (Station multi-instrumentée Mesurho, ILICO/COAST-HF ; bouée Roustan-Est).

Les difficultés à effectuer des séries temporelles pendant les évènements extrêmes (crues, tempêtes) rendent la compréhension de leurs impacts, sur les écosystèmes benthiques, très parcellaires. De même, les connaissances sur le devenir des apports de matière organique et des macronutriments, à l'océan côtier, sont limitées par ces difficultés de mesure. La campagne avait 3 buts techniques nouveaux : Déploiement de la Station Benthique (SB) de 2de génération, d'un Lander Osmosampler puis de multi-échantillonner une carotte afin de mieux corréler plusieurs marqueurs géochimiques.

Depuis plus de 10 ans le LSCE déploie sa SB qui permet d'effectuer des séries temporelles de µ-profils d'oxygène, dans les sédiments, à l'aide de µ-capteurs, d'apporter des contraintes sur leur variabilité temporelle et de calculer des taux de minéralisation du carbone organique sur une surface définie. Jusqu'à présent, la SB utilisait des capteurs en verre fragiles qui ont montré leurs limites. En collaboration avec la DT-INSU, nous avons donc décidé d'opter pour des µ-optodes plus robustes utilisant la technologie d'émission-réception par fibre optique. Ce déploiement de la SB pourvue de 6 µ-optodes, a été l'aboutissement de plus d'une année de refonte.

Ce dispositif a été complété par l'immersion d'un 2^{d} lander pourvu d'un dispositif d'échantillonnage temporel, des eaux interstitielles, par pompage osmotique et conservation dans des bobines de tuyaux de cuivre. Ce dispositif permet de mesurer des séries temporelles de CH_4, de sulfates et de DIC, à 4 profondeurs, dans le sédiment. Ce travail est le fruit d'une collaboration initiée lors du séjour de L. Lapham, de l'université du Maryland, dans l'équipe OCEANIS en 2019-2020.

En parallèle, l'équipe poursuit le suivi des dépôts organiques à l'aide de carottages. Pour la 1ère fois une carotte a été prélevée et échantillonnée pour effectuer une inter-comparaison de la mesure du CH_4 dans deux laboratoires différents et récupérer les liquides interstitiels en vue de la mesure du DIC, du NH_4, des sulfates, en lien avec les laboratoires UMCES-Maryland (USA) et GEOPS (Orsay, France).

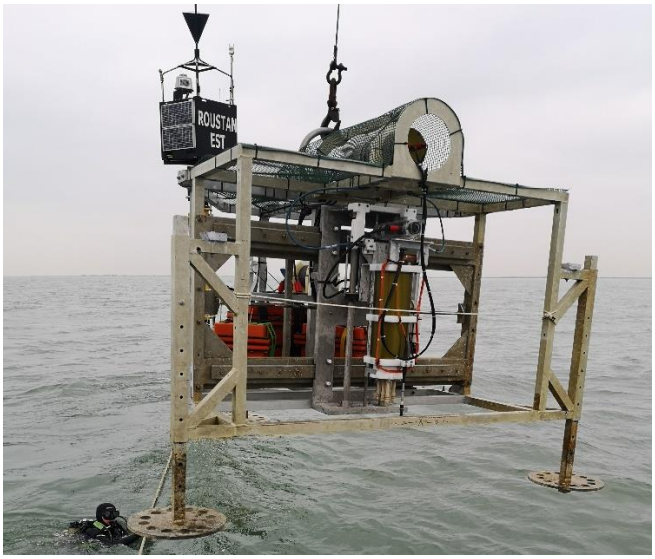

Fig 1 : Station Benthique de seconde génération en cours de déploiement à la station Mesurho (Bouée Roustan-Est)

Fig 2 : à gauche : Osmopompe et bobines de cuivre pour conservation des série temporelles d'eaux interstitielles. A droite : Carotte multi-échantillonnées, sur toute la hauteur, par pompage des eaux interstitielles à l'aide de µ-préleveurs rhizon

DEVELOPPEMENTS EXPERIMENTAUX

Acquisition d'instruments et de nouveaux matériels dans le thème

GLACCIOS

- 1 PICARRO ^{17}O et ses périphériques (SDM, passeur, vaporiseur)
- 1 SARA O_2 en développement avec AP2Eet le Liphy en test monté à l'ECOTRON
- 1 générateur de vapeur basse humidité de laboratoire développé et construit en 2020

GEOTRAC

- 1 balance Mettler-Toledo XSR105 avec kit anti-statique pour la salle blanche doté d'une précision de 0.01mg.
- 2 Stéréomicroscopes ZEISS STEMI 508 Doc, zoom gradué à crans 0,63x à 5x, système optique Apochromatique10x/23, Grossissements 6,3x à 50x Ratio Zoom 8/1, avec 1 caméra très haute résolution, sortie photo 100/100% Largeur de champ Max : 35 mm, éclairage annulaire multizones, destiné à la mesure et découpe des largeurs de cerne avec archivage des photos (panoramas) très haute résolution..

Le NGX 600 Isotopx: un spectromètre de masse pour la datation $^{40}Ar/^{39}Ar$ des téphras

Guillou H., Scao V., Nomade S.

Projet INSU SYSTER 2020

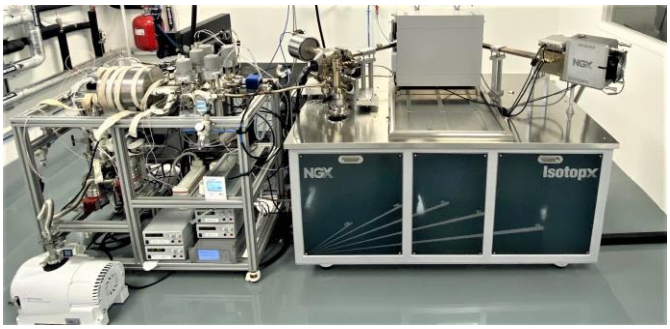

Fig.1 : Le nouveau labo Ar/Ar du LSCE.

Les éruptions volcaniques explosives peuvent disperser des cendres (téphras) qui sont retrouvées dans les séquences sédimentaires marines et lacustres et les forages des glaces polaires.

Compte tenu de leur caractère discret combiné à leur vaste répartition spatiale (i.e., parfois à l'échelle du bassin océanique e.g. éruption du Toba à 74ka) ces téphras sont des outils de corrélation stratigraphique puissants qu'il est important de dater avec justesse et précision. C'est dans cette optique qu'un nouveau spectromètre de masse (MS) dédié à la datation $^{40}Ar/^{39}Ar$ a été acquis par le LSCE et GEOPS. Ce nouveau MS installé en Novembre 2019 est équipé de 10 détecteurs (9 faradays (F) et 1 compteur d'ions (IC)) permettant la collection simultanée en deux configurations (4 F et 1 IC ou 5 F) des cinq isotopes d'Argon. Ce MS est relié à une ligne d'introduction et de purification des gaz et équipée d'un Laser CO_2 permettant la fusion à l'échelle du monocristal.

Des expériences et tests ont permis de caractériser les « blancs procéduraux », la linéarité de réponse des détecteurs et les discriminations de masse qui sont en cohérence avec celles définies au cahier des charges. Nous avons confirmé la géométrie et l'alignement des pics entre eux pour chacun des 5 isotopes de l'argon garantissant ainsi des conditions de mesures optimales en penta-collection (Fig.2).

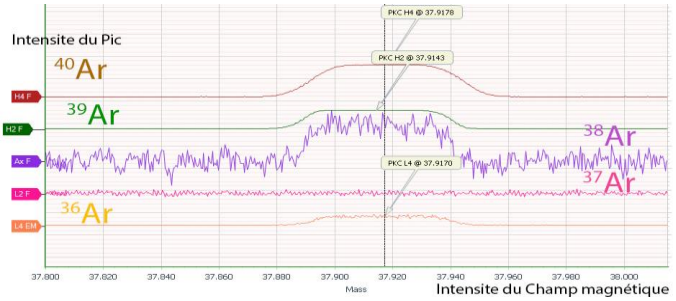

Fig.2 : Mise en évidence de la forme et de l'alignement des pics d'Argon

Sur la base de 110 mesures d'aliquotes d'air de différentes tailles, nous avons vérifié que la discrimination de masse sur le rapport $^{40}Ar/^{36}Ar$ instrumental est constante sur une large gamme de pression (Fig.3). Cela est crucial pour une détermination juste précise du pourcentage d'^{40}Ar radiogénique, paramètre décisif dans le calcul des âges.

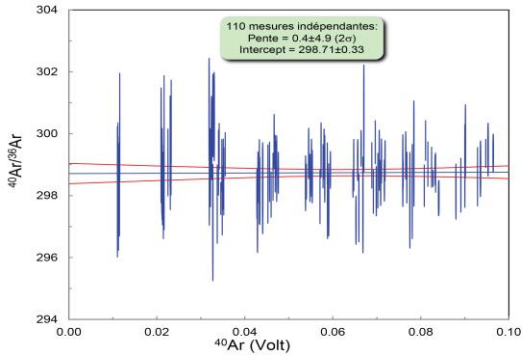

Fig.3:Variation du rapport 40Ar/36Ar vs pression 40Ar dans le MS.

L'analyse de standards internationaux a permis de vérifier que les âges obtenus avec cette machine étaient en accord avec les valeurs préconisées (Fig.4). Ainsi qualifié, ce nouvel outil complète l'éventail déjà large et puissant des outils de datation du LSCE.

Achat du CHS (carbonate handling system) : nouveau périphérique pour la mesure ^{14}C des micro-échantillons carbonatés

Participants LSCE: F. Thil, N. Tisnérat Laborde, C. Hatté, E. Michel, E. Pons-Branchu, H. Valladas ; GEOPS : D. Calmel, G. Siani.

Le CHS est un système automatisé d'introduction d'échantillons carbonatés. Couplé à *ECHo*MICADAS, spectromètre de masse par accélérateur (2015, DIM Analytics), il permettra d'une part, de dater par la méthode du carbone 14 des micro-carbonates jusqu'à présent trop petits pour être analysés et ouvre vers de nouvelles voies de recherche, et d'autre part, un gain de productivité.

L'équipement CHS permettra l'hydrolyse des carbonates et l'injection de leur CO_2 purifié directement dans *ECHo*MICADAS via son interface gaz. Il facilitera la datation ^{14}C des micro-carbonates de l'ordre de 1 à 0.5 mg et accroîtra les capacités analytiques. Le coût global de cet instrument est de 75k€. Il est co-financé par le DIM MAP (Matériaux anciens et patrimoniaux au fil de l'eau, l'ERM2020- Université Paris-Saclay (Equipement de Recherche Mutualisé) et l'ANR Apart (H. Valladas).

A la pointe de la technologie, le CHS est destiné à la recherche et aux développements en géochronologie et géochimie, dans les domaines des Sciences de l'Environnement et des Sciences Humaines. Ces analyses ^{14}C sur des µcarbonates apporteront principalement des éléments de réponses clés aux questions sur le cycle du carbone et la géochronologie.

Les premières applications développées porteront par exemple **i- sur le cycle du carbone dans l'océan** pour caractériser la variabilité temporelle et spatiale de la circulation océanique à haute résolution des différentes masses d'eau (surface, intermédiaire et profonde) afin de mieux comprendre la pompe physico-chimique et également les variations de la teneur en CO_2 atmosphérique lié au changement climatique. Les foraminifères benthiques peu abondants pourront être systématiquement dater comme les foraminifères planctoniques et les coraux ou mollusques marins afin de déterminer à haute résolution la variabilité des âges réservoirs de surface, intermédiaire et de fond **ii- sur le cycle du carbone continental** principalement dans les rivières afin de renforcer les études sur la dynamique, la réactivité du carbone et ses flux dans les différents hydrosystèmes (eaux de surface et eaux souterraines); **iii-sur la chronologie de l'évolution des cultures** tel que l'art pariétal, en datant des gravures pariétales et/ou des représentations de tracés à base de pigments minéraux lorsqu'ils sont recouverts d'un voile de calcite, **iv) sur l'amélioration du cadre chronologique des archives** avec l'étude de l'impact de la présence humaine comme par exemple « l'usage des sols », en datant des archives continentales tels que les sédiments lacustres via la datation des ostracodes ou des spéléothèmes urbains en datant les lamines à haute résolution.

Fig : Vue d'ECHoMICADAS, spectromètre de masse par accélérateur et du périphérique « carbonate Handling system » CHS permettant de dater les carbonates par injection directe du CO_2 dans la source.

PROJETS

SeMPER Arctic – un projet transdisciplinaire

Projet Belmont Forum : Gherardi, J;-M.(LSCE/UVSQ) Huctin, J.-M. et Vanderlinden J.-P. (CEARC)

Démarrage Mars 2020

Le projet transdiscipinaire " Sense Making, Place attachment, and Extended networks, as sources of Resilience in the Arctic" (SeMPER-Arctic) a pour objectif de comprendre et analyser les sources de résilience en Arctique en s'attachant à rassembler des récits locaux de changements et leurs conséquences au niveau de trois communautés arctiques : Ittoqqortoormiit, Uummannaq (Groenland) et Tiksi (Sibérie). Ce projet est financé par le Belmont Forum, dans le cadre de l'appel « Resilience in Rapidly Changing Arctic Systems – Arctic II, 2019. Il rassemble des chercheurs de 5 pays, la Russie, la Norvège, les Pays-Bas, la Suède et la France spécialisés en sociologie du développement et planification régionale, en économie écologique, en anthropologie et en sciences et études de l'environnement et du climat.

Sur la base de l'analyse des récits collectés sur le terrain, ce projet vise à comprendre et à analyser les sources de résilience en Arctique, notamment chez les populations autochtones dont on connaît les capacités singulières d'adaptation, en s'attachant plus particulièrement à des notions clés qui sont apparues lors d'enquêtes préalables : la notion de création de sens, celle de l'attachement à un lieu et enfin celle d'un réseau sociaux et économiques étendus. Outre ces trois dimensions, les travaux de co-construction du projet ont permis d'identifier deux grandes catégories de narrations externes aux communautés : les sciences environnementales et le développement des politiques publiques régionales.

Cette compréhension est essentielle pour développer des outils et des stratégies visant à accroître la résilience des communautés dans d'autres régions. Un partage des enseignements tirés dans le cadre de ce projet sera ainsi fait avec les planificateurs régionaux et les décideurs. Le consortium va donc contribuer aux connaissances de base sur l'adaptation au changement environnemental global par le biais d'une enquête respectueuse, sur ce que signifie être un être résilient dans une communauté arctique au 21e siècle.

Les partenaires français du projet sont deux laboratoires de l'OSU OVSQ : le LSCE (UMR 8212) et le CEARC (EA4455 UVSQ). Les partenaires internationaux sont l'Université de Bergen (Norvège), la Northeastern Federal University de Yakutsk (république Sakha, Fédération de Russia), Nordregio (Suède) et l'Université d'Utrecht (Copernicus Center).

Carbonate compensation in the Glacial and Future Oceans

William Gray, Nathaelle Bouttes, Didier Roche, Francois Thil, Arnaud Dapoigny, Patricia Richard, Fatima Manssouri, Hélène Rebaubier, Guy Munhoven, David Thornalley

ANR JCJC 'CARBCOMP'

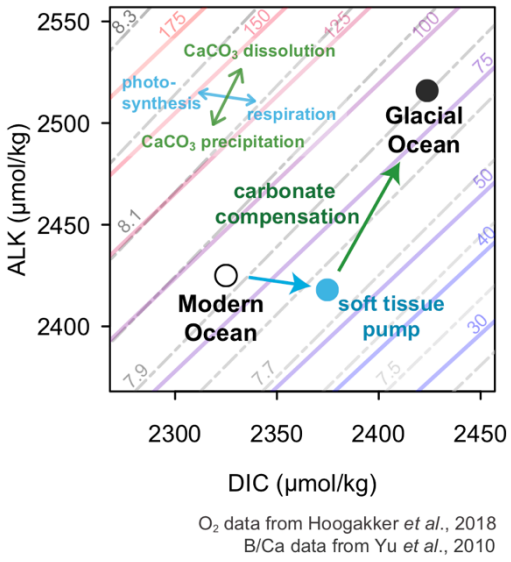

Using paired oxygen ($\Delta\delta^{13}C$) *and pH* ($\delta^{11}B$) *data to constrain glacial carbonate compensation. Dashed grey contours show pH, solid colour contours show* CO_3^{2-}.

The deep ocean carbonate system and its influence on the dissolution of $CaCO_3$ ('*carbonate compensation*') is a first order control on atmospheric CO_2 on timescales of ~10^3 to 10^5 years. Carbonate compensation is thought to account for up to ~*half* of the glacial drawdown of CO_2, and it will eventually help drawdown the CO_2 humans are currently emitting to the atmosphere. However, large uncertainties exist in our knowledge of both glacial and future carbonate compensation. Using paired carbon and boron isotopes in benthic foraminifera we will quantify glacial carbonate compensation within the Pacific Ocean, determining the timescale at which carbonate compensation can buffer the deep ocean and drawdown CO_2. We will use these new constraints from the glacial ocean, along with new boron isotope estimates of the acidification of the deep Atlantic over the industrial period, to optimise and validate carbonate compensation in a coupled Earth System-Sediment model. We will then use this model to predict the fate of anthropogenic CO_2 emissions into the long-term future.

Effondrements en masse des flancs des volcans océaniques : Une réponse aux variations rapides du niveau marin ?-CHROCOL-

Guillou H., Scao V., Nomade S., Bassinot F.

Projet INSU SYSTER 2020

Giant landslides are frequent and hazardous events shaping the intra-plate volcanic islands. They are the result of a complex interplay between intrusive and eruptive processes, the structure of the edifice itself (discontinuities, presence of weak layers, etc.), and its environment (climate and sea-level changes). The influence of external vs. internal parameters is still strongly debated. If the links between the instability of the volcanic edifice and the intrusive system have been convincingly demonstrated, it has also been proposed that the formation of shallow magmatic reservoirs may destabilize the upper part of the volcano. In the case of the Canary Islands, periods of increasing rates of lava accumulation frequently preceded flank collapses.
Alternatively to the geological triggers, it is proposed that rapid sea-level rise associated with warmer and wetter climate during the onsets of interglacials might cause increased retention of groundwater and pore pressure in volcanic islands, thus favouring their instability. However, these hypotheses rely on incomplete databases of volcano flank collapses that are often inaccurate or not precisely dated. Based on the examination of 125 volcaniclastic turbidites on the Madeira Abyssal Plain viewed as a record of large (>5 km³) flank collapses of the Canary Islands, no significant statistical correlation between the turbidite occurrence and sea-level change during the last 17 Ma was found. Plotting 28 dated flank collapses from six archipelagos against the sea-level curve of the last 1 Ma do not reveal any clear correlation with prompt changes of sea level. Depending on the accuracy of the ages, only six to ten events (20-35 %) might coincide with periods of rapid sea-level rise (> 5 m/ka, as defined by Coussens et al., 2016). In contrast, eleven events occurred during relative low-stands of sea level (glacials).

So, at first sight, external factors such as rapid rises of sea level should be discarded from the top list of collapse's triggers. That would be acceptable if the ages of these collapses were sufficiently accurate and precise. Indeed, as we will discuss in the following, most of the ages retained to date these collapses are K-Ar ages. These ages are useful for documenting the eruptive history of a volcanic edifice, but they can be questionable because they may be biased by unresolved excess argon, argon loss, fractionated ^{40}Ar, as well as K loss or gain due to alteration, leading to over- or underestimate the final ages. As an alternative, the $^{40}Ar/^{39}Ar$ technique evidence and may resolve these perturbations providing more accurate ages. Then, to state on the potential relationship between giant landslides and climate changes it is crucial to date these collapses using the $^{40}Ar/^{39}Ar$ technique. Such an approach will produce undoubtedly accurate ages that can be confronted with confidence to the isotopic curves retracing the sea level changes.

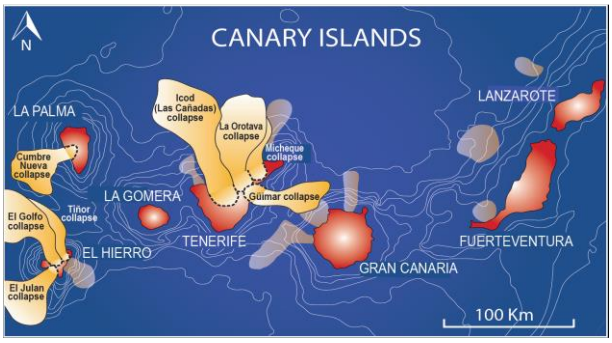

Fig. *1 : In orange, collapses retained for $^{40}Ar/^{39}Ar$ datings, in grey, other major collapses*

.

CASIMODO: Optimum Climatique médiéval et développements socio-économiques: études de la charpente de Notre-Dame de Paris et implications pour les forêts

ANR 2020, Coordinatrice : A. Dufraisse ; Responsable scientifique LSCE : V. Daux et le groupe de dendroclimatologie

Participants : C. Hatté et groupe 14C de l'équipe GeoTrAc, L. Beck et le LMC14

La charpente en chêne de Notre-Dame de Paris est l'un des plus grands chefs-d'œuvre de la charpenterie gothique en France. Elle a été construite au cours du Haut Moyen-Âge, entre le XIe et le XIIIe siècle, à une époque où de profonds changements environnementaux et sociétaux - optimum climatique médiéval (OCM), forte croissance démographique et économique - ont créé une pression importante sur les ressources forestières disponibles, l'une des principales richesses des sociétés médiévales. La destruction de la charpente de Notre-Dame de Paris dans l'incendie du 15 avril 2019 a laissé des milliers de fragments de poutres de chêne carbonisées. Analyser cette "forêt", c'est remonter le temps, reconstituer les conditions environnementales dans lesquelles les chênes ont poussé.

La contribution du LSCE dans le projet CASIMODO est de deux ordres et consiste 1) à extraire des bois de Notre-Dame une reconstitution du climat du X au XIIIème siècle, grâce une approche isotopique et 2) à préciser la courbe de calibration du ^{14}C, grâce à un enregistrement annuel des fluctuations des teneurs en ^{14}C atmosphérique.

L'OCM est une période d'investigation extrêmement intéressante : jouissant d'un climat relativement clément, elle présente certaines analogies avec l'époque actuelle. Les recherches dendroisotopiques se focaliseront sur la variabilité climatique interannuelle et la fréquence des extrêmes pendant les doux étés médiévaux. Le LSCE propose également sa force de frappe en datation ^{14}C pour préciser les chronologies nécessaires au projet CASIMODO (enregistrements palynologiques, complément à la dendrochronologie).

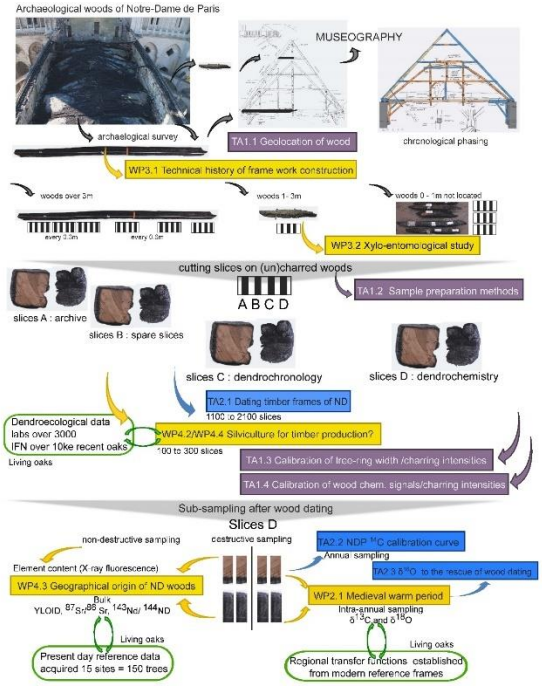

Figure 1 : schéma de principe des imbrications des actions dans CASIMODO. Le LSCE porte les TA2.2., WP2.1 et contribue à TA2.3, TA2.1

Atmospheric River Climatology in Antarctica.

ANR 2020 ; PIs: Vincent Favier (IGE) ; LSCE (PI E. Fourré) ; LOCEAN (PI F. Codron)

Démarrage 01/01/2021, 4 ans

Participants LSCE : C. Agosta, O. Cattani,E. Fourré, O. Jossoud, A. Landais, V. Masson-Delmotte, B. Minster, F. Prié

Le bilan de masse de surface (BMS) d'une grande partie de l'Antarctique est contrôlé par quelques événements extrêmes, ce qui entraîne une forte variabilité naturelle de ce paramètre. Les intrusions d'humidité extrêmes liées aux rivières atmosphériques arrivant de l'océan Austral conduisent à la fois à des accumulations de neige intenses, et à la fonte en surface sous l'effet du fort réchauffement et de l'augmentation du rayonnement infra-rouge. Pourtant, ces rivières atmosphériques sont actuellement négligées dans les études des changements climatique passés et futurs en Antarctique et de leurs impacts sur le BMS.

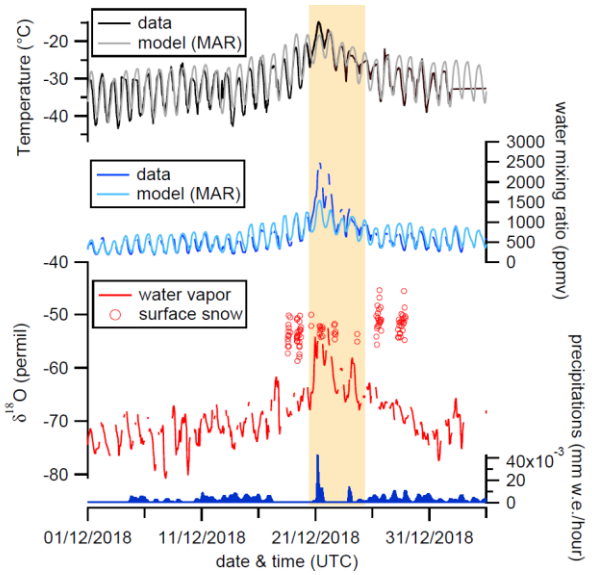

Fig. 1. Signature of an AR in temperature and humidity (in observation and MAR model outputs), in $\delta^{18}O$ signals (in water vapor and surface snow) and precipitation at Dome C in December 2018.

Le projet ARCA vise à décrire les rivières atmosphériques dans les régions polaires et leurs impacts en appliquant des algorithmes récents de détection des rivières atmosphériques à des sorties de simulations des climats passés, présents et futurs. ARCA évaluera l'impact des rivières atmosphériques sur le bilan de masse de surface de l'Antarctique et en étudiera la signature (notamment isotopique) afin d'explorer dans quelle mesure l'activité passée des rivières atmosphériques peut être reconstituée grâce aux enregistrements des carottes de glace.

Pour atteindre cet objectif, ARCA est organisé en 4 Axes. 1) ARCA utilisera des méthodes récentes d'identification des rivières atmosphériques, que nous appliquerons aux modèles de circulation globale et régionale. 2) ARCA collectera des données météorologiques, d'isotopes de l'eau et d'aérosols dans l'atmosphère et la neige de surface en Terre Adélie et de Wilkes (Antarctique de l'Est) pour définir la signature isotopique et en aérosols des rivières atmosphériques, puis 3) appliquera une modélisation des isotopes stables dans l'eau à l'échelle régionale pour mieux interpréter ces données. Enfin, 4) ARCA examinera les données des carottes de glace existantes.

.

Cadre chronologique, climatostratigraphique et paléomagnétique des tectites du Golfe de Guinée-**CHRONOTEC**

Nomade S., Rochette P., Guillou H., Scao V., Gray W., Daeron M., Jourdan F., Bassinot F., Rebaubier H., Isguder G.

Projet INSU LEFFE IMAGO 2019-2021

The CHRONOTEC project will aim at giving key information concerning the warm MIS 31 interglacial. Studying past long and warm interglacial climates is relevant in the frame of the on-going and projected global warming. The CHRONOTEC project tacked key questions that remain unanswered in particular regarding the exact orbital framework and this interglacial that currently relies on *a-priori* alignment with external forcing parameters of the climatic patterns obtained using palaeoclimatic proxy records. Ultimately, by providing a precise and accurate radio-isotopic age to the Ivory Coast microtektites layer (Fig. 1) deposition we will be able using the close temporal relationship of this event with the base of the Chron C1r.1n to calculate the absolute duration of MIS 31 (Fig. 2). Duration as well as phase relationship with the external forcing are indeed much need parameters to untangled underlying mechanisms that preside during such abnormal warm and long interglacial at the beginning of the EMPT. In order to bring such crucially needed information the general objectives of the CHRONOTEC project are listed below:

- Dated using $^{40}Ar/^{39}Ar$ the Ivory Coast tektites fallout using last generation multi-collector mass spectrometers.
- Provide the exact locating of the peak and reworked pattern of the microtektites tektites in marine sediments.
- Give to the scientific community the precise and accurate climatostratigraphic and palaeomagnetic context of the Ivory-coast microtektites deposition and as a consequence of the Bosumtwi crater formation.

Fig. 1 : Map of the Ivory Coast strewn field modified from Glass et al., (1991). The black squares are Leg 108 and Leg 159 sites were tektites layer was found and circle other cores that are not available but where tektites were found.

Innovative Training Network – DEEPICE- Research and training network on understanding Deep icE corE Proxies to Infer past antarctiC climatE dynamics

Coordination: Amaëlle Landais (2021-2025)

The new deep ice core to be drilled within the European project BEOI will enable the paleoclimate community to address major scientific questions on the role of ice sheet size and greenhouse gas concentrations on the dynamics of past climate changes. In particular a key challenge is to understand why the periodicity of glacial to interglacial cycles changed from 41 to 100 thousand of years during the so-called Mid-Pleistocene Transition, between 0.8 and 1.2 Ma, while at the same time the orbital forcing given by astronomical parameters keeps the same periodicity (Figure).

In addition to the logistical challenges associated with the drilling this ice core, large technological and scientific challenges need to be tackled in order to exploit this unique archive in the field and back in the laboratory. The new climatic records between 0.8 and 1.5 Ma will be located at the bottom of the ice core and hence, the ice will be extremely thinned. An optimal analysis of this precious ice for getting the best scientific outputs require to develop new techniques to analyse precisely very small quantity of ice. In addition, the results related to atmospheric greenhouse gas concentration and climate change will have to be confronted to climate model simulations in order to progress on the physical processes.

The DEEPICE network capitalizes on this unique European scientific endeavour, providing an educational and training program to 15 PhD students. Such subject is closely related to the major societal questions on climate change and its impact in the polar vulnerable regions. The goal of DEEPICE is hence to build a training program benefiting from the momentum created by the BEOI drilling project and its societal impact by complementing it by a program of basic and applied science questions in preparation of the Oldest Ice analysis. Moreover, DEEPICE will offer unique links with many non-academic partners that will provide the students with the extended skill-set now required for academic and non-academic careers. The study of climate change is a complex scientific subject as well as a long-term challenge for society. Hence, DEEPICE will provide a full educational program including a robust scientific understanding of climate processes and technical skills (statistics, specific instrumentation, climate modelling), transferable skills as well as a unique experience in the synthesis and communication of updated data on climate change.

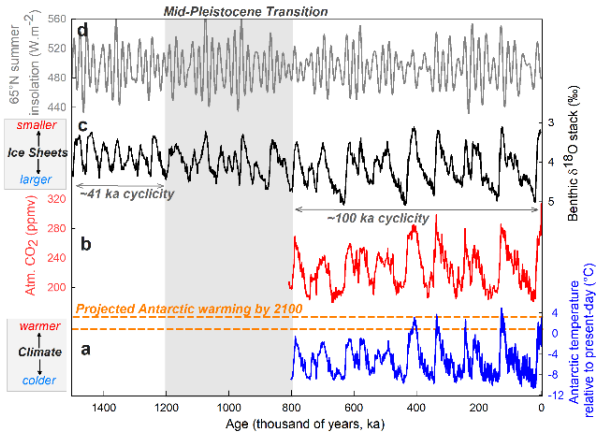

Fig. Key paleoclimatic records over the past 1.5 Myr.

ERC Synergy Grant 2020 AWACA : Atmospheric WAter Cycle over Antarctica: Past, Present and Future

Alexis Berne (EPFL), Thomas Dubos (LMD-Ecole Polytechnique), Christophe Genthon (LMD-CNRS), Valérie Masson-Delmotte (LSCE-CEA).

Autres participants LSCE : C. Agosta, O. Cattani, E. Fourré, O. Jossoud, A. Landais, B. Minster, F. Prié

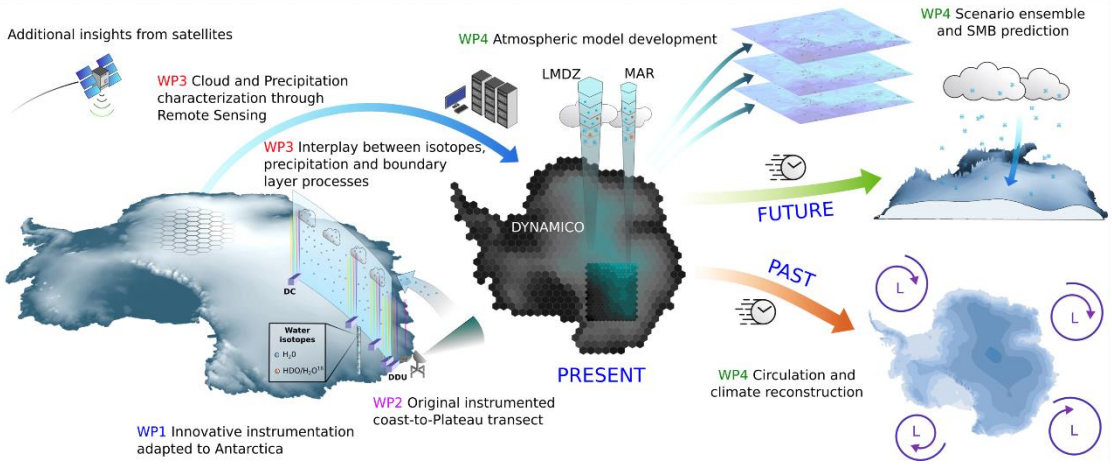

Fig. 1. Région, processus, outils et objectifs du projet AWACA.

Le Conseil Européen de Recherche a sélectionné le projet ERC Synergy AWACA, dont Valérie Masson-Delmote est l'une des quatre chercheurs porteurs. Ce projet a pour objectif de comprendre le cycle de l'eau en Antarctique en associant modélisations et mesures. Ce projet débutera mi-2021 pour une durée de 6 ans.

Résumé : Les modèles de climat projettent une augmentation des précipitations en Antarctique, qui modéreront l'augmentation globale du niveau des mers. La compréhension du cycle de l'eau atmosphérique est encore très limitée en Antarctique. La composition isotopique des précipitations neigeuses enregistre les paramètres climatiques qui peuvent être retracés dans les carottes de glaces, et apporter des informations précieuses pour mieux comprendre le cycle de l'eau atmosphérique. Le projet AWACA produira un cadre cohérent et complet, combinant observations et modélisation, pour comprendre et projeter la trajectoire de l'eau atmosphérique dans toute la colonne troposphérique. Des instruments spécifiquement adaptés/conçus seront combinés au sein de plateformes d'observations déployées sur 5 sites, le long d'un transect de 1100 km aligné sur la trajectoire principale de transport d'humidité vers la calotte. Les challenges relatifs à l'acquisition de données en totale autonomie, jamais réalisés jusqu'à présent pour un développement instrumental aussi complet, seront relevés grâce à la collaboration d'experts en technologies et en logistique polaire. Le jeu de données obtenu permettra l'étude des processus contrôlant les flux d'eau et leur composition microphysique et isotopique, qui seront utilisés pour développer de nouvelles paramétrisations physiques dans un modèle de climat global et ses configurations régionales. Une fois évalués le long du transect AWACA et pour d'autres régions Antarctique à partir d'observations satellites et des campagnes de terrain existantes, ces modèles permettront de quantifier la variabilité passée et future du cycle de l'eau atmosphérique en Antarctique.

SESAME: Human paleocology, social and cultural evolutions among first SEttlements in South AMErica (ANR 01/2021 – 12/2024)

coordinateurs : E. Boëda (ArScAn) – C. Hatté (LSCE)

Autres participants LSCE: A. Govin, C. Hatté, J. Jacob – C. Gauthier, C. Kissel, C. Noury, B. Phouybandhyt, F. Thil, A. Van Toer, C. Wandres

Qui étaient les premiers occupants des Amériques? Dans quelle mesure ces sociétés humaines ont-elles été affectées par les changements environnementaux? S'adapter, se déplacer, voire disparaître en réponse aux fluctuations climatiques sont les réactions attendues lors de changements drastiques de l'environnement.

Afin de caractériser ces différents scénarios, SESAME propose d'étudier la présence humaine attestée depuis au moins 40,000 ans dans le nord-est du Brésil. En révélant l'identité culturelle et technologique de ces sociétés passées et en confrontant la chronologie de leurs évolutions avec celle des variations climatiques et environnementales passées, SESAME ambitionne de lever le voile sur l'évolution croisée des hommes et de leur environnement à travers le Pléistocène et l'Holocène. Nous formulerons de nouvelles hypothèses sur les voies de diffusion et d'implantation, à l'échelle des Amériques, de ces cultures méconnues. Pour cela, nous utiliserons le modèle du NE Brésil pour remettre en contexte les données archéologiques disponibles (Fig. 1), dans le cadre des changements paléoenvironnementaux reconstruits.

Le projet implique les laboratoires ArScAn (Nanterre), LSCE, ISEM (Montpellier), IRAMAT (Bordeaux), EDYTEM (Chambéry), Univ. São Paulo (Brésil), Univ. Tucumán (Argentine).

La contribution du LSCE est de trois ordres et consiste 1- à conforter les cadres chronologiques (^{14}C) des phases d'occupation des sites brésiliens, 2- à préciser le cadre environnemental des occupations (biomarqueurs moléculaires, ^{13}C) et 3- à préciser le cadre paléoenvironnemental et paléoclimatique (fluorescence X, propriétés magnétiques, biomarqueurs) au niveau du bassin versant et de la région, tout au long des derniers 50 mille ans.

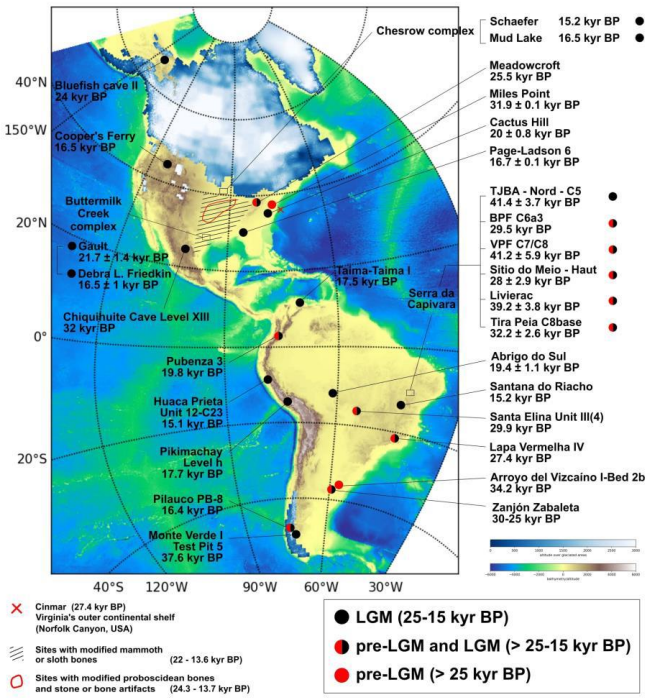

***Figure: Les plus anciens niveaux archéologiques connus en Amérique**. La carte présente l'extension de la calotte au LGM. Les sites archéologiques indiqués, sont associés à leur plus ancien âge connu. TJBA est pour Toca da Janela da Borra do Antonio, BPF pour Boqueirao da Pedra Furada, VPF fo Vale da Pedra Furada, tous dans le parc national de Capivara, Brésil. A noter que les sites brésiliens présentent les occupations les plus anciennes d'Amérique (occupation récurrentes tout au long de la période d'intérêt)*

INNOvation Isotopique pour les Paléo-Environnements et l'Océanographie: achat d'un système de micro-boucles pour injection directe sur MC-ICPMS(INNO)

Arnaud Dapoigny, Edwige Pons-Branchu, Matthieu Roy-Barman, William Gray, Jocelyn Barbarand, Valérie Plagnes
Projet IPSL

Le projet a pour objectif de mettre en place des analyses isotopiques haute précision sur le spectromètre de masse MC-ICPMS Neptune^{plus} ouvert à la communauté scientifique.

Le projet INNO a pour objectif l'achat d'un système de micro-boucles qui sera couplé au MC-ICPMS du LSCE afin d'injecter directement des microéchantillons de quelques dizaines de microlitres permettant ainsi un gain important en termes de capacités analytiques. Cette innovation technique permettra de développer de nouveaux axes de recherche dans le domaine des paléoenvironnements et de l'océanographie. Ce projet d'achat s'inscrit dans une démarche d'amélioration technique plus large qui a démarré par la mise en place en 2019 de nouveaux amplificateurs pour les cages de faraday (coût 16.5k€HT supporté pour partie par un projet « émergence » du département des sciences de l'université Paris-Saclay, pour une autre partie par la plateforme analytique PANOPLY, et enfin par des ressources propres de deux équipes du LSCE). Ces amplificateurs ont rendu possible la mesure fiable de petits signaux sur cage de faraday (l'erreur standard sur la mesure de petits signaux a été divisée par trois) et a permis d'envisager de nouvelles applications des mesures isotopiques. Il est donc nécessaire de compléter ce package avec des systèmes d'introduction adaptés tel que INNO.

Première application : mesure de la composition isotopique du bore dans des microéchantillons (foraminifères …)

Deuxième Application : la datation uranium-thorium (U-Th) de microéchantillons de carbonates secondaires et d'échantillons jeunes et pauvres en uranium et/ou thorium.

Troisième Application : la mesure de l'actinium dans l'eau de mer

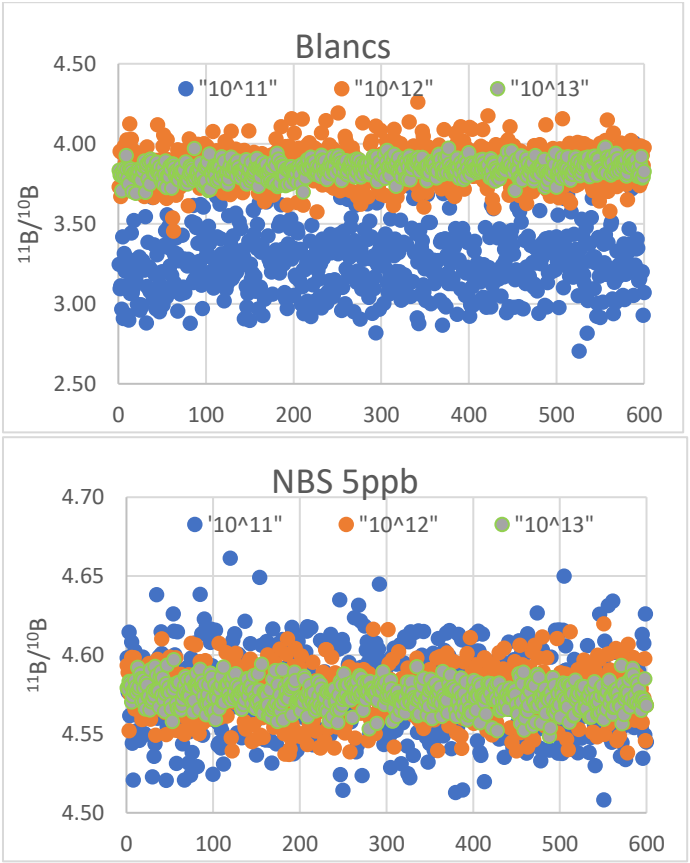

Figure : Reproductibilité du rapport isotopique du Bore sur le blanc et le standard en fonction des amplificateurs utilisés. Les analyses classiques sur le bore sont réalisées à 100ppb

ARTICLES

Southern Ocean upwelling, Earth's obliquity, and glacial-interglacial atmospheric CO_2 change

Ai, X., Studer, A., Sigman, D., Martınez-Garcıa, A., Fripiat, F., Thole, L., Michel, E., Gottschalk, J., Arnold, L., Moretti, S., Schmitt, M., Oleynik, S., Jaccard, S., and Haug, G.

Science (2020) Vol.370, 1348-1352

Previous studies have suggested that during the late Pleistocene ice ages, surface-deep exchange was somehow weakened in the Southern Ocean's Antarctic Zone (AZ), which reduced the leakage of deeply sequestered carbon dioxide and thus contributed to the lower atmospheric carbon dioxide levels of the ice ages. Here, high-resolution diatom-bound nitrogen isotope measurements from the Indian sector of the Antarctic Zone reveal three modes of change in Southern Westerly Wind–driven upwelling, each affecting atmospheric carbon dioxide. Two modes, related to **1** global climate and **2** the bipolar seesaw, have been proposed previously. The third mode **3**—which arises from the meridional temperature gradient as affected by Earth's obliquity (axial tilt)—can explain the lag of atmospheric carbon dioxide behind climate during glacial inception and deglaciation. This obliquity-induced lag, in turn, makes carbon dioxide a delayed climate amplifier in the late Pleistocene glacial cycles.

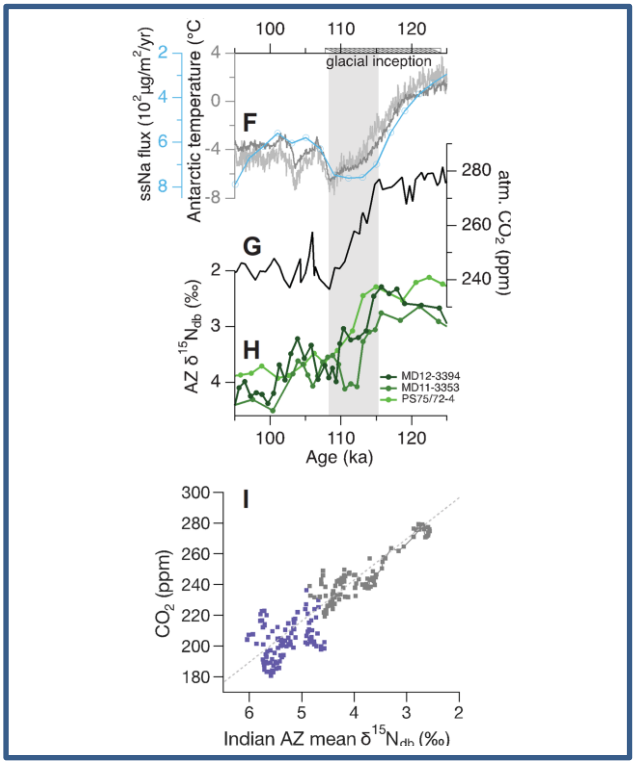

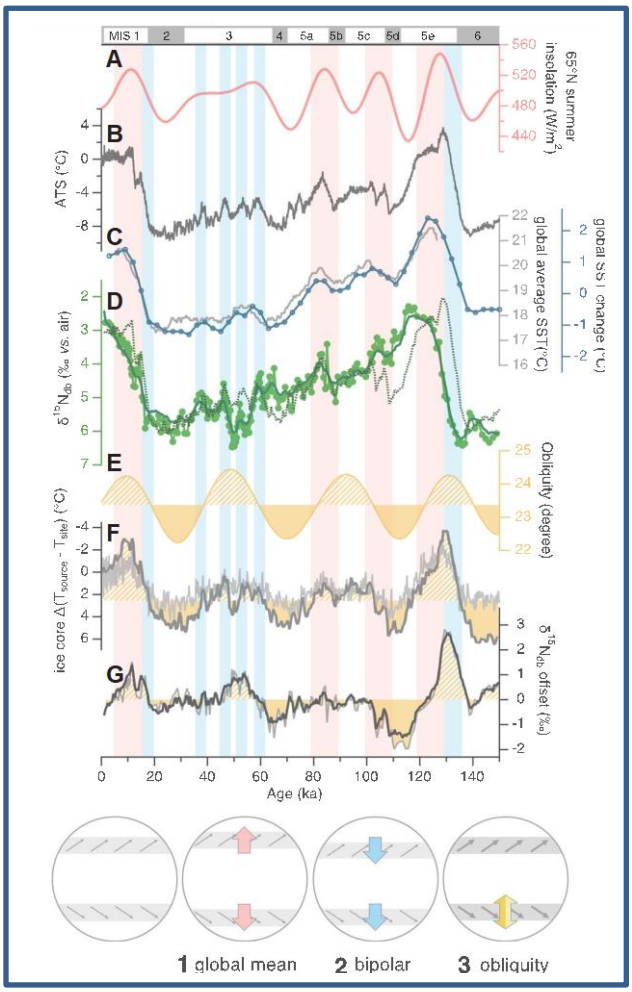

Fig. 1. Evidence for three modes of change in SWW-driven upwelling in the AZ. A: insolation at 65°N summer solstice. B: Antarctic temperature stack (ATS). C: Two reconstructions of global SST. D: $\delta^{15}N_{db}$ -from MD12-3394 -mean from MD12-3394 and MD11-3353 -predicted $\delta^{15}N_{db}$ if it strictly follows ATS (green dots, green line and grey line). E: Obliquity. F: Changes in the difference between the air temperature at the moisture source and the ice core site, Vostok and Dome Fuji, (dark, light grey) G: $\delta^{15}N_{db}$ offset : measured minus predicted.

Fig. 2. Last glacial inception : F: temperature : ATS and EDC (dark and light grey) with a proxy of sea ice (blue), G: atmospheric CO_2 and H: $\delta^{15}N_{db}$ of 3 AZ cores. I: cross plot CO_{2atm} and Indian AZ $\delta^{15}N_{db}$ grey dots: glacial inception.

Spatio-temporal dynamics of sedimentary phosphorus along two temperate eutrophic estuaries: A data-modelling approach

Ait Ballagh, F.E., Rabouille, C., Andrieux-Loyer, F., Soetaert, K., Elkalay, K., Khalil, K.

Continental Shelf Research, (2020) vol.193, 104037

Sediments play an important role in dissolved inorganic phosphorus (DIP) recycling, which needs to be precisely quantified in eutrophic estuaries. A coupled field data and diagenetic modelling approach was used to study P dynamics in two estuaries (Elorn and Aulne, Brittany, France). An existing model (OMEXDIA) was extended with phosphorus (P) benthic cycle by adding dissolved inorganic phosphorus (DIP) and particulate P fractions (organic P, Fe-bound P and Ca-bound P). The model was fitted to pore water oxygen, nitrate, ammonium, oxygen demand units (reduced substances that were produced by the anoxic mineralization; Fe2þ, Mn2þ and H2S; ODU), DIP, sediment organic P and C, Fe-bound P and Ca-bound P data from four seasons (February, May, July and October 2009) in two eutrophic estuaries (Elorn and Aulne). These two systems were investigated along the salinity gradient with 3 stations per estuary. The model shows that high organic C fluxes deposited in the sediments (23–98 mmol m-2 d-1) caused high organic P mineralization rates, which is the modeled main benthic source of DIP (77%). The DIP recycling fluxes were calculated in Elorn (463 ± 122 µmol m-2 d-1) and in Aulne (320 ± 137 µmol m-2 d-1) estuaries, and overall 85% of DIP produced in the sediment was recycled to the overlying water. A limited but substantial proportion (15%) was precipitated as Ca-bound P except in the upstream reach of the Aulne in February, where the integrated rate of Ca-bound P precipitation constitutes a major sink of DIP (83%). The high DIP recycling fluxes in Elorn and Aulne estuaries, integrated over the entire area, were 3–20 times larger than the river DIP input. This comparison of external and internal DIP loads shows the major role of these sediments as sources of DIP to the estuary and the potential storage of formerly discharged nutrients.

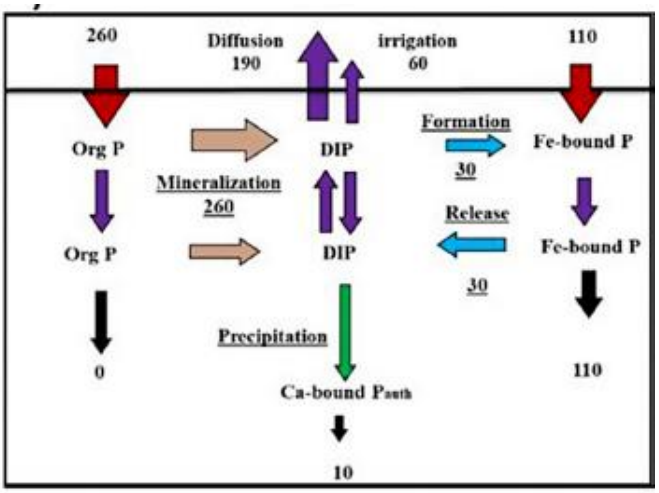

Fig. 1. Phosphorus mass balance in sediment of the downstream site of the Elorn estuary in October. It clearly shows the large recycling flux (Diffusion+Irrigation), the balanced Fe bound P fluxes which constitutes a shuttle of P to the anoxic zone and the limited (but not insignificant) CaP precipitation and burial.

CMIP5 model selection for ISMIP6 ice sheet model forcing: Greenland and Antarctica

Barthel, A., Agosta, C., Little, C., Hattermann, T., Jourdain, N., Goelzer, H., Nowicki, S., Seroussi, H., Straneo, F., and Bracegirdle, T.

The Cryosphere, Vol. 14, pages 855–879, 2020

The ice sheet model intercomparison project for CMIP6 (ISMIP6) effort brings together the ice sheet and climate modeling communities to gain understanding of the ice sheet contribution to sea level rise. ISMIP6 conducts stand-alone ice sheet experiments that use space- and time-varying forcing derived from atmosphere–ocean coupled global climate models (AOGCMs) to reflect plausible trajectories for climate projections. The goal of this study is to recommend a subset of CMIP5 AOGCMs (three core and three targeted) to produce forcing for ISMIP6 stand-alone ice sheet simulations, based on (i) their representation of current climate near Antarctica and Greenland relative to observations and (ii) their ability to sample a diversity of projected atmosphere and ocean changes over the 21st century. The selection is performed separately for Greenland and Antarctica. Model evaluation over the historical period focuses on variables used to generate ice sheet forcing. For stage (i), we combine metrics of atmosphere and surface ocean state (annual- and seasonal-mean variables over large spatial domains) with metrics of time-mean subsurface ocean temperature biases averaged over sectors of the continental shelf. For stage (ii), we maximize the diversity of climate projections among the best-performing models. Model selection is also constrained by technical limitations, such as availability of required data from RCP2.6 and RCP8.5 projections. The selected top three CMIP5 climate models are CCSM4, MIROC-ESM-CHEM, and NorESM1-M for Antarctica and HadGEM2-ES, MIROC5, and NorESM1-M for Greenland. This model selection was designed specifically for ISMIP6 but can be adapted for other applications.

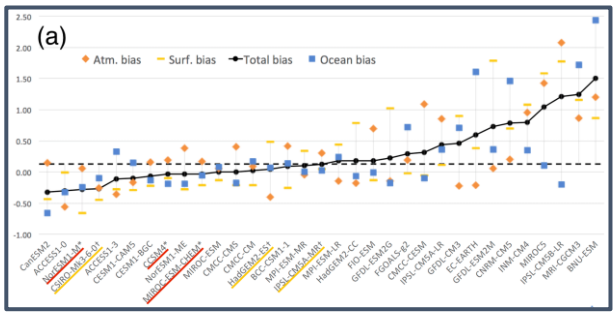

Fig. 1. Ranking of models according to total bias (black) over the Antarctic domain, with a breakdown of the ocean (blue), atmosphere (orange), and surface (yellow) contributions. Models are ranked according to total bias. Models selected in the top three (core) ensemble are underlined in red with an asterisk, and models in the top six (targeted) ensemble are underlined in yellow with a † symbol.

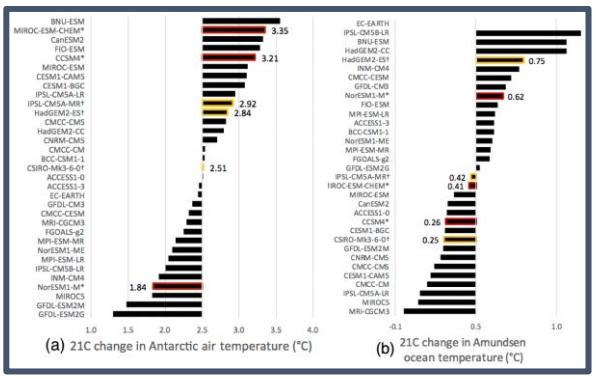

Fig. 2. Projected RCP8.5 warming for each CMIP5 model in the Antarctic region.

Routing of terrestrial organic matter from the Congo River to the ultimate sink in the abyss: a mass balance approach

Baudin, F., Rabouille, C., and Dennielou, B.

Geologica Belgica (2020) 23/1-2: 41-52

We address the role of the Congo River sediment dispersal in exporting and trapping organic carbon into deep offshore sediments. Of particular interest is the Congo submarine canyon, which constitutes a permanent link between the terrestrial sediment sources and the marine sink. The Congo River delivers an annual sediment load of ~40 Tg (including 2 Tg of C) that feed a mud-rich turbidite system. Previous estimates of carbon storage capacity in the Congo turbidite system suggest that the terminal lobe complex accounts for ~12% of the surface area of the active turbidite system and accumulates ~18% of the annual input of terrestrial particulate organic carbon exiting the Congo River. In this paper, we extend the approach to the whole active turbidite depositional system by calculating an average burial of terrestrial organic matter in the different environments: canyon, channel, and levees. We estimate that between 33 and 69% (average of 45%) of terrestrial carbon exported by the Congo River is ultimately trapped in the different parts of turbidite system and we evaluate their relative efficiency using a source to sink approach. Our carbon budget approach, which consider annual river discharge *versus* offshore centennial accumulation rates, indicates that about half of the total particulate organic matter delivered yearly by the Congo River watershed escapes the study area or is not correctly estimated by our deep offshore dataset and calculations.

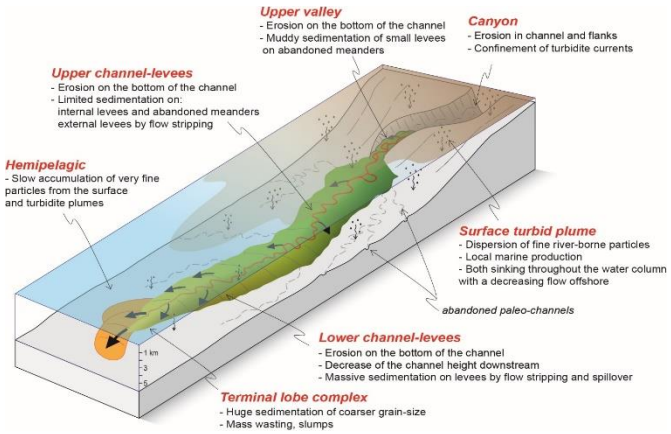

Fig. 1. Sedimentary processes in the surface and submarine environment off the Congo River mouth with the main characteristics of the different environments of the turbidite system (inspired from Babonneau, 2002).

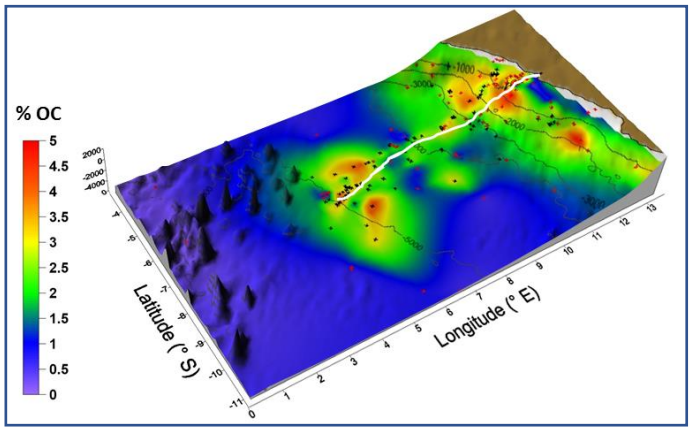

Fig. 2. Map of the Corg content (wt% of dry and desalted sediment) in topmost sediments (< 3 cm depth) in the Southeastern Atlantic Ocean off the Congo River (modified from Baudin et al., 2017a). Sediments related to the Congo turbidite system are significantly enriched in Corg, until the abyssal plain. The white line corresponds to the path of the present-day active turbidite channel.

Carbon 13 Isotopes Reveal Limited Ocean Circulation Changes Between Interglacials of the Last 800 ka

Bouttes N., Vazquez Riveiros N., Govin A., Swingedouw D., Sanchez-Goni M.F., Crosta X., Roche D.M.

Reference: *Paleoceanography Paleoclimatology* 35, e2019PA003776, https://doi.org/10.1029/2019PA003776.

Ice core data have shown that atmospheric CO_2 concentrations during interglacials were lower before the Mid-Brunhes Event (MBE, ~430 ka), than after the MBE by around 30 ppm. To explain such a difference, it has been hypothesized that increased bottom water formation around Antarctica or reduced Atlantic Meridional Overturning Circulation could have led to greater oceanic carbon storage before the MBE, resulting in less carbon in the atmosphere. However, only few data on possible changes in interglacial ocean circulation across the MBE have been compiled, hampering model-data comparison.

Here we present a new global compilation of benthic foraminifera carbon isotopic ($\delta^{13}C$) records from 31 marine sediment cores covering the last 800 ka (Fig. 1) in order to evaluate possible changes of interglacial ocean circulation across the MBE. We show that a small systematic difference between pre- and post-MBE interglacial $\delta^{13}C$ is observed. In pre-MBE interglacials, northern source waters tend to have slightly higher $\delta^{13}C$ values (Fig. 2) and penetrate deeper, which could be linked to an increased northern sourced water formation or a decreased southern sourced water formation.

Numerical model simulations tend to support the role of abyssal water formation around Antarctica: Decreased convection there associated with increased sinking of dense water along the continental slopes results in increased $\delta^{13}C$ values in the Atlantic, in agreement with pre-MBE interglacial data. It also yields reduced atmospheric CO_2 as in pre-MBE records, despite a smaller simulated amplitude change compared to data, highlighting the need for other processes to explain the MBE transition.

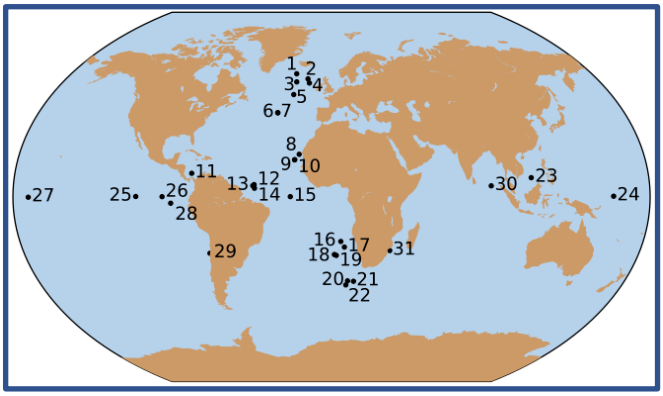

Fig. 1. Compilation of selected marine sediment cores with available $\delta^{13}C$ records over the last 800 ka (at least partially).

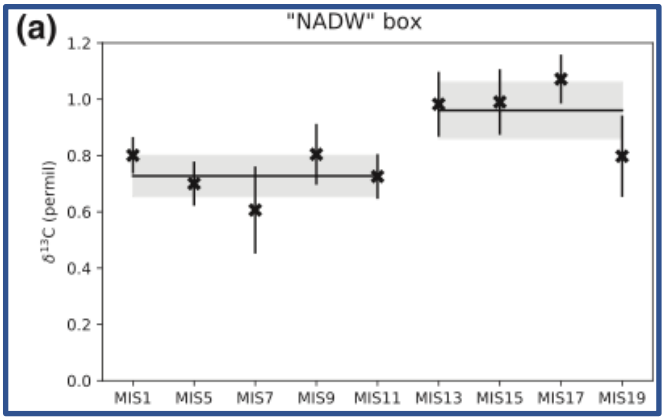

Fig. 2. Mean benthic $\delta^{13}C$ value calculated for nine interglacials in the "NADW" box (North Atlantic sites with water-depths between 1000 and 4000 m,) after correcting for global mean ocean $\delta^{13}C$ changes using the mean deep equatorial Pacific signal.

Productivité exceptionnelle de la biosphère il y a 420 000 ans

Brandon, M., Landais, A., Duchamp-Alphonse, S., Favre, V., Schmitz, L., Abrial, H., Prié, F., Extier, T., Blunier, T.

Nature Communications volume 11, Article number: 2112 (2020)

Une équipe franco-danoise a étudié les flux liés à la productivité biosphérique sur la période de la Terminaison V, pour mieux comprendre leurs impacts sur les variations de CO_2 atmosphérique. Pour ce faire, les scientifiques ont développé au LSCE la seule ligne expérimentale d'Europe d'extraction de l'oxygène de l'air piégé dans la glace, qui permet de mesurer avec précision la composition isotopique triple de l'oxygène ($\Delta^{17}O$ de O_2) dans les bulles d'air piégées dans la glace, et l'ont utilisée pour effectuer des mesures sur la carotte antarctique Epica Dome C (EDC) pour la période comprise entre 445 et 405 000 ans. La composition isotopique triple de l'oxygène échangé avec la biosphère lors des processus associés à la productivité biologique (photosynthèse vs respiration) ayant une signature significativement différente de celle de l'oxygène n'ayant pas subi de tels échanges, les variations enregistrées dans l'atmosphère « fossile » permettent de retracer la productivité biosphérique passée.

Les flux d'oxygène associés à la productivité biosphérique et reconstitués à partir des données de cette étude montrent que, durant la Terminaison V et le début de l'interglaciaire qu'elle précède, la productivité était de 10 à 30 % supérieure à celle observée durant la période préindustrielle. C'est le niveau de productivité biologique le plus élevé jamais observé durant les 450 000 dernières années.

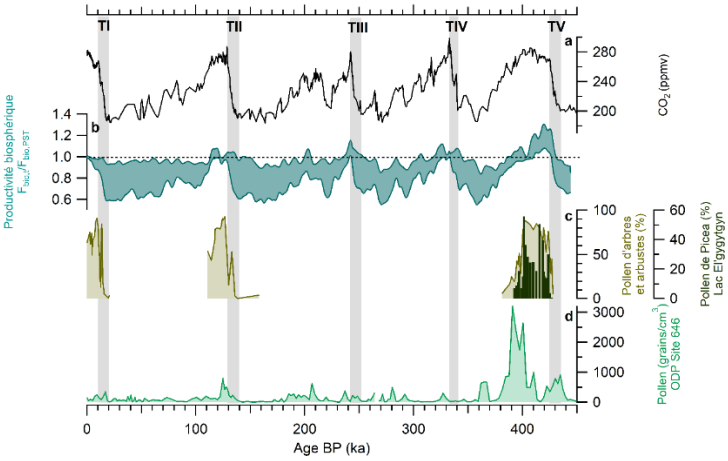

Figure : Evolution de la productivité biosphérique au cours des 445 derniers milliers d'années. En haut : courbe de CO_2 composite (Bereiter et al., 2015). 2ème courbe depuis le haut : reconstitution du ratio de productivité biosphérique entre un temps donné t et la période préindustrielle, calculée à partir des données de $\Delta^{17}O$ de O_2. 3ème courbe depuis le haut : Enregistrement de pollen d'arbres, d'arbustes et de Picea dans le lac El'Gygytgyn, Sibérie (Melles et al., 2012). En bas : Enregistrement de pollen dans la carotte sédimentaire marine ODP Site 646 au Sud du Groenland (De Vernal et Hillaire-Marcel, 2008)

Editorial: Facing Marine Deoxygenation

Capet, A., Cook, P., Garcia-Robledo, E., Hoogakker, B., Paulmier, A., Rabouille C., and Vaquer-Sunyer, R.

Frontiers in Marine Science (2020) vol. 7, article 46

This paper is the editorial for the special issue of Frontiers in Marine Science on Marine deoxygenation for which all the authors were associate guest editors. The special issue contains 11 papers.

Marine deoxygenation is increasingly recognized as a major environmental threat (Breitburg et al., 2018).

Global warming drives a substantial part of this deoxygenation trend (Keeling et al., 2010), which is projected to continue during the next decades both in the open ocean and in the coastal waters. Future increasing anthropogenic pressures (e.g., eutrophication) are expected to further exacerbate this trend (Fennel and Testa, 2019).

Several main challenges need to be addressed by the scientific community:

1) To understand natural variability in marine oxygenation. As observations only cover the last ca. 60 years, we lack information about longer-term variability and trends in ocean oxygenation and associated drivers (Kamykowski and Zentara, 1990; Schmidtko et al., 2017; Oschlies et al., 2018).

2) To understand and predict the response of global biogeochemical cycles to deoxygenation. In particular, how lower oxygen conditions affect community respiration, the nitrogen (Zehr, 2009; Lam and Kuypers, 2011) and phosphorus cycles (Conley et al., 2002;Watson et al., 2017) across the estuarine-shelves-ocean continuum, including feed-backs on the climate system.

3) To evaluate and mitigate the threat posed by deoxygenation on valuable marine goods and services (Cooley, 2012) and on marine biodiversity (Vaquer-Sunyer and Duarte, 2008).

Open ocean (Paulmier and Ruiz-Pino, 2009) and coastal (Diaz and Rosenberg, 2008; Rabalais et al., 2009) deoxygenation differ in terms of temporal scale, morphology, driving processes, and implications. However, we gathered contributions related to both typologies in order to highlight interactions, differences and similarities, and to promote a common concern on marine deoxygenation so as to raise public awareness and facilitate mitigation strategies (Levin and Breitburg, 2015).

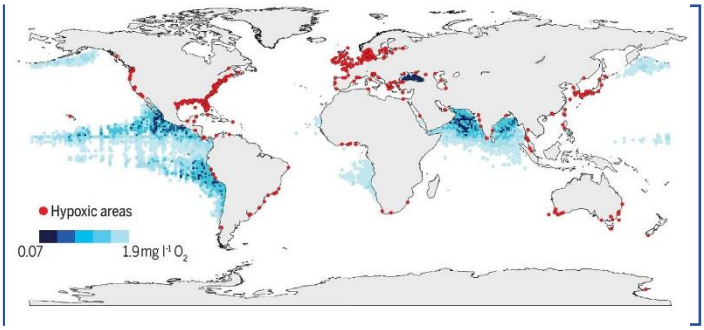

Fig. 1 (from Breitburg et al., 2018). Deoxygenation in the world ocean. Red dots indicate site that are hypoxic in the coastal ocean due to increased nutrient input and blue symbols indicate the oxygen concentration in oxygen minimum zones at 300 meters water in the open ocean.

Building a three dimensional model of the active Plio-Quaternary basin of Argostoli (Cephalonia Island, Greece): An integrated geophysical and geological approach

Cushing ME., Hollender F., Moiriat D., Guyonnet-Benaize C., Theodoulidis N., Pons-Branchu E., Sépulcre S., Bard PY., Cornou C., Dechamp A., Mariscal, A., Roumelioti Z.

Engineering Geology 265 (2020) 105441 - doi: 10.1016/j.enggeo.2019.105441

This work is a multidisciplinary approach from geological and geophysical surveys to build a 3D geological model of Argostoli Basin (Cephalonia Island, Greece) aiming to be used for computational 3D simulation of seismic motion. Cephalonia Island is located at the north-western end of the Aegean subduction frontal thrust that is linked to the dextral Cephalonia Transform Fault (west of Cephalonia) where the seismic hazard is high in terms of earthquake frequency and magnitude. The Plio-Quaternary Koutavos-Argostoli basin site was selected within the French Research Agency PIA SINAPS@ project (www.institut-seism.fr/projets/sinaps/ - last accessed on November 25th 2019) to host a vertical accelerometer array. The long-term goal is to validate three-dimensional nonlinear numerical simulation codes to assess the site-specific amplification and nonlinearity. Herein the geological and geophysical surveys carried out from 2011 to 2017 are presented and in particular the complementary investigations that led to the identification of the main stratigraphic units and their structures. In addition, coral debris sampled from the vertical array deep borehole cores were used for $^{230}Th/^{234}U$ measurements, which confirmed the Pleistocene age of the Koutavos basin. The characterization of the three-dimensional structure of the stratigraphic units was achieved by coupling geological cross-sections (i.e., depth geometry) and geophysical surveys based of surface wave analysis.

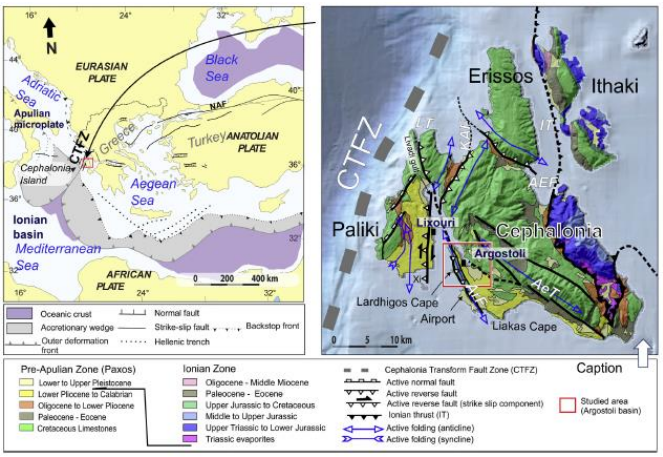

Fig.: Location of the studied site, and Geodynamic map of the broader southeastern Mediterranean.

Magnesium in subaqueous speleothems as a potential palaeotemperature proxy

Drysdale R., Couchoud I., Zanchetta G., Isola I., Regattieri E., Hellstrom J., Govin A., Tzedakis P.C., Ireland T., Corrick E., Greig A., Wong H., Piccini L., Holden P., Woodhead

Nature Communications 11, 5027-5037, https://doi.org/10.1038/s41467-020-18083-7.

Records of Quaternary temperature change are derived primarily from polar ice cores and ocean sediments. Beyond the polar regions, long terrestrial records of palaeotemperatures are sparse, because most archives lack chemical, biological, and/or physical properties that behave consistently as a palaeothermometer. This hampers efforts to develop a more coherent picture of global patterns of past temperatures.

Here we investigate the potential of using Mg palaeothermometry in a subaqueous speleothem from Corchia Cave (Italy). The cave is located close to the North Atlantic, whose ocean heat transport modulates the climate of Western Europe and the Mediterranean (Fig. 1).

We show Mg concentrations in Corchia Cave's speleothem track regional sea surface temperature over the last 350 ka. The Mg shows higher values during interglacials and converse patterns during glacial times (Fig. 2). In contrast to previous studies, this result implies that temperature, not rainfall, is the principal driver of Mg variability.

High-resolution Mg concentrations also faithfully track regional temperatures during Termination II, despite a deglacial offset of several ka between Mg and $\delta^{18}O$ records. Thus, the subaqueous speleothem Mg is a far more robust and direct palaeotemperature proxy than δ18O, particularly during millennial-scale Heinrich events.

The depositional setting of the speleothem gives rise to Mg partition coefficients that are more temperature dependent than other calcites, enabling the effect of temperature change on Mg partitioning to greatly exceed the effects of changes in source-water Mg/Ca. Subaqueous speleothems from similar deep-cave environments should be capable of providing palaeotemperature information over multiple glacial-interglacial cycles.

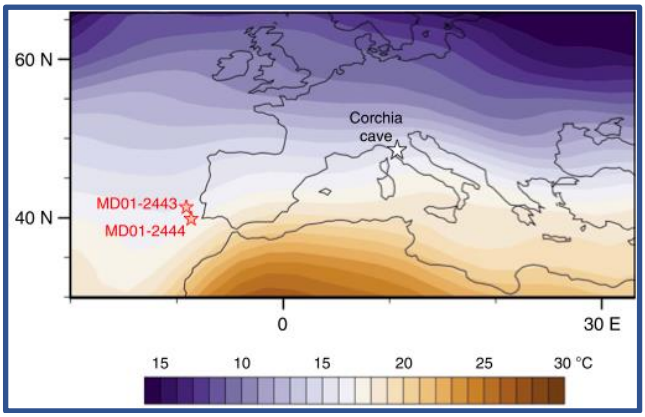

Fig. 1. Mean annual (1981-2010) regional air temperatures and study sites: Corchia Cave and two North Atlantic cores.

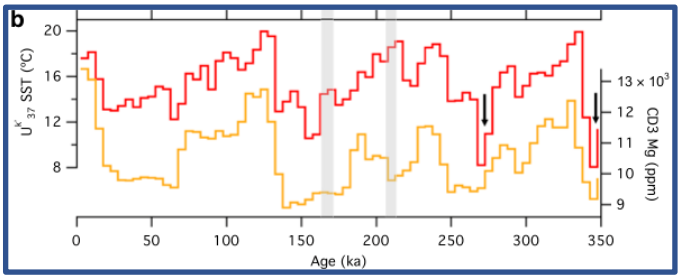

Fig. 2. Comparison of Corchia Cave Mg record (in orange) to the composite Sea Surface Temperature record of the two North Atlantic cores over the last 350 ka.

Variations in eastern Mediterranean hydrology during the last climatic cycle as inferred from neodymium isotopes in foraminifera

Duhamel, M., Colin, C., Revel, M., Siani, G., Dapoigny, A., Douville, E., Wu, J., Zhao, Y., Liu, Z., and Montagna, P.

Quaternary Science Reviews (2020) 237, 10.1016/j.quascirev.2020.106306.

The Nd isotopic compositions (ε_{Nd}) of mixed planktonic foraminifera have been analyzed in two sediment cores collected in the Nile deep-sea fan in order to reconstruct past ε_{Nd} of the Eastern Mediterranean Deep Water (EMDW) and to assess the relative contributions of Nile discharge and Modified Atlantic Water (MAW) inflow to the Eastern Mediterranean Sea hydrology, as well as their potential control on anoxic events over the last climatic cycle. The two foraminiferal ε_{Nd} records are similar and display an increase in ε_{Nd} values during the African Humid Periods. Superimposed on this precession-forced variability (insolation received by the Earth at low latitudes), the record of variations in foraminiferal ε_{Nd} indicates a 2-unit decrease in ε_{Nd} during the interglacial Marine Isotope Stages (MIS) 5 and 1 compared to glacial MIS- 6, 4, 3 and 2. The ε_{Nd} results suggest that the long-term glacial to interglacial changes in Nd isotopic composition of EMDW were not entirely induced by variations in Nile River discharge and Saharan dust inputs. Decreases in ε_{Nd} during MIS-5 and MIS-1 interglacials indicate an increase in the contribution of unradiogenic MAW to the eastern Mediterranean Sea related to high sea-level stands and greater seawater exchange between the North Atlantic and Mediterranean basins. In addition, radiogenic seawater ε_{Nd} values observed during African Humid Periods (and sapropel events) are associated with an intensification of Nile discharge and an increase in residence time of deep-water masses in the eastern Mediterranean Sea, which induces an increase in the interaction between deep-water masses and radiogenic sediments along the margin of the eastern Mediterranean Sea. Results confirm that an intensification of the hydrological exchanges between the western and eastern Mediterranean basins during high sea-level stand and the subsequent higher proportion of Atlantic Water in the Levantine Basin may have preconditioned the eastern Mediterranean Sea to sapropel depositions during the last climatic cycle.

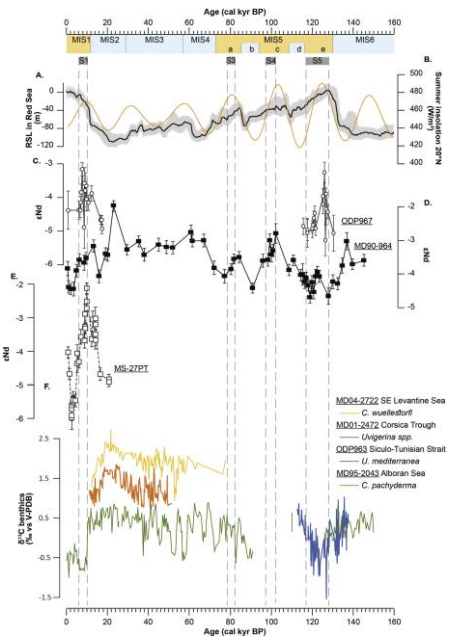

Fig. 1. (A) Variations in Relative Sea Level (RSL) (Grant et al., 2014); (B) summer insolation (June and July) received by the Earth at 20°N, calculated using Analyseries software (Paillard et al., 1996) for last 160 kyr. (CC) ε_{Nd} record obtained from ODP Site 967C (Osborne et al., 2010); (DD) ε_{Nd} record obtained from non-reductively cleaned mixed planktonic foraminifera of core MD90-964 (this study); (EE) ε_{Nd} record obtained from non-reductively cleaned mixed planktonic foraminifera of core MS27PT (this study). See paper for the others sources.

The nature of deep overturning and reconfigurations of the silicon cycle across the last deglaciation

Dumont, M., Pichevin, L., Geibert, W., Crosta, X., Michel, E., Moreton, S., Dobby, K., Ganeshram, R.

Nature Communications (2020) vol.11 :1534., doi.org/10.1038/s41467-020-15101-6

Changes in ocean circulation and the biological carbon pump have been implicated as the drivers behind the rise in atmospheric CO_2 across the last deglaciation; however, the processes involved remain uncertain. Previous records have hinted at a partitioning of deep ocean ventilation across the two major intervals of atmospheric CO_2 rise, but the consequences of differential ventilation on the Si cycle has not been explored. Here we present three new records of silicon isotopes in diatoms and sponges from the Southern Ocean that together show increased Si supply from deep mixing during the deglaciation with a maximum during the Younger Dryas (YD). We suggest Antarctic sea ice and Atlantic overturning conditions favored abyssal ocean ventilation at the YD and marked an interval of Si cycle reorganization. By regulating the strength of the biological pump, the glacial–interglacial shift in the Si cycle may present an important control on Pleistocene CO_2 concentrations.

During glacials, the stratification of the ocean stored a large amount of DSi in the deeper ocean. However the reduction in DSi uptake by diatoms through a combination of iron-induced alteration of diatom Si:C stoichiometric demand as well as a reduction in biogenic silica export in the more extensively ice-covered waters of the glacial Antarctic allowed more DSi to be exported and sustained diatom growth in lower latitudes. A higher whole ocean glacial DSi inventory, due to reduced opal burial in response to sea ice cover in the Antarctic and reduced silification of iron replete diatoms might have also increase the availiability of DSi in the upper ocean.

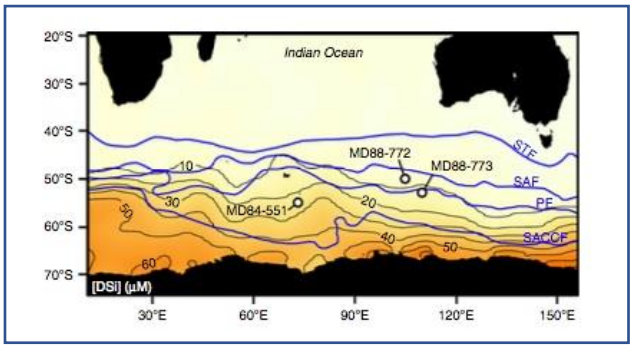

Fig. 1. Core location and Dsi distribution in the surface (10m depth) Indian Ocean.

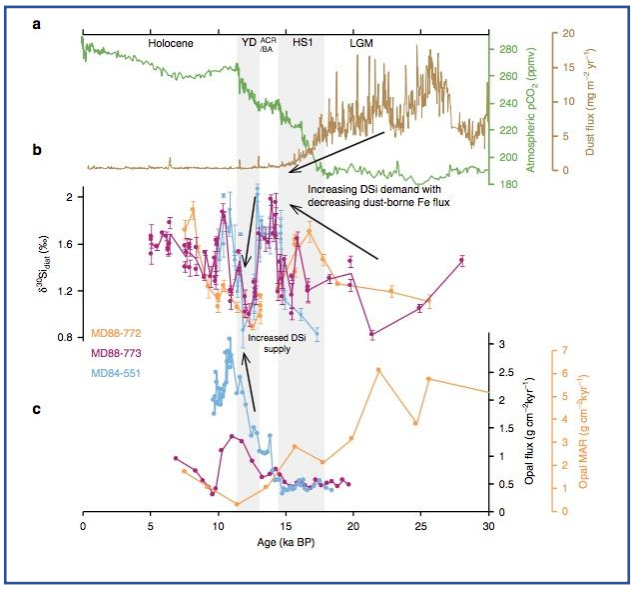

Fig. 2. Deglacial $\delta^{30}Si_{diat}$ and opal records from the three Southern Ocean Indian sector cores. a Atmospheric CO_2 and Antarctic dust flux recorded in EPICA Dome C. b $\delta^{30}Si_{diat}$ data from MD84-551, MD88-773 and MD88-772 with ± 1SE. c ^{230}Th-normalised opal flux records from MD84-551 and MD88-773 and opal mass accumulation rate from MD88-772.

Tara Pacific Expedition's Atmospheric Measurements of Marine Aerosols across the Atlantic and Pacific Oceans

Flores J.M. et al., including Douville E.

Bull. Amer. Meteor. Soc. (2020) 101 (5): E536–E554, 10.1175/BAMS-D-18-0224.1Geost

Marine aerosols play a significant role in the global radiative budget, in clouds' pro-cesses, and in the chemistry of the marine atmosphere. There is a critical need to better understand their production mechanisms, composition, chemical properties, and the contribution of ocean-derived biogenic matter to their mass and number concentration. Here we present an overview of a new dataset of in situ measurements of marine aerosols conducted over the 2.5-yr Tara Pacific Expedition over 110,000 km across the Atlantic and Pacific Oceans. Preliminary results are presented here to describe the new dataset that will be built using this novel set of measurements. It will characterize marine aerosols properties in detail and will open a new window to study the marine aerosol link to the water properties and environmental conditions.

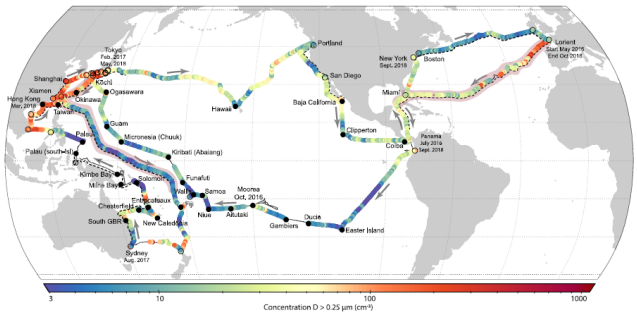

Fig. 1. Route of the Tara Pacific Expedition 2016–18 visualized by the OPC aerosol concentration of D > 0.25 µm. The black line shows the full route of the expedition, but where no aerosol data were collected. The gray arrows indicate the direction Tara sailed. The black dotted line shows the areas the SMPS was working. The black full circles denote coral holobionte sampling sites, and the black open circles denote any other stopover.

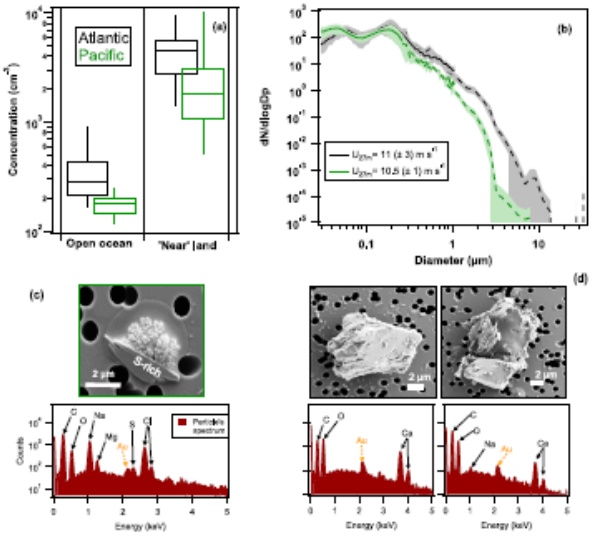

Fig. 2. Differences in concentration, size distribution, and composition between the Atlantic and Pacific Oceans.

^{231}Pa and ^{230}Th in the Arctic Ocean: Implications for boundary scavenging and ^{231}Pa-^{230}Th fractionation in the Eurasian Basin

Gdaniec, S., Roy-Barman, M., Levier, M., Valk, O., Rutgers van der Loeff, M., Foliot, L., Dapoigny, A., Missiaen, L., Mörth, C.-M., and Andersson, P.

Chemical Geology, Elsevier, 2020, 532, pp.119380. ⟨10.1016/j.chemgeo.2019.119380⟩

^{231}Pa, ^{230}Th and ^{232}Th were analyzed in filtered seawater (n = 70) and suspended particles (n = 39) collected along a shelf-basin transect from the Barents shelf to the Makarov Basin in the Arctic Ocean during GEOTRACES section GN04 in 2015. The distribution of dissolved ^{231}Pa and ^{230}Th in the Arctic Ocean deviates from the linear increase expected from reversible scavenging. Higher ^{232}Th concentrations were observed at the shelf, slope and in surface waters in the deep basin, pointing at lithogenic sources. Fractionation factors ($F_{Th/Pa}$) observed at the Nansen margin were higher compared to $F_{Th/Pa}$ in the central Nansen Basin, possibly due to the residual occurrence of hydrothermal particles in the deep central Nansen Basin. Application of a boundary scavenging model quantitatively accounts for the dissolved and particulate ^{230}Th distributions in the Nansen Basin. Modelled dissolved ^{231}Pa distributions were largely overestimated, which was attributed to the absence of incorporation of water exchange with the Atlantic Ocean in the model. ^{231}Pa/^{230}Th ratios of the suspended particles of the Nansen Basin were below the ^{231}Pa/^{230}Th production ratio, but top-core sediments of the Nansen margin and slope have high ^{231}Pa/^{230}Th-ratios, suggesting that scavenging along the Nansen margin partly acts as a sink for the missing Arctic ^{231}Pa.

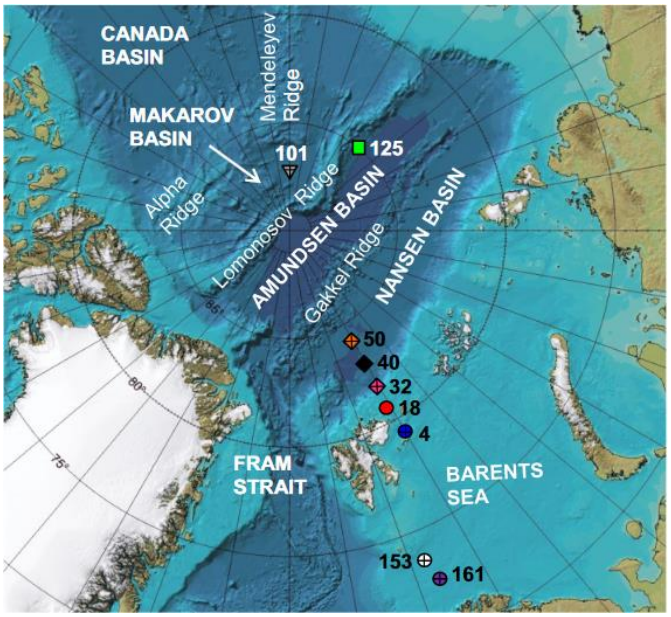

Fig.1. Samples for the analysis of dissolved and particulate ^{231}Pa, ^{230}Th and ^{232}Th were collected at 9 stations along the GEOTRACES GN04 section in the Arctic Ocean. Crossed symbols denote sampling for particulate and dissolved samples and non-crossed points are stations which were sampled for the analysis of dissolved concentrations.

Expanding Tara Oceans protocols for underway, ecosystemic sampling of the Ocean-Atmosphere interface during Tara Pacific expedition (2016-2018)

Gorsky G. et al. including Douville, E., …

Front.Mar. Sci. 6:750. doi: 10.3389/fmars.2019.00750

Interactions between the ocean and the atmosphere occur at the air-sea interface through the transfer of momentum, heat, gases and particulate matter, and through the impact of the upper-ocean biology on the composition and radiative properties of this boundary layer. The *Tara* Pacific expedition, launched in May 2016 aboard the schooner Tara, was a 29-month exploration with the dual goals to study the ecology of reef ecosystems along ecological gradients in the Pacific Ocean and to assess inter-island and open ocean surface plankton and neuston community structures. In addition, key atmospheric properties were measured to study links between the two boundary layer properties. A major challenge for the open ocean sampling was the lack of ship-time available for work at "stations". The time constraint led us to develop new underway sampling approaches (Fig. 1) to optimize physical, chemical, optical, and genomic methods to capture the entire community structure of the surface layers, from viruses to metazoans in their oceanographic and atmospheric physicochemical context. An international scientific consortium was put together to analyze the samples, generate data, and develop datasets in coherence with the existing *Tara* Oceans database. Beyond adapting the extensive *Tara* Oceans sampling protocols for high-resolution underway sampling, the key novelties compared to *Tara* Oceans global assessment of plankton include the measurement of (i) surface plankton and neuston biogeography and functional diversity; (ii) bioactive trace metals distribution at the ocean surface and metal-dependent ecosystem structures; (iii) marine aerosols, including biological entities; (iv) geography, nature and colonization of microplastic; and (v) high-resolution underway assessment of net community production via equilibrator inlet mass spectrometry. We are committed to share the data collected during this expedition, making it an important resource to address a variety of scientific questions.

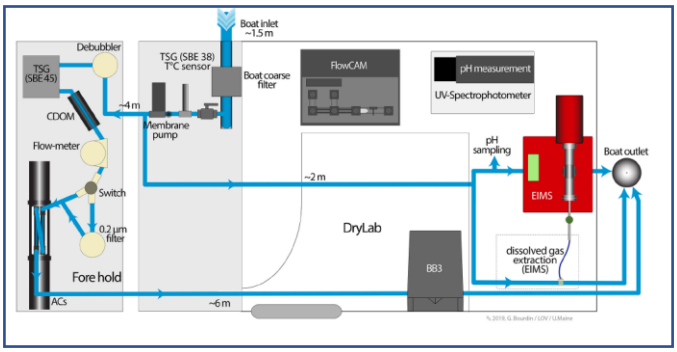

Fig. 1. Schematic diagram of the underway, continuous sampling system, showing the setup of the various flow-through instruments and the distance between the water intake and each instrument. The water flow is shown in blue. The FlowCam and the UV-spectrophotometer were installed in the drylab for live imaging of microplankton and pH measurements.

Glacial heterogeneity in Southern Ocean carbon storage abated by fast South Indian deglacial carbon release

Gottschalk, J., Michel, E., Thöle, L. M., Studer, A. S., Hasenfratz, A. P., Schmid, N., Butzin, M., Mazaud, A., Martínez-García, A., Szidat, S., Jaccard, S.

Nature Communications (2020) vol.11, doi.org/10.1038/s41467-020-20034-1

Past changes in ocean ^{14}C disequilibria have been suggested to reflect the Southern Ocean control on global exogenic carbon cycling. Yet, the volumetric extent of the glacial carbon pool and the deglacial mechanisms contributing to release remineralized carbon, particularly from regions with enhanced mixing today, remain insufficiently constrained. Here, we reconstruct the deglacial ventilation history of the South Indian upwelling hotspot near Kerguelen Island, using high-resolution ^{14}C-dating of smaller-than-conventional foraminiferal samples and multi-proxy deep-ocean oxygen estimates. We find marked regional differences in Southern Ocean overturning with distinct South Indian fingerprints on early de-glacial atmospheric CO_2 change. The dissipation of this heterogeneity commenced 14.6 kyr ago, signaling the onset of modern-like, strong South Indian Ocean upwelling, likely promoted by rejuvenated Atlantic overturning. Our findings highlight the South Indian Ocean's capacity to influence atmospheric CO_2 levels and amplify the impacts of inter-hemispheric climate variability on global carbon cycling within centuries and millennia.

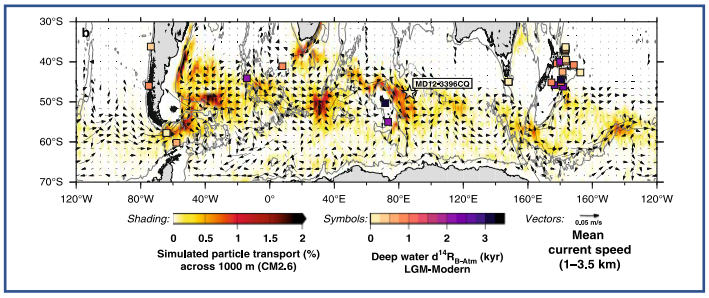

Fig. 1. Regions of intense interaction of the Antarctic Circumpolar Current with local bathymetry in Southern Ocean upwelling hotspots. Spatial changes in particle transport in percent across the 1000 m-depth surface, with vectors showing the average speed and direction of ocean currents at mid-depth (1–3.5 km) based on (GODAS) database representing the Antarctic Circumpolar Current between 40–60°S. Squares indicate reconstructed deep-water 14C ages in the Southern Ocean during the last glacial maximum (LGM) referenced to preindustrial.

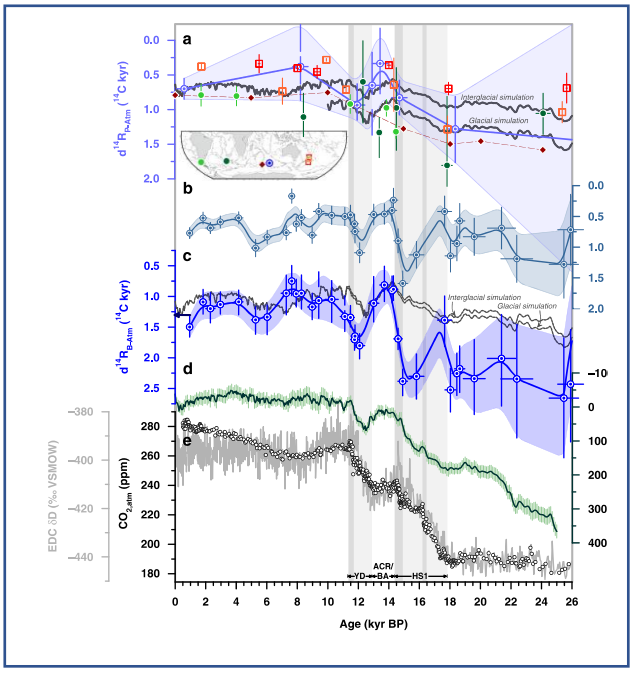

Fig. 2. Deglacial ocean reservoir age variations reconstructed in core MD12-3396CQ. a: Surface-ocean reservoir age ($d^{14}R_{P\text{-}Atm}$), b: benthic-to- planktic foraminiferal ^{14}C age offsets ($d^{14}R_{B\text{-}P}$) in MD12-3396CQ, c: ^{14}C age offsets of benthic foraminifera in MD12-3396CQ from the contemporaneous atmosphere, $d^{14}R_{B\text{-}Atm}$, d: $\Delta^{14}C_{atm}$ variations corrected for changes in cosmogenic ^{14}C production, and e: atmospheric CO_2 (black) and EPICA Dome C (EDC) δD variations (grey). Grey lines in a and c show simulated $d^{14}R_{P\text{-}Atm}$ changes at the study site at 25 m and 3.5 km depth, respectively.

Wind-driven evolution of the North Pacific subpolar gyre over the last deglaciation.

Gray, W. R., Wills, R. C. J., Rae, J. W. B., Burke, A., Ivanovic, R. F., Roberts, W. H. G., et al.

Geophysical Research Letters 47, e2019GL086328. https://doi.org/ 10.1029/2019GL086328

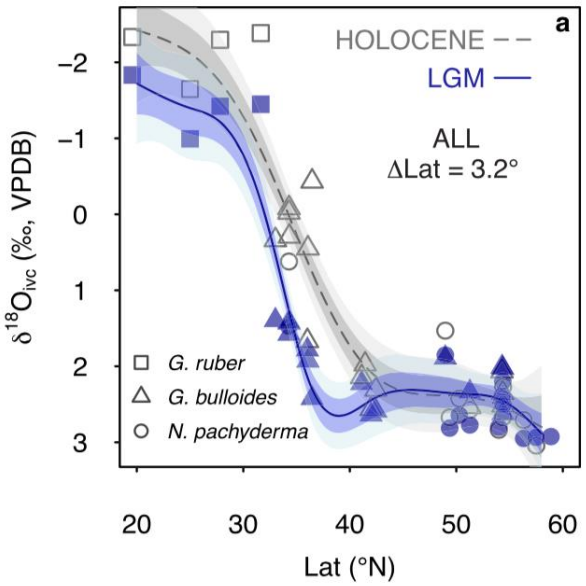

Holocene and LGM meridional profiles of planktic foraminiferal $\delta^{18}O$ from the North Pacific. The steep part of the curve represents the gyre boundary, which is shifted equatorward during the LGM

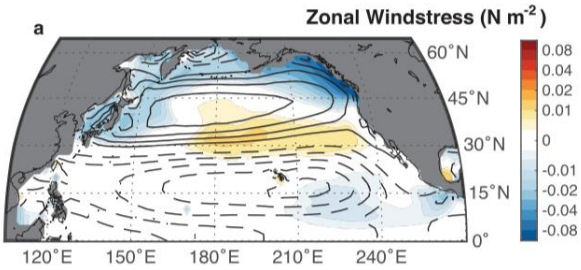

LGM-PI zonal windstress in the PMIP3 ensemble demonstrating a southward shift and strengthening of the westerlies during the LGM, leading to the expansion of the subpolar gyre seen in the data in the top figure.

North Pacific atmospheric and oceanic circulations are key missing pieces in our understanding of the reorganization of the global climate system since the Last Glacial Maximum. Here, using a basin-wide compilation of planktic foraminiferal $\delta^{18}O$, we show that the North Pacific subpolar gyre extended ~3° further south during the Last Glacial Maximum, consistent with sea surface temperature and productivity proxy data. Climate models indicate that the expansion of the subpolar gyre was associated with a substantial gyre strengthening, and that these gyre circulation changes were driven by a southward shift of the mid-latitude westerlies and increased wind stress from the polar easterlies. Using single-forcing model runs, we show that these atmospheric circulation changes are a nonlinear response to ice sheet topography/albedo and CO_2. Our reconstruction indicates that the gyre boundary (and thus westerly winds) began to migrate northward at ~16.5 ka, driving changes in ocean heat transport, biogeochemistry, and North American hydroclimate.

Sub-permil inter-laboratory consistency for solution-based Boron isotope analyses on marine carbonates

Gutjahr, M., Bordier L., Douville, E. et al., including Thil, F

Geostandards and Geoanalytical Research (2020) 10.1111/ggr.12364

Boron isotopes in marine carbonates are increasingly used to reconstruct seawater pH and atmospheric pCO_2 through Earth's history. While isotopic measurements from individual laboratories are often of high quality, it is important that records generated in different laboratories can equally be compared. Within this Boron Isotope Intercomparison Project (BIIP), we characterised the boron isotopic composition (commonly expressed in $\delta^{11}B$) of two marine carbonates: Japanese Geological Survey carbonate standard materials JCp-1 (coral *Porites*) and JCt-1 (giant clam *Tridacna gigas*). Our study has three foci:

(i) to assess the extent to which oxidative pre-treatment, aimed at removing organic material from carbonate, can influence the resulting $\delta^{11}B$;

(ii) to determine to what degree the chosen analytical approach may affect the resultant $\delta^{11}B$, and (iii) to provide well-constrained consensus $\delta^{11}B$ values for JCp-1 and JCt-1.The resultant robust mean and associated robust standard deviation (σ^*) for un-oxidized JCp-1 is 24.36 ± 0.45 ‰ ($2\sigma^*$), compared with 24.25 ± 0.22 ‰ ($2\sigma^*$) for the same oxidized material. For un-oxidized JCt-1, respective compositions are 16.39 ± 0.60 ‰ ($2\sigma^*$; un-oxidized) and 16.24 ± 0.38 ‰ ($2\sigma^*$; oxidized). The consistency between laboratories is generally better if carbonate powders were oxidatively cleaned prior to purification and analysis.

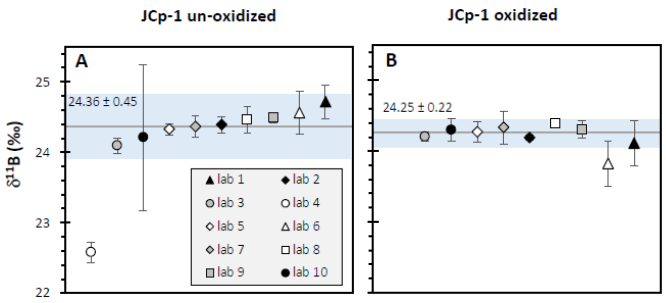

Fig. 1. $\delta^{11}B$ results for modern Porites sp. coral JCp-1, presented in delta notation relative to NIST SRM 951, presenting the mean $\delta^{11}B$ for each laboratory with resultant 2σ for (A) un-oxidized samples and (B) aliquots that underwent preceding oxidative treatment. Shaded area corresponds to the $\delta^{11}B$ range enclosed by the double robust standard deviation $2\sigma^*$. Values for the robust mean and double robust standard deviation are equally displayed and indicated by the grey lines in (A) and (B).

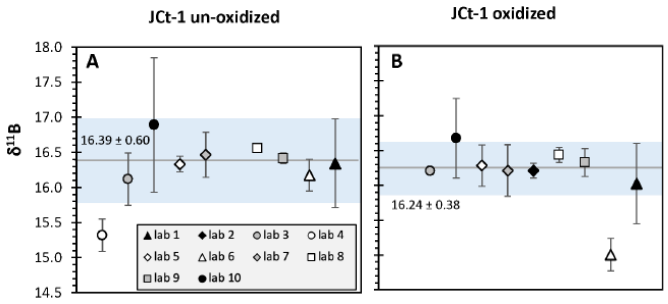

Fig. 2. $\delta^{11}B$ results for Tridacna gigas JCt-1 standard, presented in delta notation relative to NIST SRM 951, showing the mean $\delta^{11}B$ for each laboratory with resultant 2σ for (A) un-oxidized samples and (B) aliquots that underwent prior oxidative treatment. Shaded area corresponds to the $\delta^{11}B$ range enclosed by the double robust standard deviation $2\sigma^*$. Values for the robust mean and double robust standard deviation are equally displayed and indicated by the grey lines in (A) and (B).

Ventilation and Expansion of Intermediate and Deep Waters in the Southeast Pacific During the Last Termination

Haddam, N., Michel E., Siani, G., Licari, L., and Dewilde, F.

Paleoceanography and Paleoclimatology (2020) 35, doi.org/10.1029/2019PA003743

We investigate the geometry and ventilation of the water masses within bathyal depths (~1,500 to ~2,500 m) of the Southeast Pacific (SEP), inferring the lower depth limit variations of the Antarctic Intermediate Water (AAIW) since ~22 kyr cal. BP. We use three cores collected at the upper limit of the Pacific deep waters, between 41°S and 49°S, and one core at a greater depth within this same water mass, at 46°S. The benthic foraminiferal assemblages and carbon and oxygen isotopes are used to show strong linkages between the timing of the deglacial Southern Ocean upwelling events and changes in the vertical extension and ventilation of the AAIW. In accordance with local/sublocal oxygen reconstructions, we propose at least three states of ventilation-AAIW vertical extension: (i) the late glacial and the Antarctic Cold Reversal (ACR): AAIW depth-limit shoals, as its formation zone moves northward; (ii) the deglaciation (excluding the ACR): the [O2] enrichment of the AAIW and the dominance of benthic species Trifarina angulosa indicate ventilated AAIW, along with a deepening of its lower limit; and (iii) the Holocene: enhanced influence of the Pacific deep water at bathyal depths (1,500–2,500 m) in the SEP north of ~46°S and the circumpolar deep water south of ~46°S.

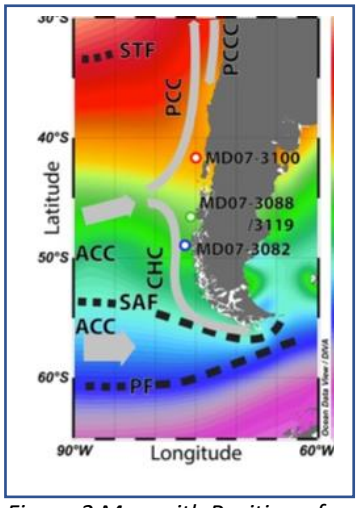

Figure 2 Map with Position of the cores studied and the sea surface temperature WOA, Boyer et al., 2013)

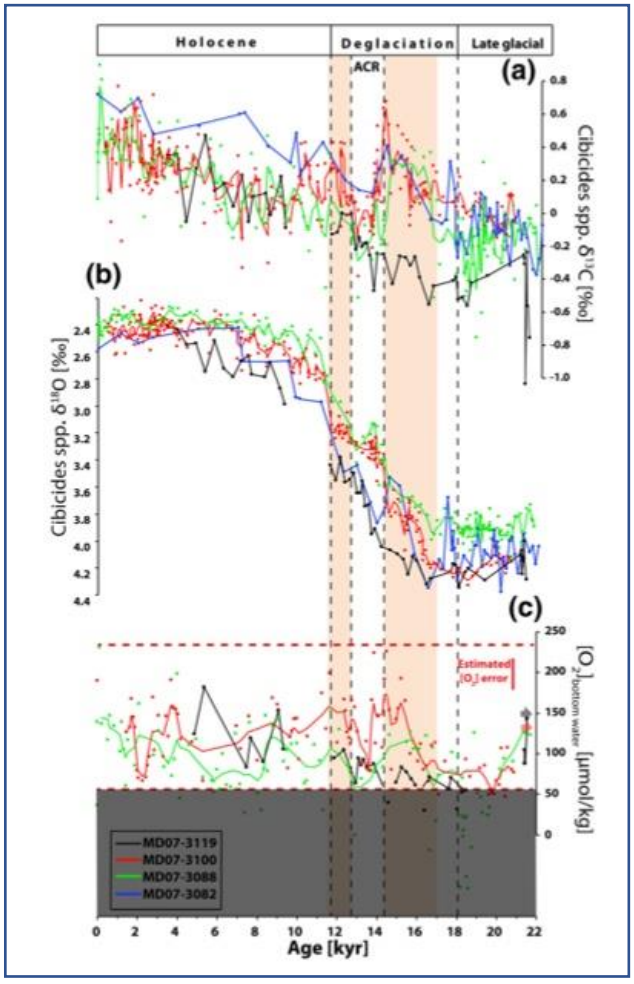

Fig. 2. (a) Cibicides spp. $\delta^{13}C$ and (b) Cibicides spp. $\delta^{18}O$ measured on the three considered cores. (c) [O_2] reconstructed in cores MD07–3100, MD07–3119, and MD07–3088 with the horizontal red dashed lines representing the sensitivity limits of Hoogakker et al. (2015) calibration; the lower limit is shaded. The vertical red line represents the estimated error for the estimations (± ~30 µmol/kg). The red and black arrows represent the actual [O2] value at 1500 and 2500 m (Silva et al. (2009), and WOA Boyer et al., 2013 respectively). Pink shading indicates the periods of Southern Ocean upwelling increase (Siani et al., 2013).

The radiocarbon age of the mycoheterotrophic plants

Hatté C., Zazzo A., Sélosse M.-A.

New Phytologist (2020), 227(5):1284–1288

Mycorrhizal symbiosis, a widespread, > 400 million-year-old mutualism, consists of soil fungi associated with plant roots. In this symbiosis, soil mineral nutrients are exchanged for photosynthetic products. In plant evolution, the fungi involved in this association diversified, and the exchange was modified in some cases. Several groups of achlorophyllous plants associated with fungi independently emerged, which reversed the ancestral carbon flow. The so-called mycoheterotrophic plants exploit carbon substrates from their fungal hosts. These fungi obtain their own carbon from other sources: some are saprotrophic and exploit dead organic matter, whereas others are mycorrhizal on autotrophic plants that provide the carbon and energy for the whole consortium. In the recently published article in New Phytologist, Suetsugu et al. (2020) elegantly use radiocarbon to assess the age of carbon in diverse mycoheterotrophic plants. Our study carried out a few years earlier but which we had not published, had similar objectives on different ecosystems and is therefore very well positioned to complement Suetsugu et al.'s work. Results are shown in the figure.

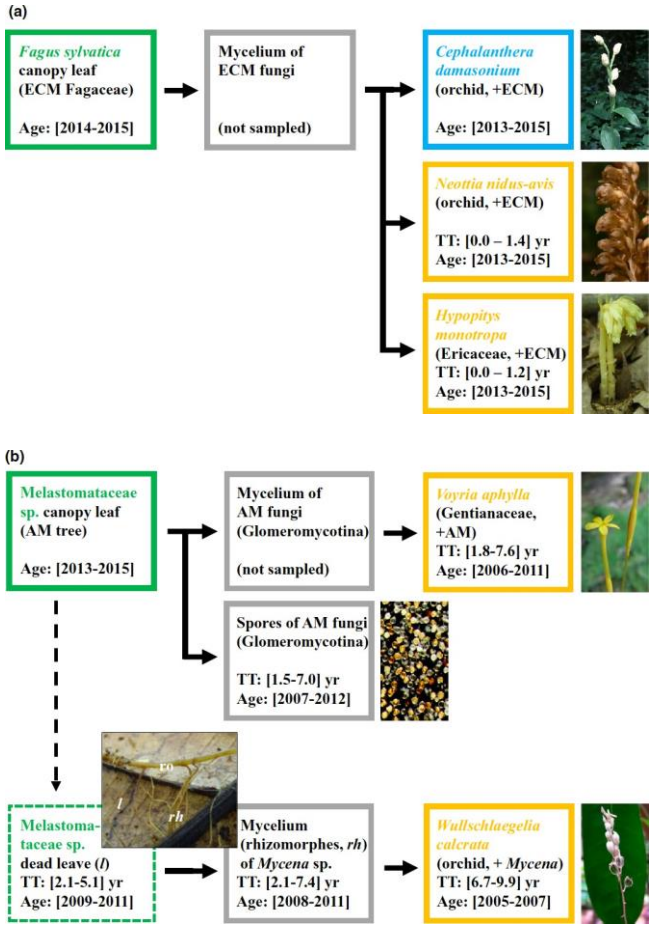

Figure: Age of carbon in samples from 2014 at two sites with mycoheterotrophic (orange) and mixotrophic (blue) plants, linked by various fungi (grey) and trophic chains to autotrophic plants (green), with 95% confidence intervals for transit time (TT) since initial photosynthesis and for carbon age [in brackets]. (a) An ectomycorrhizal (ECM) network in a French temperate forest (Pagny-la-Blanche-Côte) links Fagus sylvatica to mixotrophic Cephalanthera damasonium and mycoheterotrophic Neottia nidus-avis and Hypopitys monotropa monotropa

High-resolution sedimentary record of anthropogenic deposits accumulated in a sewer decantation tank

Jacob, J., Thibault, A., Simonneau, A., Sabatier, P., Le Milbeau, C., Gautret, P., Ardito, L. and Morio, C. High

https://doi.org/10.1016/j.ancene.2020.100238

To test the extent to which sediments accumulated in sewers may serve as high-resolution archives of urban evolution, this study examined a sedimentary succession deposited in a decantation tank of the combined sewer network of Orléans (France). The focus was on a 1.43 m sediment core drilled after 10 months of operation since the last cleaning. Sediments were stratigraphically organized into three distinct facies. The lower unit comprised organic remains, the middle unit gravels and sands and the upper unit was fine sands. The evolution of radionuclide activities, bile acid concentrations, and glass microspheres enabled sediments from wastewater and storm-water inputs to be distinguished. Precipitation events that affected the area were the main control on sediment deposition with organic-rich sediments accumulating from wastewater during dry weather and coarser, mineral sediments accumulating from storm-water during precipitation events. These results enable development of a chronological framework for sediment deposition. These findings reveal the potential of sewer sediment accumulations to record relevant information on the evolution of urban socio-ecosystems on monthly to annual scales with a relatively high time resolution.

OUTIL. En 2017, un forage avait permis des prélèvements dans les couches plus anciennes qui restent à étudier. PH. D'ARCHIVES

The Zanclean palaeofloras around the Mont-Dore strato-volcano: A window into upper Neogene vegetation and environments in the Massif Central (Puy de Dome, France)

Jolly-Saad, M.-C., Pastre, J.-F., and Nomade, S.

GEOBIOS 59, 29-46 (2020)

New Pliocene macrofloras and microfloras perfectly preserved from the Mont-Dore cinerite (Puy-de-Dôme, Massif central, France) have been reinvestigate. The 40Ar/39Ar radiometric datings bracketing the Chambon Lake and La Gratade fossil-bearing horizons give 4.46 ± 0.05 Ma and 3.94 ± 0.04 Ma respectively, (Fig.1).

They belong to the Zanclean Stage of the early Pliocene (5.32 to 3.6 Ma) therefore much older than previously thought (i.e., Piacenzian). Detailed morphological evaluation of leaf morphotypes completed with pollen analysis contributed to the better taxonomic knowledge of these palaeofloras. All the taxa (Fig. 2) described contribute to a rich biodiversity of these Pliocene assemblages. All three sites investigated point towards riverine forest habitats dominated by hygrophilic diversified woody plants while in the surrounding plains and slopes the thermophilic elements were scarce and mesophilic taxa abundant as temperate elements. This vegetation can be compared with mixed mesophytic forests depicting a climate cooling during the two considered periods (ca. 4.46 and 3.95 Ma).

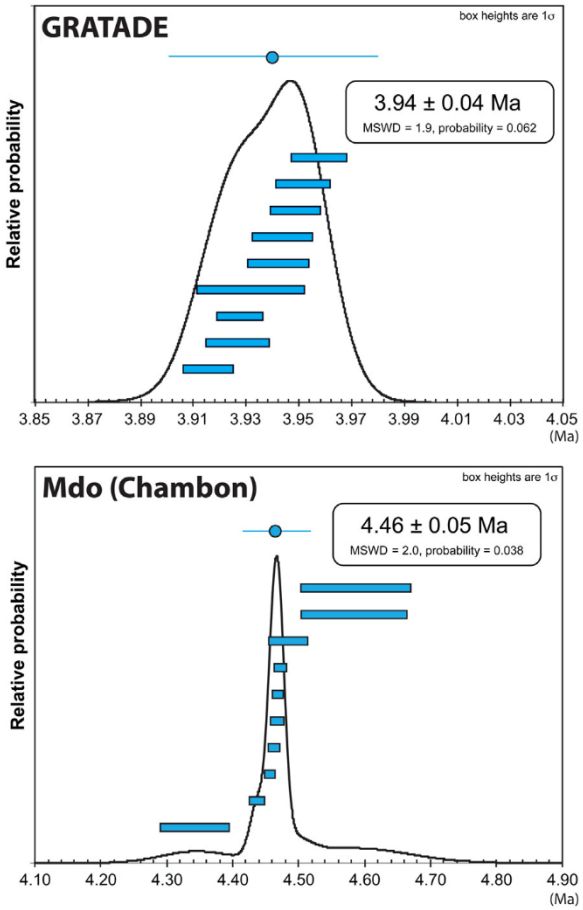

Fig.1 $^{40}Ar/^{39}Ar$ relative probability distributions for the Chambon Lake and La Gratade outcrops.

A global database of Holocene paleo-temperature records

Kaufman, D. and the Temperature-12ka consortium, including A. Orsi.

Reference : Scientific Data | (2020) 7:115 | https://doi.org/10.1038/s41597-020-0445-3

A comprehensive database of paleoclimate records is needed to place recent warming into the longer-term context of natural climate variability. We present a global compilation of quality-controlled, published, temperature-sensitive proxy records extending back 12,000 years through the Holocene. Data were compiled from 679 sites where time series cover at least 4000 years, are resolved at sub-millennial scale (median spacing of 400 years or finer) and have at least one age control point every 3000 years, with cut-off values slackened in datasparse regions. The data derive from lake sediment (51%), marine sediment (31%), peat (11%), glacier ice (3%), and other natural archives. The database contains 1319 records, including 157 from the Southern Hemisphere. The multi-proxy database comprises paleotemperature time series based on ecological assemblages, as well as biophysical and geochemical indicators that reflect mean annual or seasonal temperatures, as encoded in the database. This database can be used to reconstruct the spatiotemporal evolution of Holocene temperature at global to regional scales, and is publicly available in Linked Paleo Data (LiPD) format.

Past environmental and circulation changes in the South China Sea: Input from the magnetic properties of deep-sea sediment

Kissel, C., Laj, C., Jian, Z., Wang, P., Wandres, C., Rebolledo-Vieyra, M.

Quaternary Science Reviews 236 (2020) 106263

The enormous mass of continental sediments delivered every year in the South China Sea constitute a unique archive for past environmental studies in this region. The magnetic fraction of deep-sea sediments, though forming a minority in volume, provides incredibly valuable information for paleoceanographic reconstructions, as long as its provenance and source-to-sink processes are well constrained.

The review of the information available so far about the magnetic properties of SCS sediments shows that the large variety of interpretations/ conclusions finally results in a rather unclear picture. Because in such a context, the characterization of the sediment at the source is critical, the magnetic properties recently obtained from a set of samples from rivers (Kissel et al., 2017 ; 2018) and modern marine surface sediments (Kissel et al., 2018) are summarized to describe the present day situation. They are then used to interpret paleorecords from a set of seven marine cores distributed from the southern to the northern basins at different water depths and all covering at least the last climatic cycle.

The results reported here for the first time suggest that the magnetic mineralogy remains rather stable in time on land and that its time and spatial distribution at sea is an interplay of changes in sea level and deep-sea circulation. During low sea level periods, bottom deep-sea circulation is weak and the deposited sediment originates from the proximal rivers. On the contrary, during high sea level, the circulation is enhanced, transporting more sediment most likely from Taiwan and Luzon, to the northwestern part of the SCS and also, in smaller proportion, to the southern basin where it mixes with the local river-borne sediment.

The two longest records indicate that this pattern is repeated over the last 900 ka (□S-ratio, Fig. 1). Superimposed to the 100 kyr cyclicity we also observe a longer-term evolution with a maximum in the bottom current strength around 500 ka coinciding with global changes in the deep ocean circulation and carbon cycle.

Fig

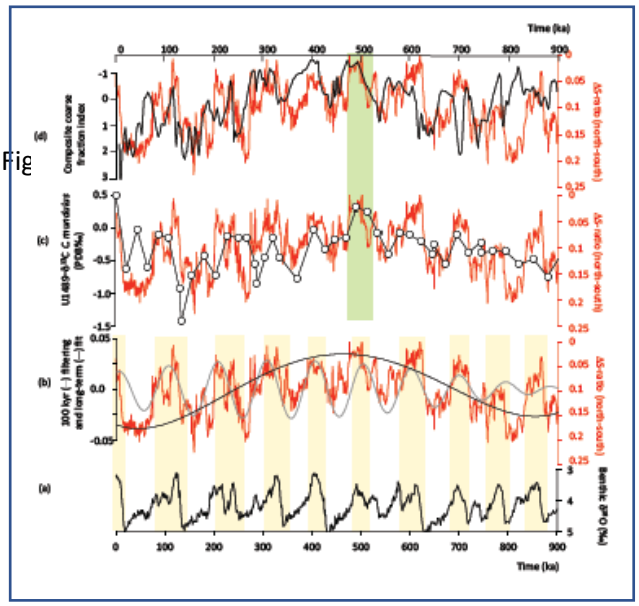

Fig. 1. The ΔS-ratio between the north and the south is reported in (b) with the 100 kyr filtering and long-term polynomial fit (grey and black curves, respectively). The LR04 stack is given as a guide for the climatic stages in (a). The same ΔS-ratio is compared in (c) to the benthic δ13C record from the western equatorial Pacific (Dang et al., 2020) and in (d) to the coarse fraction index produced by Bassinot et al. (1994). The green rectangle is for the δ13C max II coinciding with the lowest carbonate dissolution and the lowest ΔS-ratio, all illustrating enhanced deep-sea circulation.

An open-source database for the synthesis of soil radiocarbon data: International Soil Radiocarbon Database (ISRaD) version 1.0

Lawrence C.R., et al… including Hatté C.

Earth System Science Data (2020), 12, 61-76 – doi: 10.519/essd-12-61-2020

Radiocarbon is a critical constraint on our estimates of the timescales of soil carbon cycling that can aid in identifying mechanisms of carbon stabilization and destabilization and improve the forecast of soil carbon response to management or environmental change. Despite the wealth of soil radiocarbon data that have been reported over the past 75 years, the ability to apply these data to global-scale questions is limited by our capacity to synthesize and compare measurements generated using a variety of methods. Here, we present the International
Soil Radiocarbon Database (ISRaD[1]), an open-source archive of soil data that include reported measurements from bulk soils, distinct soil carbon pools isolated in the laboratory by a variety of soil fractionation methods, samples of soil gas or water collected interstitially from within an intact soil profile, CO_2 gas isolated from laboratory soil incubations, and fluxes collected in situ from a soil profile. The core of ISRaD is a relational database structured around individual datasets (entries) and organized hierarchically to report soil radiocarbon data, measured at different physical and temporal scales as well as other soil or environmental properties that may also be measured and may assist with interpretation and context. Anyone may contribute their own data to the database by entering it into the ISRaD template and subjecting it to quality assurance protocols. ISRaD can be accessed through (1) a web-based interface, (2) an R package (ISRaD), or (3) direct access to code and data through the GitHub repository, which hosts both code and data. The design of ISRaD allows for participants to become directly involved in the management, design, and application of ISRaD data. The synthesized dataset is available in two forms: the original data as reported by the authors of the datasets and an enhanced dataset that includes ancillary geospatial data calculated within the ISRaD framework. ISRaD also provides data management tools in the ISRaD-R package that provide a starting point for data analysis; as an open-source project, the broader soil community is invited and encouraged to add data, tools, and ideas for improvement. As a whole, ISRaD provides resources to aid our evaluation of soil dynamics across a range of spatial and temporal scales. The ISRaD v1.0 dataset is archived and freely available at https://doi.org/10.5281/zenodo.2613911 (Lawrence et al., 2019).

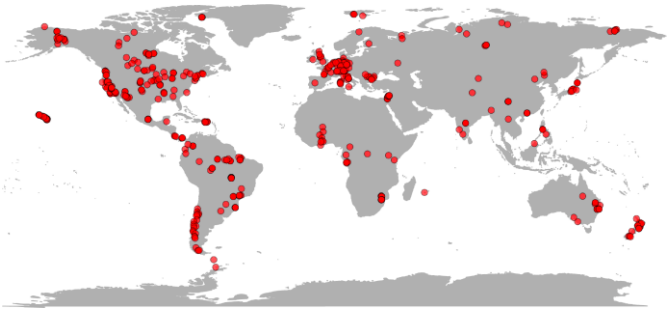

Fig. 1. Geographic location of sites currently included in ISRaD v1.0. Circles that appear darker in color indicate multiple overlapping sites at the resolution of the map.

[1] http://soilradiocarbon.org, last access: 16 December 2019

A 4.5 year-long record of Svalbard water vapor isotopic composition documents winter air mass origin

Leroy-Dos Santos, C., Masson-Delmotte, V., Casado, M., Fourré, E., Steen-Larsen, H., Maturilli, M., Orsi, A., Berchet, A., Cattani, O., Minster, B., Gherardi, J., and Landais, A.

Journal of Geophysical Reearch, doi.org/10.1029/2020JD032681

From May 2014 to September 2018, a laser spectrometer analyzer provided a 4.5 years continuous record of water vapor isotopic composition at Ny-Ålesund (8 m a.s.l.), Svalbard. It corresponds to the longest dataset published in polar regions. A comparison of this dataset with a parallel similar dataset obtained during 20 days by a second laser spectrometer installed at the near Mount Zeppelin (474 m a.s.l.) shows that this dataset is representative of a regional signal. In addition, the observation of insignificant diurnal cycles in the isotopic signal compared to the strong isotopic signature of synoptic events and the comparison of simultaneous measurements in the vapor and in rain or snow samples lead to the conclusion that our record reflects a large part of the regional dynamics of the atmospheric water cycle driven by large scale variability. This study focuses on winters dominated by the occurrence of synoptic events associated with humidity peaks. Using statistics and back-trajectories calculations, we link high humidity peaks characterized by an anti-correlation between δ18O and d-excess in the water vapor to a rapid shift of air mass source regions from the Arctic to the North Atlantic Ocean below 60°N. On the other hand, correlation between δ18O and d-excess may be associated with a shift of air mass sources within the Arctic. These results demonstrate the added value of long-term water vapor isotopic monitoring to better understand the moisture origin in the Arctic and the atmospheric dynamics.

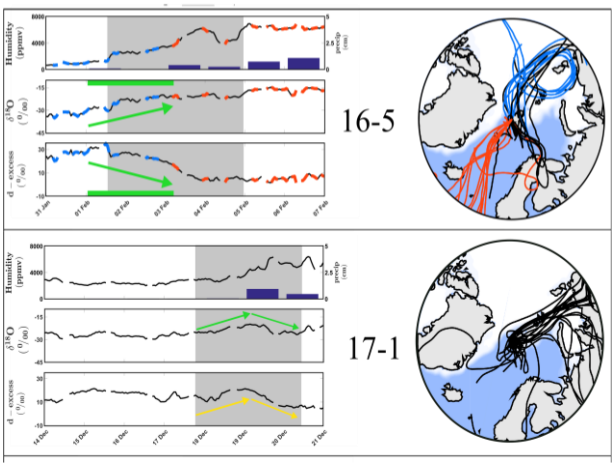

Fig. 1. Examples of typical winter humidity peak events (grey). The left panels display the humidity, precipitation, $\delta^{18}O$ and d-excess records over 7 days. The right panels display the associated 5 days back-trajectories computed with Hysplit. During event 16-5, a clear anticorrelation between $\delta^{18}O$ and d-excess is associated to a shift of air origin from the Arctic to the Atlantic sector. On the contrary, an event like 17-1 displays no isotopic anti-correlation while the origin of air parcels remains within the Northern sector

Climate variability during MIS20-18 as recorded by alkenone-SST and calcareous plankton in the Ionian basin (central Mediterranean)

Marino, M., Girone, A., Gallicchio, S., Herbert, T., Addante, M., Bazzicalupo, P., Quivelli, O., Bassinot, F., Bertini, A., Nomade, S., Ciaranfi, N., and Maiorano, P.

Palaeogeography, Palaeoclimatology, Palaeocology 560 110027 (2020)

This study shows the first Mediterranean high-resolution record of alkenone-derived sea surface temperature (SST) in the marine sediments outcropping at the Ideale section (IS) (southern Italy, central Mediterranean) from late marine isotope stage (MIS) 20 - through early MIS 18. The SST pattern evidences glacial-interglacial up to submillennial-scale temperature variation, with lower values (~13 °C) in late MIS 20 and substage 19b, and higher values (up to 21 °C) in MIS 19c and in the interstadials of MIS 19a. The SST data are combined with the new calcareous plankton analysis and the available, chronologically well-constrained carbon and oxygen isotope records in the IS. The combined proxies reveal the occurrence of a terminal stadial event in late MIS 20 (here Med-HTIX), and warm-cold episodes (here Med-BATIX and Med-YDTIX) during Termination IX (TIX), which recall those that occurred through the last termination (TI). During these periods and the following ghost sapropel layer (insolation cycle 74, 784 ka) in the early MIS 19, high frequency internal changes are synchronously recorded by all proxies. The substage MIS 19c is warm but quite unstable (Fig. 1), with several episodes of paleoenvironmental changes, associated with fluctuating tropical-subtropical water inflow through the Gibraltar Strait, variations of the cyclonic regime in the Ionian basin, and the southward shift of westerly winds and winter precipitation over southern Europe and Mediterranean basin.

Three high-amplitude millennial-scale oscillations in the patterns of SST and calcareous plankton key taxa during MIS 19a are interpreted as linked to changes in temperature as well as in salinity due to periodical water column stratification and mixing. The main processes involved in the climate variability include changes in oceanographic exchanges through the Gibraltar Strait during modulations of Atlantic meridional overturning circulation and/or variations in atmospheric dynamics related to the influence of westerly and polar winds acting in the paleo-Ionian basin. A strong climate teleconnection between the North Atlantic and Mediterranean is discussed, and a prominent role of atmospheric processes in the central Mediterranean is evidenced by comparing data sets at the IS with Italian and extra-Mediterranean marine and terrestrial records.

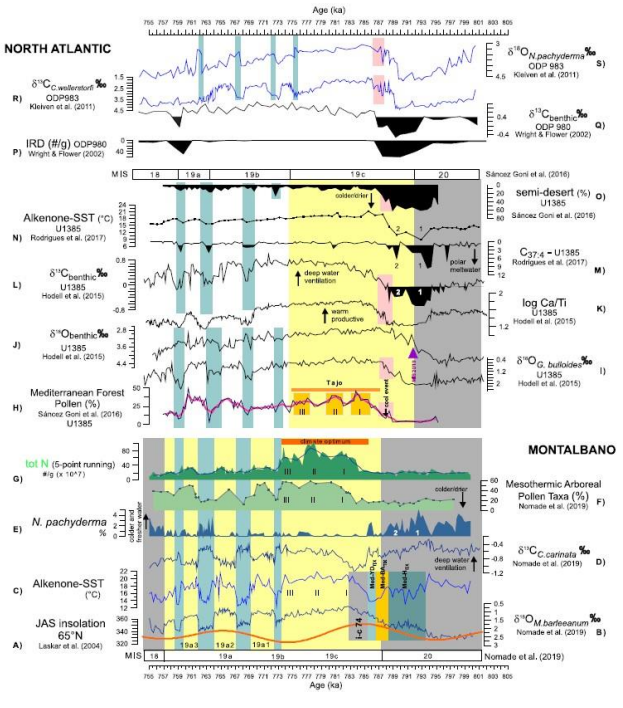

Fig. 1: Synthesis of Montalbano results (A to G) compared to Iberian margin U1385 record (H to O) and Northern Atlantic ODP 983 and 980 records (P to S).

From “source to sink” – A new perspective on the past dynamics of the T Murray Canyon Group from benthic foraminiferal communities

Mojtahid, M., Michel, E., and De Deckker, P.

Marine Micropaleontology (2020) Vol.160, doi.org/10.1016/j.marmicro.2020.101877

We present fossil benthic foraminiferal assemblage data from marine sediment core SS02/06-GC2 located in the abyssal plain of the Murray Canyon Group (offshore South Australia). The sedimentological characteristics in- dicate the presence of turbidite deposits showing classical Bouma-like sequences, dated between ~40 and 12 cal ka BP. These results confirm the previous interpretation of the observed large deep-water holes in the abyssal area where the core was sampled as being gouged by surges of high-energy turbidity currents. The presence of good indicator taxa and unique assemblages occupying specific bathymetric depths allows the de- termination of the source origin of the sediments making the turbidites. Three distinct faunal groups are found: 1) mostly shelf species, 2) mostly bathyal species and 3) mostly abyssal species. In the sediment core, these groups present a quasi-systematic succession, with nearly all Bouma-like sequences starting with the dominance of bathyal species in the coarse-grained base, followed by the dominance of shallow species in the silty part, and finally with abyssal species in the clays. To explain such phenomena, turbidites triggered by mixed hyperpycnal/ hypopycnal flow processes and turbidity currents during periods of river floods are considered for the first time within the Murray Canyon Group. They are mostly related to periods of increased fluvial discharges during wet phases in the Murray-Darling Basin.

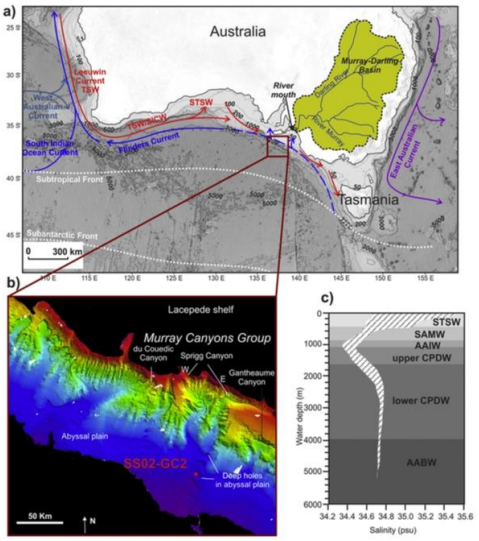

Fig. 1. a) Map showing the location of the study area, the outlet of one of Australia's largest river systems, the Murray–Darling and the main currents and water masses b) 3-D morphobathymetric map of the Murray Canyon Group (Hill and De Deckker, 2004) with the position of the study core SS02/06-GC2 in one of the deep holes of the abyssal plain.

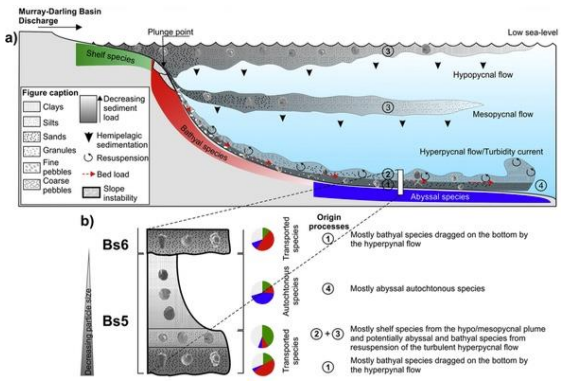

Fig. 2. Interpretative summary scheme of the hydro-sedimentary processes leading the deposition of the Bouma-like sequences in core SS2-CG2.

The origin of early Acheulean expansion in Europe 700 ka ago: new findings at Notarchirico (Italy)

Moncel, M.-H., Biddittu, I., Manzi, G., Saracino, B., Pereira, A., Nomade, S., Hertler, C., Voinchet, P., and Bahain, J.-J.

Scientific reports https://doi.org/10.1038/s41598-020-68617-8 (2020)

Notarchirico (Southern Italy) has yielded the earliest evidence of Acheulean settlement in Italy and four older occupation levels have recently been unearthed, including one with bifaces, extendingthe roots of the Acheulean in Italy even further back in time.
New 40Ar/39Ar on tephras and ESR dates on bleached quartz securely and accurately place these occupations between 695 and 670 ka (MIS 17, Fig. 1), penecontemporaneous with the Moulin-Quignon and la Noira sites (France).

These new data demonstrate a very rapid expansion of shared traditions over Western Europe during a period of highly variable climatic conditions, including interglacial and glacial episodes, between 670 and 650 (i.e., MIS17/MIS16 transition). The diversity of tools and activities observed in these three sites (Fig. 2). shows that Western Europe was populated by adaptable hominins during this time These conclusions question the existence of refuge areas during intense glacial stages and raise questions concerning understudied migration pathways, such as the Sicilian route.

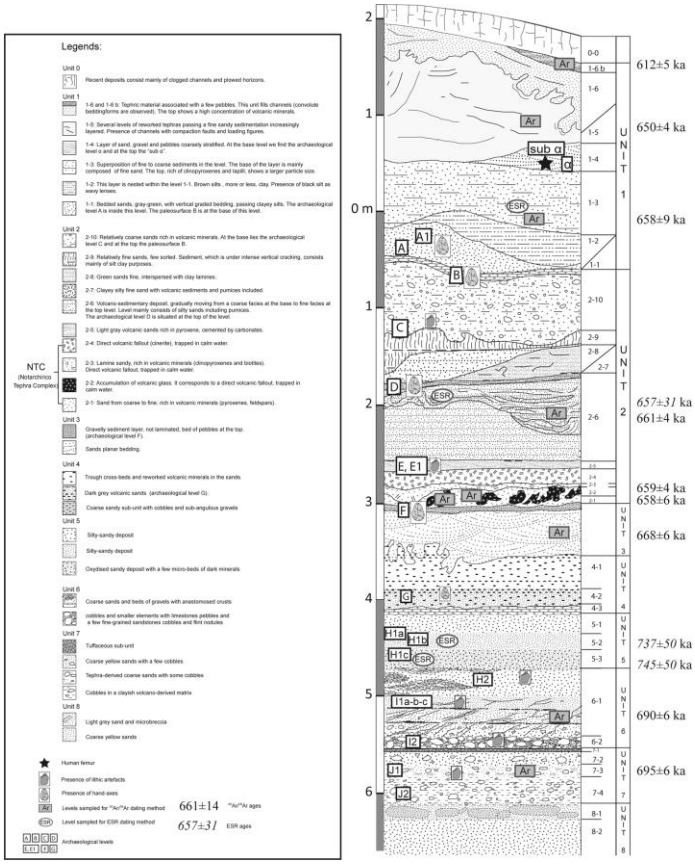

Fig.1 Stratigraphic log of the Notarchirico sequence (Modified from Raynal et al., 1999) with the 40Ar/39Ar and ESR dates.

Geochemical proxies in marine biogenic carbonates: New developments and applications to global change

Montagna P., Douville E.

Chemical Geology 533 (2020), 10.1016/j.chemgeo.2019.119411

This special issue of Chemical Geology comprises a selection of papers presented at the Goldschmidt Conference held in Paris in 2017 within the Session 10a Geochemical proxies in marine biogenic carbonates: new developments and applications to global change. The session brought together experts in carbonate biogeochemistry to discuss issues related to the potential of geochemical proxies to precisely quantify recent trends in acidification and/or warming of the surface, intermediate and deep oceans as well as to identify the limits of these proxies (e.g. calibration and analytical issues) and their application to understanding biomineralisation mechanisms. Special emphasis was placed on the role of biomineralisation processes in controlling the trace element and isotopic composition of marine carbonates and how they relate to ambient seawater conditions. The session started with the keynote given by Malcolm McCulloch from the University of Western Australia on Coral calcification in a changing world and the interactive dynamics of pH and DIC up-regulation, followed by the invited talk of Jonathan Erez from The Hebrew University on Light enhanced calcification in corals, foraminifera and clams and their implications for carbon isotopes in their shells, and 9 oral presentations. The session continued in the afternoon with the second invited talk given by Henry Wu from LOCEAN and LSCE (France) on 320 years of modern sea surface pH and SST variability in the South Pacific from coral proxy records, followed by 11 oral presentations and 16 posters. The 8 contributions of this special issue deal with the main topics presented and discussed during the Conference session, with a specific focus on the geochemistry of the mineralised portions of benthic and planktonic foraminifera, scleractinian and gorgonian corals, bivalves, and brachiopods.

All of the contributions in this special issue apply micro-analytical techniques to investigate the fine scale geochemical composition of the biogenic carbonates to: 1) provide a better understanding of the bio-mineralisation processes, and/or 2) select the most promising portion of the skeleton/shell/test for paleoceanographic studies. There is also a common approach using modern material to relate geochemical signals to ambient environmental parameters, which attempts to deconvolve the biological factors and the various environmental parameters that overprint the geochemical signals, as also recently suggested by D'Olivo et al. (2019). This will eventually lead to properly quantifying the uncertainties of geochemical proxies and greater confidence in paleoceanographic reconstructions. It is important that future investigations integrate both geochemistry and biology to gain a holistic understanding of the biomineralisation processes, which is necessary for fully exploiting biogenic carbonates as reliable archives of ocean conditions through time. A better understanding of the influence of the skeletal/shell microstructures on the geochemistry and proxy-based reconstructions requires a multi-disciplinary approach that combines newly-developed nano-micro-sampling capabilities (e.g. NanoSIMS, synchrotron-based X-ray fluorescence or femto laser ICP-MS) with specific morphological-petrographic-mineralogical techniques that can also be applied at microscale (e.g. mRaman, CT "micro"-tomography), laboratory and/or field calibration exercises, biomineralisation models and the integration of multiple proxies.

A Large Paleoearthquake in the Central Apennines, Italy, Recorded by the Collapse of a Cave Speleothem

Pace B., Valentini A. , Ferranti L., Vasta M., Vassallo M. , Montagna P., Colella A., Pons-Branchu E.

Tectonics - 10.1029/2020TC006289 - doi.org/10.1029/2020TC006289

Speleoseismological research carried out in the Central Apennines (Italy) contributed to understanding the behavior of active normal faults that are potentially able to generate Mw 6.5–7 earthquakes documented by paleoseismology and by historical and instrumental seismology. Radiometric (U-Th, AMS-14C, and bulk-14C) dating of predeformation and postdeformation layers from collapsed speleothems found in Cola Cave indicates that at least three speleoseismic events occurred in the cave during the last ~12.5 ka and were ostensibly caused by seismic slip on one or more of the active faults located in the region surrounding the cave. We modeled the collapse of a tall (173 cm high) stalagmite to find a causative association of this event with one among the potential seismogenic sources. We defined the uniform hazard spectrum (UHS) for each seismogenic source at the site, and we used the calculated spectra in a deterministic approach to study the behavior of the speleothem, through a numerical finite element modeling (FEM). Although our analysis suggests the "Liri" fault as the most likely source responsible for the ground shaking recorded in the cave, the "Fucino" fault system, responsible for a Mw 7 earthquake in 1915, cannot be excluded as a potential source of speleoseismic damage. Results of this work provide new constraints on the seismotectonic history of this sector of Central Apennines and highlight the performance of integrated speleoseismological, seismic hazard, and numerical studies.

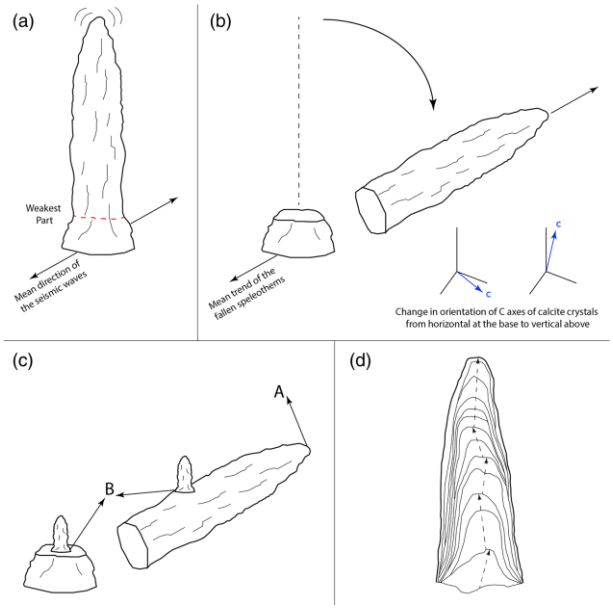

Fig. : seismic record in speleothems. (a) oscillation of the speleothem due to the passage of the seismic waves. (b) Speleothem breaks in the weakest part, (c) After the collapse, new speleothems grow on top of the base and the fallen part of the broken speleothem. Dating the tip of the fallen part (A) and the base of the new speleothems (B) help to constrain the age of the collapse. (d) If the speleothem is not vulnerable enough, instead of collapsing, it could change its growth axis. In this case, the evidences of earthquakes are in the inner structure of it.

La datation des archives glaciaires

Parrenin, F., et Landais, A.

La Météorologie, n° 110, Août 2020

Les glaces en Antarctique et au Groenland sont une archive de premier plan pour reconstruire le climat du Quaternaire. Une datation précise est nécessaire pour exploiter cette archive. Les méthodes de datation peuvent être tirées de l'analyse de la glace, des bulles d'air piégées, de la comparaison à d'autres archives ou aux variations des paramètres orbitaux de la Terre, ou de la modélisation du processus de sédimentation glaciaire. Ces méthodes étant complémentaires, un modèle probabiliste a été développé pour les combiner de manière optimale.

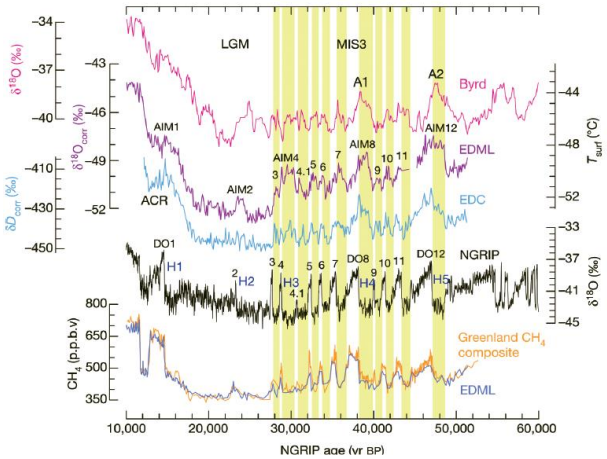

Figure: Synchronisation méthane et explication de la bascule bipolaire. Les trois courbes en haut représentent les variations isotopiques de la glace enregistrées dans trois forages antarctiques : Byrd, EDML et EDC. La courbe en noir au milieu représente les variations isotopiques de la glace au Groenland à partir du forage NGRIP. Les deux courbes du bas représentent le méthane enregistré au Groenland et à EDML qui a permis la synchronisation. La bascule bipolaire décrit le fait que, sur la variabilité millénaire à centennale de la dernière période glaciaire, l'Antarctique se réchauffe (respectivement se refroidit) pendant les phases froides (respectivement chaudes) du Groenland.

^{13}C-^{14}C relations reveal that soil ^{13}C-depth gradient is linked to historical changes in vegetation ^{13}C

Paul A., Balesdent J, Hatté C.

Plant Soil (2020), 447, 305-317 – doi: 10.1007/s11104-019-04384-4

Aims The understanding of the dynamics of subsoil (>30 cm) soil organic matter (SOM) is critical to predict the future evolution of the carbon cycle. Stable carbon isotopes ratios ($^{13}C/^{12}C$) are helpful to study the dynamics of SOM, but their variations with depth are still speculative.

Methods Several studies indicated that the $^{13}C/^{12}C$ ratio of C3 vegetation decreased over time more than that of atmospheric CO2 did. From these studies, we modelled the average variation of $\delta^{13}C$ values of vegetation from 20,000 years Before Present (BP) to today. Then, we conducted a meta-analysis of the $\delta^{13}C$ vs $\Delta^{14}C$ values relations in forty-five soil profiles sampled all around the world. *Results* We first found evidence of the change in SOM $\delta^{13}C$ values with the sampling year of the profile. Then, by converting $\Delta^{14}C$ values into mean calendar age of SOM, we showed that 40% of the change in SOM $\delta^{13}C$ values was explained by the historical change in plant $\delta^{13}C$ values.

Conclusion We conclude that the average increase of SOM $\delta^{13}C$ values with depth was mostly linked to the change in vegetation $\delta^{13}C$ values over the last 20,000 years. The variance around the trend was attributed to the contribution of root derived carbon and to soil processes such as interaction of SOM with minerals or to microbial processes.

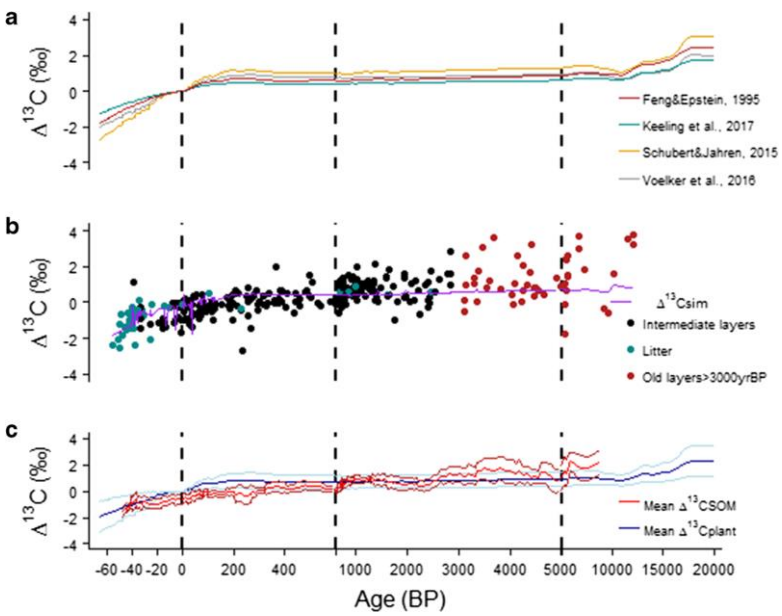

Figure: a. Reconstruction of $\Delta^{13}C_{plant}$ values from 20,000 BP to today from 4 different studies. b. $\delta^{13}C_{SOM}$ values as a function of mean calendar age of each SOM sample and calculated $\delta^{13}C_{sim}$. The age was inferred from $\Delta^{14}C_{SOM}$ and sampling date. Mean values of $\Delta^{13}C_{plant}$ and $\Delta^{13}C_{SOM}$ (moving average of 10 points). The light-blue lines represent two standard errors of the estimated mean value $\Delta^{13}C_{plant}$ from the four scenarios; it does not take into account the error of each individual scenario. The light-red lines represent the confidence interval of the mean value $\Delta^{13}C_{SOM}$ (95%). Note that the x axis is divided into 4 scales.

Tephrochronology of the central Mediterranean MIS11c interglacial (~425-395 ka): new constraints from the Vco volcano and Tiber delta, central Italy

Pereira, A., Monaco, L., Marra, F., Nomade, S., Gaeta, M., Leicher, N., Palladino, D., Sottili, G., Guillou, H., Scao, V., and Giaccio, B.

Quaternary Science Reviews **243, 106470 (2020)**

Through a systematic integrated approach, which combined lithostratigraphic, geochronological and geochemical analyses of tephra from near-source sections of the peri-Tyrrhenian volcanoes and mid to distal settings, here we provide an improved tephrochronological framework for the Marine Isotope Stage 11c interglacial (MIS 11c, 425-395 ka) in the Central Mediterranean area. Specifically, we present the complete geochemical dataset and new high-precision 40Ar/39Ar ages of the previously poorly characterized earliest pyroclastic products of the Vico volcano (420-400 ka, Fig. 1).

Five pyroclastic units were recognized in Vico volcanic area, four out of which, Vico α, Vico β, Vico β top (a minor eruption immediately following Vico β and temporally very close to it) and Vico d were directly dated at 414.8 ± 2.2 ka, 406.5 ± 2.4 ka, 406.4 ± 2.0 ka and 399.7 ± 3.2 ka respectively (2σ analytical uncertainties).

These new data allow a critical reappraisal of the previously claimed identifications of Vico tephra from mid-distal to ultra-distal successions (i.e., Vico-Sabatini volcanic districts, Roman San Paolo Formation and Castel di Guido archaeological site, Sulmona Basin, Valdarno and Lake Ohrid), which were unavoidably biased by the poor and incomplete geochemical and geochronological reference datasets previously available (Fig. 2).

Such an improvement of the tephrochronological framework brings great benefits to any future investigations (e.g., paleoclimatology, archaeology, active tectonic, volcanology) in the dispersal areas of the studied eruptions at the key point in time that is MIS 11.

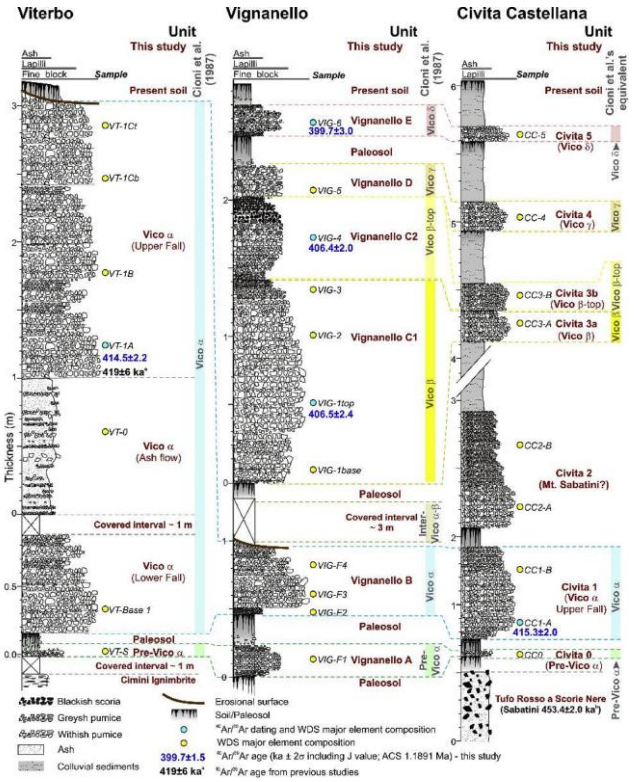

Fig. 1 Stratigraphic successions of the Vico α and Vico β sections including the Plinian eruptions of Vico α and Vico β and the immediately post-dating lower magnitude explosive events. Furthermore, we also provide new geochronological and geochemical data for the distal tephra layers preserved in the aggradational succession of the Tiber delta (San Paolo Formation), Roman area, which records sea level rise relating to the MIS 12 (glacial) to MIS 11 (interglacial) transition.

The Tara Pacific expedition—A pan-ecosystemic approach of the "-omics" complexity of coral reef holobionts across the Pacific Ocean

Planes S., Allemand D., Agostini S., Banaigs B., Boissin E., Boss E., Bourdin G., Bowler C., Douville E., … & The Tara Pacific Consortium

PLoS Biol 17(9): e3000483. https://doi.org/10.1371/journal.pbio.3000483

Coral reefs are the most diverse habitats in the marine realm. Their productivity, structural complexity, and biodiversity critically depend on ecosystem services provided by corals that are threatened because of climate change effects—in particular, ocean warming and acidification. The coral holobiont is composed of the coral animal host, endosymbiotic dinoflagellates, associated viruses, bacteria, and other microeukaryotes. In particular, the mandatory photosymbiosis with microalgae of the family Symbiodiniaceae and its consequences on the evolution, physiology, and stress resilience of the coral holobiont have yet to be fully elucidated. The functioning of the holobiont as a whole is largely unknown, although bacteria and viruses are presumed to play roles in metabolic interactions, immunity, and stress tolerance. In the context of climate change and anthropogenic threats on coral reef ecosystems, the *Tara* Pacific project aims to provide a baseline of the "-omics" complexity of the coral holobiont and its ecosystem across the Pacific Ocean and for various oceanographically distinct defined areas. Inspired by the previous *Tara* Oceans expeditions, the *Tara* Pacific expedition (2016–2018) has applied a pan-ecosystemic approach on coral reefs throughout the Pacific Ocean (Fig. 1) sampling corals throughout 32 island systems with local replicates. *Tara* Pacific has developed and applied state-of-the-art technologies in very-high-throughput genetic sequencing and molecular analysis to reveal the entire microbial and chemical diversity as well as functional traits associated with coral holobionts, together with various measures on environmental forcing. This ambitious project aims at revealing a massive amount of novel biodiversity, shedding light on the complex links between genomes, transcriptomes, metabolomes, organisms, and ecosystem functions in coral reefs and providing a reference of the biological state of modern coral reefs in the Anthropocene.

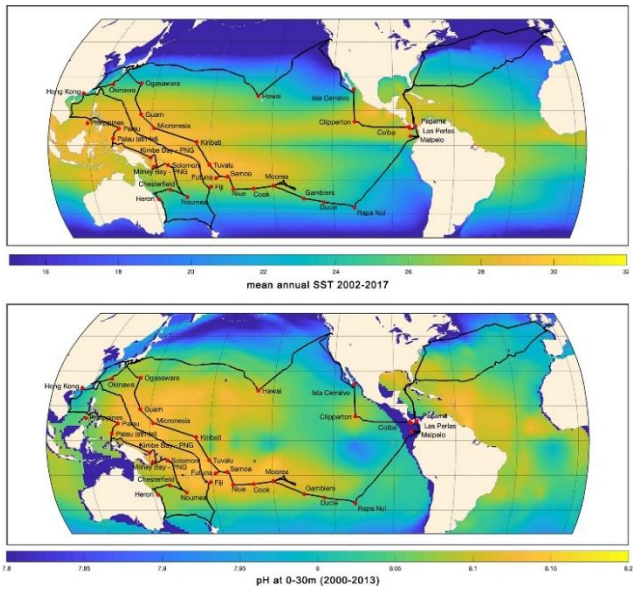

Fig. 1. Map showing the route of the Tara Pacific expedition and the sampling sites (red spots)

U-series dating at Nerja cave reveal open system. Questioning the Neanderthal origin of Spanish rock art

Pons-Branchu E., Sanchidrian JL., Fontugne M., Medina-Alcaide MA, Quiles A., Thil F., Valladas H.

Journal of Archaeological Science. (2020) 117, 105120. doi. org/10.1016/j.jas.2020.105120. Project: ANR ApART

Des fins voiles de carbonate secondaires recouvrant des parois ornées de grottes préhistoriques (gravures ou dessins) ou leur servant de support sont utilisés pour donner l'âge relatif de ces œuvres. Nous montrons par l'étude d'échantillons prélevés dans la grotte de Nerja (Andalousie, Espagne) que les datations par la méthode uranium thorium (U/Th) présentent dans certains cas un biais due à la mobilisation de radionucléides (perte d'uranium), faisant paraitre plus vieux les échantillons par rapport à leur âge réel. Ce cas d'étude permet de discuter des publications récentes de datations U/Th de voiles de calcite qui suggèrent des âges beaucoup plus vieux que ce qui était admis jusque-là pour l'Art pariétal préhistorique, avec des peintures attribuées à l'homme de Neandertal.

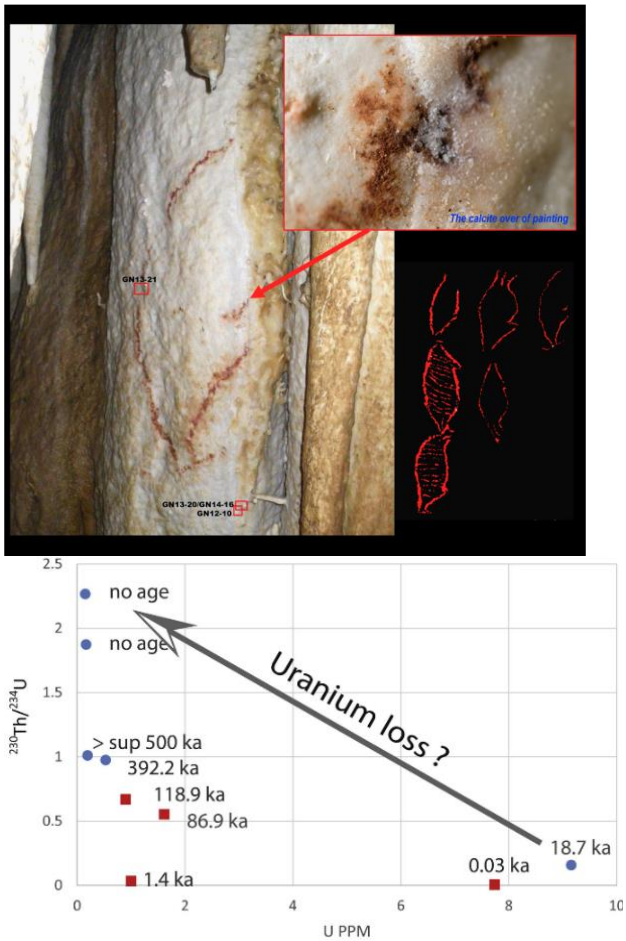

Figure: en haut, Paroi Ornée de la grotte de Nerja, avec dessin partiellement recouvert de voile de $CaCO_3$: (« panneau des pisciformes»). En bas : rapports $^{230}Th/^{234}U$ (liés aux âges) en fonction des teneurs en uranium. On note ici une tendance avec des teneurs en uranium plus faibles pour les échantillons présentant les plus forts rapports (donc les âges les plus élevés) suggérant un possible lessivage de l'uranium et un biais sur les âges.

Overturning circulation, nutrient limitation, and warming in the Glacial North Pacific

Rae, J., Gray, W., Wills, R., Eisenman, I., Fitzhugh, B., Fotheringham, M., Littley, E., Rafter, P., ReesOwen, R., Ridgwell, A., Taylor, B., and Burke, A.

Science Advances, 6(50):eabd1654, December 2020. doi: 10.1126/sciadv.abd1654.

Although the Pacific Ocean is a major reservoir of heat and CO_2, and thus an important component of the global climate system, its circulation under different climatic conditions is poorly understood. Here, we present evidence that during the Last Glacial Maximum (LGM), the North Pacific was better ventilated at intermediate depths and had surface waters with lower nutrients, higher salinity, and warmer temperatures compared to today. Modeling shows that this pattern is well explained by enhanced Pacific meridional overturning circulation (PMOC), which brings warm, salty, and nutrient-poor subtropical waters to high latitudes, analogous to the circulation of the glacial North Atlantic. Enhanced PMOC at the LGM lowers atmospheric CO_2—in part through synergy with the Southern Ocean—and supports an equable regional climate, which may have aided human habitability in Beringia, and migration from Asia to North America.

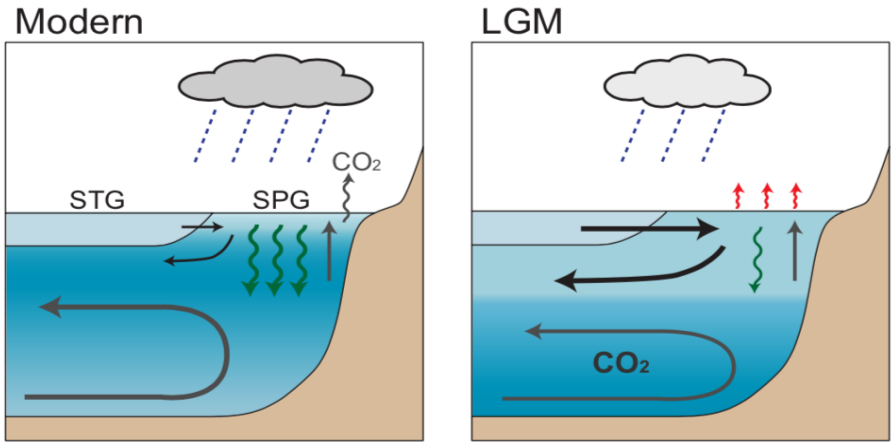

The modern North Pacific (left) lacks vigorous local ventilation, because of low salinity in surface waters of the subpolar gyre (SPG). This is a result of high net precipitation (P-E) and minimal exchange with the saltier waters of the subtropical gyre (STG). The modern subpolar North Pacific is thus dominated by upwelling of nutrient- and CO2-rich subsurface waters, driving relatively high export productivity and CO2 outgassing. During the LGM (right), our data compilation suggests that ventilation at intermediate depths was enhanced, export productivity was reduced, and subpolar surface waters were saltier and warmer. This is consistent with an invigorated meridional overturning circulation, with enhanced formation of intermediate waters and advection of warm, salty, and nutrient-depleted subtropical waters to high latitudes, analogous to a shallower version of the overturning circulation seen in the modern North Atlantic.

Les sédiments des deltas contribuent-ils à l'absorption du CO_2 atmosphérique ?

Rassmann, J., Eitel, E., Lansard, B., Cathalot, C., Brandily, C., Taillefert, M., and Rabouille, C.

Biogeosciences (2020), vol. 17, 13-33, https://www.biogeosciences.net/17/13/2020/

L'alcalinité d'une eau, c'est-à-dire sa capacité à neutraliser les acides, est une grandeur utile pour l'étude du cycle du carbone dans les milieux aquatiques, par exemple les estuaires et les deltas. En effet, le CO_2, qui est le principal responsable du réchauffement climatique, est aussi un acide faible lorsqu'il est dissous dans l'eau. Le CO_2 peut donc être neutralisé par l'alcalinité de l'eau et, dans certaines conditions, quitter définitivement l'atmosphère et ainsi limiter l'effet de serre. Dans les conditions de réchauffement planétaire largement dû au CO_2, il est donc essentiel de connaître toutes les sources d'alcalinité et d'en comprendre le fonctionnement.

Dans cette étude, nous avons mesuré les sources d'alcalinité venant des sédiments marins du prodelta du Rhône (de 20 à 75 m de profondeur) et contraint les processus dans la colonne sédimentaire qui génèrent cette alcalinité. En effet, les sédiments échangent des éléments chimiques avec les eaux océaniques par le biais de la diffusion et des transferts provoqués par l'activité biologique. Ces flux totaux ont été mesurés lors de la mission océanographique AMOR-B-Flux que nous avons menée conjointement avec le Georgia Institute of Technology en Septembre 2015 dans le cadre du projet ANR-AMORAD et du programme national de l'INSU MISTRAL-MERMEX.

Lors de cette mission, nous avons déployé une chambre benthique autonome apportée par Georgia Tech afin d'incuber les sédiments pendant 10-12h et quantifier les flux d'échanges *in situ*. Les flux d'alcalinité (TA) et de CO_2, sous la forme de carbone inorganique dissous (DIC), sont très importants dans la zone proximale, la plus proche du Rhône (≈ 50 mmol m^{-2} d^{-1}), et sont beaucoup plus faibles sur le plateau continental (4 mmol m^{-2} d^{-1}). Les sédiments du delta du Rhône, et plus particulièrement ceux de la zone proximale (stations Z et A), sont donc des sources d'alcalinité pour les eaux côtières.

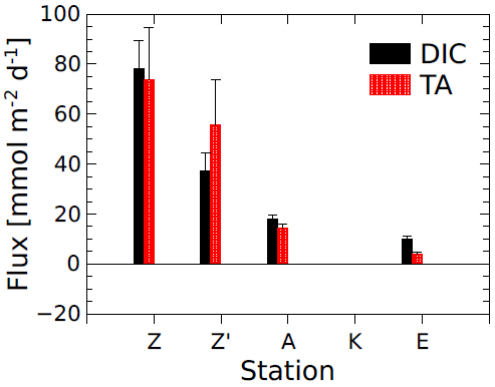

Fig. 1. Flux d'alcalinité (TA) et de carbone inorganique dissous (DIC) mesurés avec la chambre benthique in situ de Georgia Tech dans la zone proximale (A, Z) et sur le plateau continental (E). Les flux positifs indiquent des flux allant du sédiment vers la colonne d'eau.

En utilisant d'autres techniques de mesures *in situ* à l'aide d'électrodes, ainsi que des prélèvement sous-échantillonnés en atmosphère inerte à bord du navire puis analysés au laboratoire, nous avons pu mettre en évidence le mécanisme responsable de ces flux importants d'alcalinité hors des sédiments du prodelta : la précipitation d'une phase de sulfure de fer dans la partie réduite des sédiments (>20cm) et sa préservation dans les sédiments plus profonds. Au contraire, dans les sédiments plus oxydés du plateau continental, ces mécanismes sont très faibles et ne contribuent que marginalement au flux d'alcalinité.

L'impact que peut avoir ce flux d'alcalinité sur la captation de CO_2 du milieu côtier dépend du rapport entre le flux d'alcalinité (TA) et le relargage de carbone inorganique dissous (DIC). On voit sur la Fig. 2 que ce rapport est proche de 1 pour les sédiments du delta (profondeur de 20 m), plus élevé que la plupart des zones côtières, ce qui indique un rôle non négligeable dans le bilan local de carbone.

The Middle to Upper Palaeolithic transition in Hohlenstein-Stadel cave (Swabian Jura, Germany): A comparison between ESR, U-series and radiocarbon dating

Richard, M., C. Falgueres, C., Pons-Branchu, E., Richter, D., Beutelspacher, T., Conard, N.J., Kindh, C.-J.

Quaternary International 556, -49-57. doi.org/10.1016/j.quaint.2019.04.009.

The Swabian Jura is a key region for the early Aurignacian. Sites such as Geisenklosterle, Hohle Fels, Vogelherd and Hohlenstein-Stadel have produced the earliest evidence of figurative and musical art, such as ivory figurines and flutes made of bone and ivory, attributed to *Homo sapiens*. To date, radiocarbon (14C) and thermoluminescence dating have been applied in the region, providing a precise chronology for the Upper Palaeolithic levels, especially the Aurignacian. At Hohlenstein-Stadel, Upper and late Middle Palaeolithic levels were dated using 14C. This study focuses on the chronology of the Middle Palaeolithic levels of this site using electron spin resonance (ESR) on herbivorous tooth enamel, in order to constrain the timing of the earliest human occupation at the cave, attributed to Neanderthals. An age was also obtained for the early Aurignacian level, allowing a comparison with available 14C ages. Furthermore, U-series dating was applied to three samples from a flowstone located at the base of the sequence, in order to provide a maximum age (*terminus post quem*) for the beginning of human occupation at the cave. ESR results obtained on the Middle Palaeolithic levels ranged from 40 +/- 5 ka to 35 + /- 3 ka (weighted mean ages), suggesting that these levels were deposited during a short period of time. The early Aurignacian level (Geological Horizon, GH, Au) was dated by ESR to 34 +/- 11 ka, in agreement with previously published 14C dates, despite a large error range due to the heterogeneity of the sedimentological environment. The flowstone overlying the oldest deposit at the base of the stratigraphy was dated to between 351 +/- 10 ka (MIS 10–9) and 229 +/- 10 ka (MIS 7), providing a maximum age for the deposits. These new chronological data confirm that Neanderthals occupied Hohlenstein-Stadel during MIS 3. Radiocarbon ages suggest that the replacement of Neanderthals by *Homo sapiens* occurred during a brief period of time, probably before or during Heinrich Stadial 4 (around 40–38 ka).

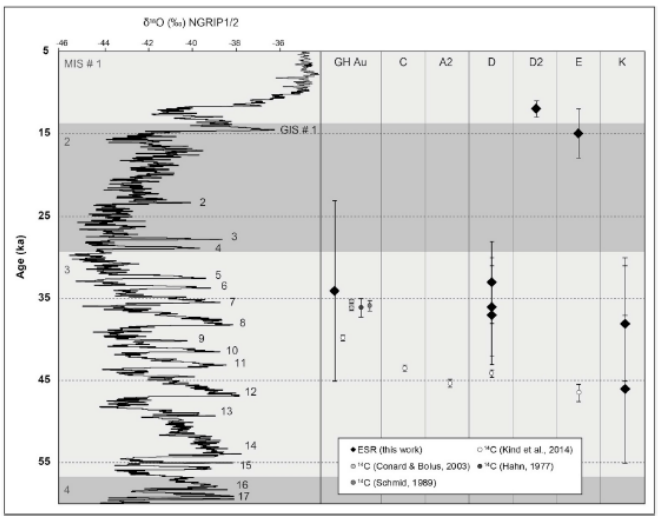

Illustration : Graphic representation of the ESR and 14C ages obtained for Hohlenstein-Stadel as a function of the δ18O variations (NGRIP data from Rasmussen et al., 2014). 14C ages are calibrated using IntCal13 (Reimer et al., 2013) and Oxcal 4.3 (Bronk Ramsey, 2009).

Dansgaard-Oeschger-like events of the penultimate climate cycle: the loess point of view

Rousseau D.D., et al… including Hatté C., Gauthier C.

Climate of the Past (2020), 16, 713-727 – doi: 10.5194/cp-16-713-2020

The global character of the millennial-scale climate variability associated with the Dansgaard–Oeschger (DO) events in Greenland has been well-established for the last glacial cycle. Mainly due to the sparsity of reliable data, however, the spatial coherence of corresponding variability during the penultimate cycle is less clear. New investigations of European loess records from Marine Isotope Stage (MIS) 6 reveal the occurrence of alternating loess intervals and paleosols (incipient soil horizons), similar to those from the last climatic cycle. These paleosols are correlated, based on their stratigraphical position and numbers as well as available optically stimulated luminescence (OSL) dates, with interstadials described in various Northern Hemisphere records and in GLt_syn, the synthetic 800 kyr record of Greenland ice core $\delta^{18}O$. Therefore, referring to the interstadials described in the record of the last climate cycle in European loess sequences, the four MIS 6 interstadials can confidently be interpreted as DO-like events of the penultimate climate cycle. Six more interstadials are identified from proxy measurements performed on the same interval, leading to a total of 10 interstadials with a DO-like event status. The statistical similarity between the millennial-scale loess–paleosol oscillations during the last and penultimate climate cycle provides direct empirical evidence that the cycles of the penultimate cycle are indeed of the same nature as the DO cycles originally discovered for the last glacial cycle. Our results thus imply that their underlying cause and global imprint were characteristic of at least the last two climate cycles.

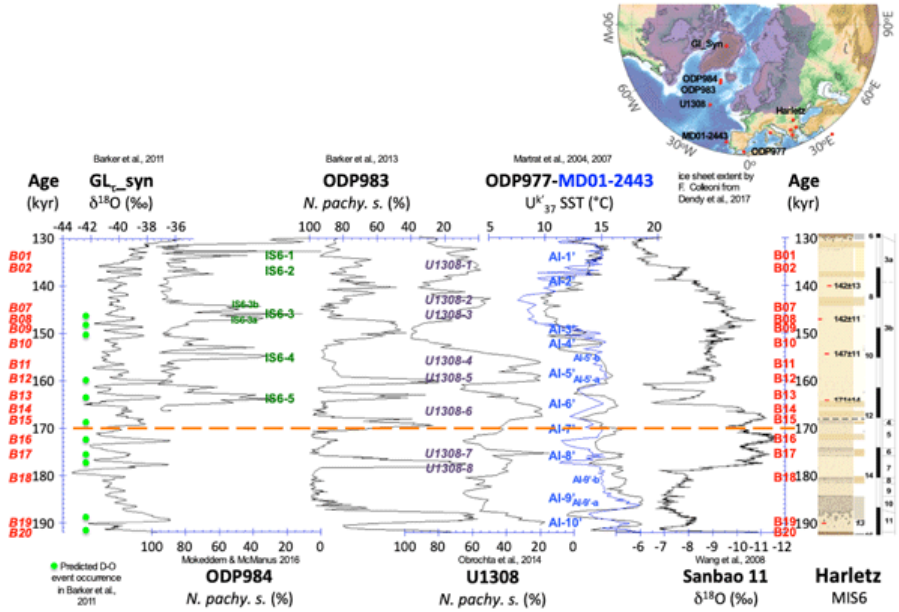

Figure: Western to eastern Mediterranean records of MIS 6 compared with summer insolation. The pedostratigraphy of the Harletz MIS 6 record is added with the newly described paleosols and pedogenic horizons for comparison. MIS 6 ice sheet extent by Florence Colleoni in Dendy et al. (2017.

Direct dating reveals the early history of opium poppy in western Europe

Salavert, A., Zazzo, A., Martin, L., Antolin, F., Gauthier, C., Thil, F., Tombret, O., Bouby, L., Manen, C., Mineo, M., Mueller-Bieniek, A., Piqué, R., Rottolli, M., Rovira Buendia, N., Toulemonde,F., and Vostrovska, I.

Scientific Reports (2020) 10:20263. https://doi.org/10.1038/s41598-020-76924-3

This paper aims to define the first chrono-cultural framework on the domestication and early diffusion of the opium poppy using small-sized botanical remains from archaeological sites, opening the way to directly date minute short-lived botanical samples. We produced the initial set of radiocarbon dates on *ECHo*MICADAS directly from the opium poppy remains of 11 Neolithic sites (5900–3500 cal BCE) in central and western Mediterranean, northwestern temperate Europe, and western Alps. When possible, we also dated the macrobotanical remains originating from the same sediment sample. In total, 22 samples were taken into account, including 12 dates directly obtained from opium poppy remains. The radiocarbon chronology ranges from 5622 to 4050 cal BCE. The results show that opium poppy is present from at least the middle of the sixth millennium in the Mediterranean, where it possibly grew naturally and was cultivated by pioneer Neolithic communities. Its dispersal outside of its native area was early, being found west of the Rhine in 5300–5200 cal BCE. It was introduced to the western Alps around 5000–4800 cal BCE, becoming widespread from the second half of the fifth millennium. This research evidences different rhythms in the introduction of opium poppy in western Europe.

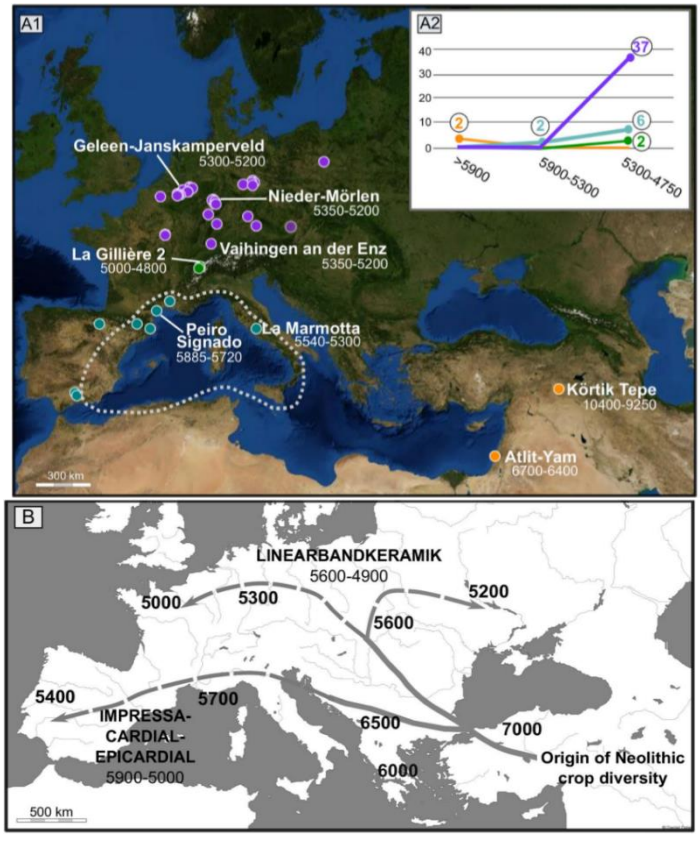

Figure 1 : (A1) Dataset of the Early Neolithic sites *where opium poppy remains have been identified with the locations of the earliest records in the Near East (orange circles), Mediterranean (blue circles), temperate Europe (purple circles), the western Alps (green circles), and current wild poppy populations (dotted line)11.* ***(A2) Number of Early Neolithic sites*** *where the plant is identified by chronological ranges corresponding to the period before the arrival of the first European farmers (< 5900 BCE); to the beginning of the Early Neolithic in the Mediterranean and temperate Europe (5900–5300 BCE); to the second stage of the LBK (LBK II–V) and the beginning of the Early Neolithic in the western Alps until the end of the period in western Europe (5300–4750 BCE).;* ***(B) Overview of the spatial and temporal framework for the diffusion of the "Neolithic crop package"*** *from the Near East to western Europe and the two European pioneer Neolithic complexes. The main chronological points are in cal BCE18. Contains*

Snowfall and Water Stable Isotope Variability in East Antarctica Controlled by Warm Synoptic Events

Servettaz, A., Orsi, A., Curran, M., Moy, A. D., Landais, A., Agosta, C., Holly L. Winton, V., Touzeau, A., McConnell, J. R., Werner, M., and Baroni, M.

Journal of Geophysical Research: Atmospheres, 125, e2020JD032863. https://doi.org/10.1029/2020JD032863

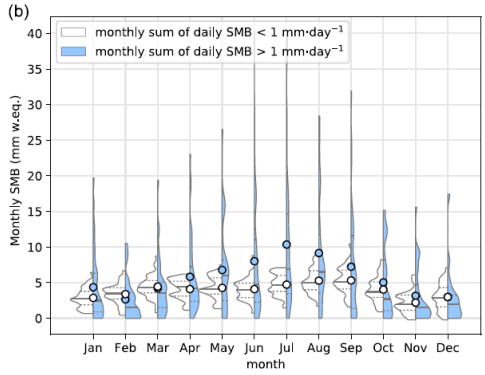

Figure 1. Probability density function of monthly SMB due to low (<1 mm w.eq. day−1, white) and high (>1 mm w.eq. day−1,blue) daily SMB rates. Mean (colored circles), median (plain lines), and quartiles(dashed lines) are indicated for each monthly distribution. Most of the variability is due to the presence or absence of large precipitation events.

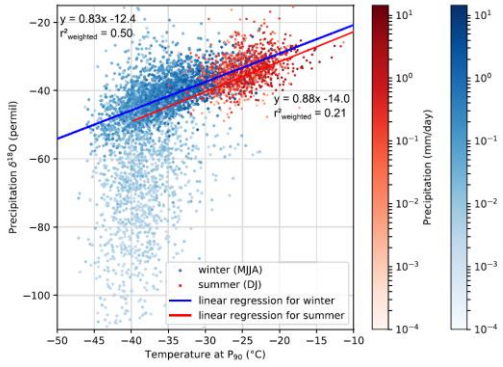

Figure 2. Scatter plot of daily δ18O in precipitation and temperature at P90 at the ABN grid point, for summer (December–January, red) and winter (May–August, blue). The color scales indicate the daily precipitation amount.

Understanding climate proxy records that preserve physical characteristics of past climate is a prerequisite to reconstruct long-term climatic conditions. Water stable isotope ratios (δ18O) constitute a widely used proxy in ice cores to reconstruct temperature and climate. However, the original climate signal is altered between the formation of precipitation and the ice, especially in low-accumulation areas such as the East Antarctic Plateau. Here, we characterize atmospheric conditions under which the isotopic signal is acquired at Aurora Basin North (ABN), East Antarctica. 50% of the snow is accumulated in less than 24 days per year (Fig. 1). Snowfall occurs throughout the year and intensifies during winter, with 64% of total accumulation between April and September, leading to a cold bias of −0.86°C. Large snowfall events are associated with high-pressure systems forcing warm oceanic air masses toward the Antarctic interior, which causes a warm bias of +2.83°C. The temperature-δ18O relationship is primarily constrained by the winter variability, but the observed slope is valid year-round (Fig 2.). Three snow δ18O records covering 2004–2014 indicate that the anomalies recorded in the ice core are attributable to the occurrence of warm winter storms bringing precipitation to ABN and support the interpretation of δ18O in this region as a marker of temperature changes related to large-scale atmospheric conditions, particularly blocking events and variations in the Southern Annular Mode.

Millennial-scale atmospheric CO_2 variations during the Marine Isotope Stage 6 period (190–135 ka)

Shin, J., Nehrbass-Ahles, C., Grilli, R., Chowdhry Beeman, J., Parrenin, F., Teste, G., Landais, A., Schmidely, L., Silva, L., Schmitt, J., Bereiter, B., Stocker, T. F., Fischer, H., Chappellaz, J.

Clim. Past, 16, 2203–2219, https://doi.org/10.5194/cp-16-2203-2020, 2020

Using new and previously published CO_2 data from the EPICA Dome C ice core (EDC), we reconstruct a new high-resolution record of atmospheric CO_2 during Marine Isotope Stage (MIS) 6 (190 to 135 ka) the penultimate glacial period. Similar to the last glacial cycle, where high-resolution data already exists, our record shows that during longer North Atlantic (NA) stadials, millennial CO_2 variations during MIS 6 are clearly coincident with the bipolar seesaw signal in the Antarctic temperature record. However, during one short stadial in the NA, atmospheric CO_2 variation is small (~5 ppm) and the relationship between temperature variations in EDC and atmospheric CO_2 is unclear. The magnitude of CO_2 increase during Carbon Dioxide Maxima (CDM) is closely related to the NA stadial duration in both MIS 6 and MIS 3 (60–27 ka). This observation implies that during the last two glacials the overall bipolar seesaw coupling of climate and atmospheric CO_2 operated similarly. In addition, similar to the last glacial period, CDM during the earliest MIS 6 show different lags with respect to the corresponding abrupt CH_4 rises, the latter reflecting rapid warming in the Northern Hemisphere (NH). During MIS 6i at around 181.5 ± 0.3 ka, CDM 6i lags the abrupt warming in the NH by only 240 ± 320 years. However, during CDM 6iv (171.1 ± 0.2 ka) and CDM 6iii (175.4 ± 0.4 ka) the lag is much longer: 1290 ± 540 years on average. We speculate that the size of this lag may be related to a larger expansion of carbon-rich, southern-sourced waters into the Northern Hemisphere in MIS 6, providing a larger carbon reservoir that requires more time to be depleted.

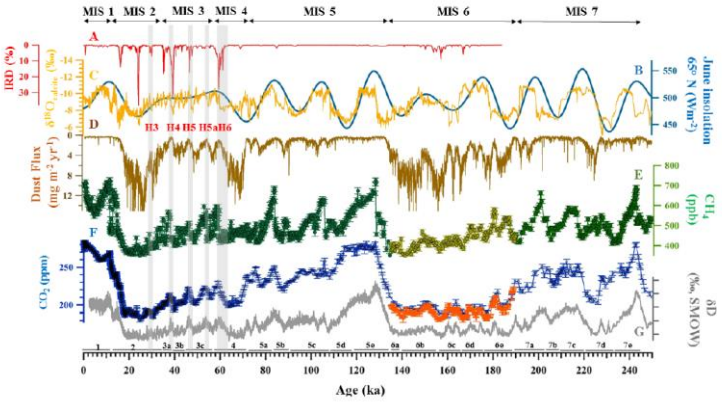

Figure: Proxy data over the last 250 ka. (a) Ice-rafted debris (IRD) input in the Iberian Margin core MD95-2040. (b) The 21 June insolation for 65°N (Berger, 1978).(c)The $\delta^{18}O$calcite from Sanbao cave, indicative of the strength of the East Asian monsoon (Cheng et al., 2016). (d) Dust flux in the EDC ice core (Lambert et al., 2012). (e) Published atmospheric CH4 in EDC (dark green dots) (Loulergue et al., 2008) and a composite atmospheric CH4 record from EDC derived in this study (light yellow dots). (f) Composite CO_2 record from the EDC ice core derived in this study (orange dots) and a published composite CO_2 record from Antarctic ice cores (dark blue dots) (g) The δD in the EDC ice core, Antarctica.

Bipolar volcanic synchronization of abrupt climate change in Greenland and Antarctic ice cores during the last glacial period

Svensson A. et al. including Landais, A.

Clim. Past, 16, 1565–1580, 2020

The last glacial period is characterized by a number of millennial climate events that have been identified in both Greenland and Antarctic ice cores and that are abrupt in Greenland climate records. The mechanisms governing this climate variability remain a puzzle that requires a precise synchronization of ice cores from the two hemispheres to be resolved. Previously, Greenland and Antarctic ice cores have been synchronized primarily via their common records of gas concentrations or isotopes from the trapped air and via cosmogenic isotopes measured on the ice. In this work, we apply ice core volcanic proxies and annual layer counting to identify large volcanic eruptions that have left a signature in both Greenland and Antarctica. Generally, no tephra is associated with those eruptions in the ice cores, so the source of the eruptions cannot be identified. Instead, we identify and match sequences of volcanic eruptions with bipolar distribution of sulfate, i.e. unique patterns of volcanic events separated by the same number of years at the two poles. Using this approach, we pinpoint 82 large bipolar volcanic eruptions throughout the second half of the last glacial period (12–60 ka). This improved ice core synchronization is applied to determine the bipolar phasing of abrupt climate change events at decadal-scale precision. In response to Greenland abrupt climatic transitions, we find a response in the Antarctic water isotope signals (^{18}O and deuterium excess) that is both more immediate and more abrupt than that found with previous gas-based interpolar synchronizations, providing additional support for our volcanic framework. On average, the Antarctic bipolar seesaw climate response lags the midpoint of Greenland abrupt δ^{18}O transitions by 122 +/- 24 years. The time difference between Antarctic signals in deuterium excess and δ^{18}O, which likewise informs the time needed to propagate the signal as described by the theory of the bipolar seesaw but is less sensitive to synchronization errors, suggests an Antarctic δ^{18}O lag behind Greenland of 152 +/- 37 years. These estimates are shorter than the 200 years suggested by earlier gas-based synchronizations.

As before, we find variations in the timing and duration between the response at different sites and for different events suggesting an interaction of oceanic and atmospheric teleconnection patterns as well as internal climate variability.

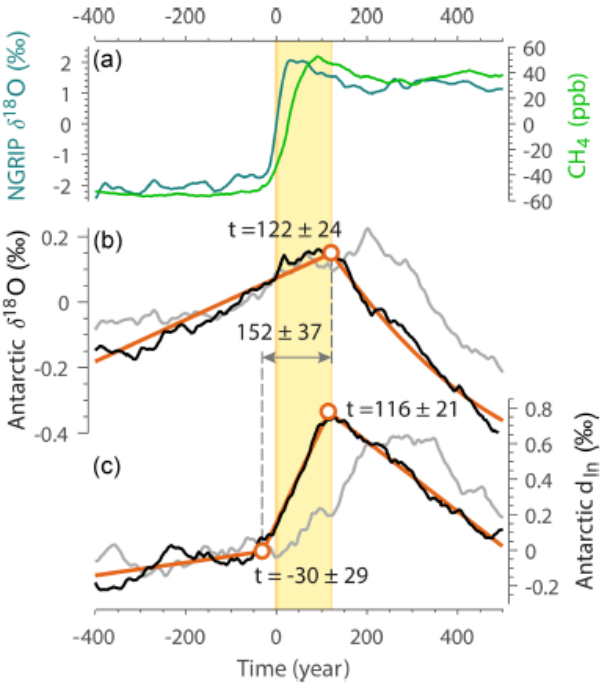

*Figure: (a) Stack of Greenland NGRIP isotopes and CH_4 for the onsets of GI events. (b) Antarctic five-core mean $\delta^{18}O$ (stack of 5*21 warming events); grey curve applies the bipolar methane synchronization of WAIS Divide Project Members (2015); (c) Antarctic five-core mean deuterium excess (d_{ln})*

Marine and terrestrial climate variability in the western Mediterranean sea during marine isotope stages 20 and 19

Toti , F., Bertini, A., Girone, A., Marino, M., Maiorano, P., Bassinot, F., Combourieu-Nebout, N., Nomade, S., and Buccianti, A.

Quaternary Science Reviews 243 106486 (2020)

The climate variability within late Marine Isotope Stage (MIS) 20 and MIS 19 is examined with particular reference to the response of marine and terrestrial realms in the area surrounding the Alboran Sea (western Mediterranean Sea). Sediment samples from the Ocean Drilling Program Site 976 (Fig.1) were used to derive high temporal resolution (average resolution of 450 years) palynological (pollen and spores) and calcareous plankton (coccolithophores and foraminifera) records.

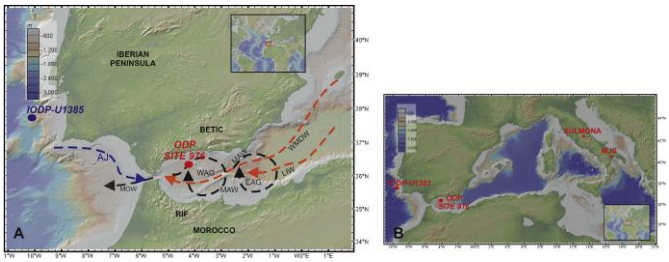

Fig.1 location of ODP Site 976, Bathymetry of the area and modern day oceanic conditions.

These data, together with the new $\delta^{18}O$ G.bulloides, make it possible to discuss the paleoenvironmental changes within a well constrained chronological frame. Cooler phases, including late MIS 20 and several cold spells during MIS 19b-a, are marked, on land, by the expansion of open vegetation formations dominated by steppe and semi-desert taxa. At the same time, the western Mediterranean Sea is marked by the incursion of North Atlantic polar-water planktonic taxa. MIS 19c and interstadials of MIS 19b-a are characterized by the spread of prevalent temperate forest taxa that parallel the expansion of warm-water calcareous plankton taxa during periods of lighter $\delta^{18}O$ (Fig. 2). Climate variations at both precessional and millennial to sub-millennial time-scales, expressed by on land and marine signals, highlight the sensitivity of the western Mediterranean area to both orbital forcing and rapid internal oscillations of the climate systems involving remote connections with North Hemisphere high latitudes. The correlation within the central-western Mediterranean and North Atlantic climate dynamics including the time/spatial gradients related to regional and global climate processes contributes to the reconstruction of the Earth climate dynamics and marine vs land responses, in full Early-Middle Pleistocene transition. These new evidences also provide an opportunity to improve knowledge of MIS 19c now considered, due to its orbital geometry, the best orbital analogue to the Holocene

Interpreting Inverse Magnetic Fabric in Miocene Dikes

Trippanera D., Porreca M., Urbani S., Kissel C., Winkler A., Sagnotti L., Nazzareni S., Acocella V.

Journal of Geophysical Research: Solid Earth, *125*, e2020JB020306. https://doi.org/10.1029/2020JB020306

Anisotropy of Magnetic Susceptibility (AMS) is a unique tool to investigate magma flow direction within dikes. However, as already shown in Icelandic dikes (Kissel et al., 2010), its interpretation in terms of flow trajectories may be complicated by geometrically inverse magnetic fabric characterized by maximum magnetic susceptibility axis (kmax) perpendicular to the dike wall. To better understand the nature and the origin of this fabric, we present a multiscale study of 19 dikes (383 samples) located in the Miocene Alftafjordur volcanic system (Iceland), where 80% of the samples show a geometrically inverse magnetic fabric.

We carried out (1) AMS measurements at different magnetic fields and temperatures, along with Anisotropy of Anhysteretic Remanent Magnetization (AARM) analysis; (2) hysteresis loops and FORC diagrams; (3) thin section analysis; (4) structural fieldwork.

All these analyses allow us to describe the magnetic mineralogical content of the studied rocks. The contribution of paramagnetic elongated crystals to the magnetic fabric is negligible, the latter being carried by variable Ti-content ($0.1 < x < 0.6$, $Fe_{3-x}Ti_xO_4$) titanomagnetite. Single domain is not the dominating the domain state of the magnetic particles, ruling out the relationship between its occurrence and inverse fabrics. AMS analyses at different fields and temperatures along with AARM allow us to exclude any mineral phase change of the titanomagnetite across the dike.

Nevertheless, kmax is parallel to a diffuse horizontal column-like fracture pattern perpendicularly oriented to the dike strike. This suggests that the Ti-magnetite mineral orientation during dike cooling was affected by the fracture network progressively developing columnar basalts. This study demonstrates that the interpretation of AMS data on old and deep volcanic bodies is not straightforward and observations at different scales are required.

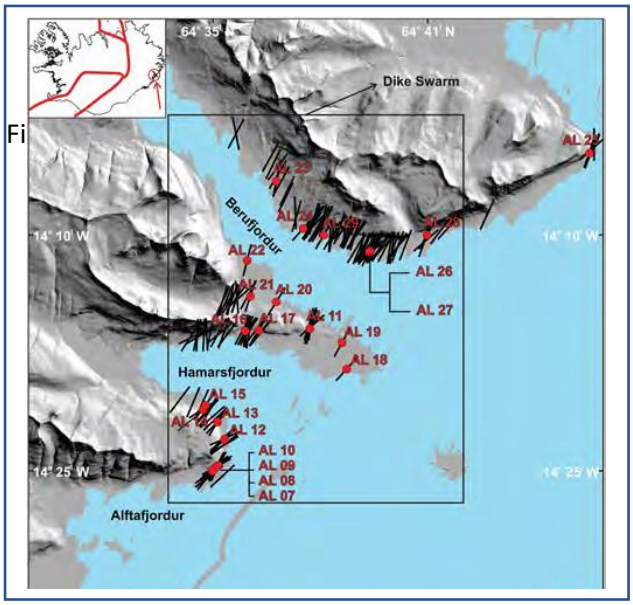

Fig. 1. Map of the Alftafjordur dike swarm in Eastern Iceland (see inset). The orientation of the measured dikes in the field along with locations of sampling sites for AMS (e.g., AL26) is indicated.

Seismo-Turbidites in Aysén Fjord (Southern Chile) Reveal a Complex Pattern of Rupture Modes Along the 1960 Megathrust Earthquake Segment

Wils, K., Van Daele, M., Kissel, C., Moernaut, J., Schmidt, S., Siani, G., and Lastras, G.

Journal of Geophysical Research: Solid Earth, *125*, e2020JB019405.

Multiple studies in south-central Chile have aimed at finding traces of giant, tsunamigenic megathrust earthquakes leading to the current 5,500-year-long paleoseismological record of the Valdivia segment. However, none of these cover the southern third of the segment. The Aysén Fjord located in southern Chile allows to fill this data gap.

In a long core retrieved during the oceanographic cruise PACHIDERME on board the R. V. *Marion Dufresne,* a series of 25 seismo-turbidites (MTD : mass-transport deposits) has been recognized. Identified by magnetic and sedimentary grain-size analyses and end-member modelling and dated by radiocarbon, they occurred during the last 9,000 years.

Considering the shaking intensities required to trigger these turbidites (V1/2-VI1/2), the majority can be related to megathrust earthquakes. This study therefore presents the first, crucial paleoseismic data in this region. Its demonstrates that the 1960 event was not unique for the Valdivia segment, yielding a recurrence rate of 321 ± 116 years in the last two millennia. Moreover, the oldest identified events in Aysén Fjord date back to 9,000 cal years BP and, thus, also extend the regional paleoseismological record in time.

We infer a large temporal variability in rupture modes, with successions of full-segment ruptures alternating with partial and cascading ruptures. The latter seems to significantly postpone the occurrence of another full rupture when consecutively occurring in different parts of the segment.

Additionally, one outstanding period of seismic quiescence - during which no megathrust earthquake evidence has been found at any paleoseismic site - occurred after a full rupture in AD ~745 that presents an unusual uplift/subsidence pattern. Such variability makes it highly speculative to anticipate the rupture mode of the next megathrust earthquake along the Valdivia segment.

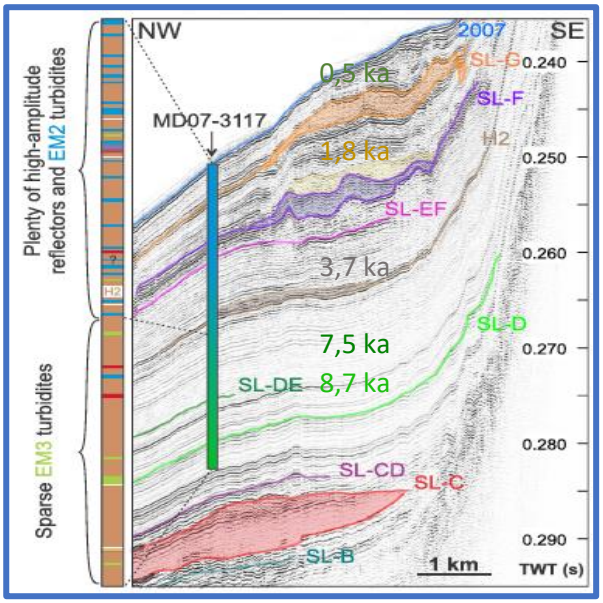

Fig. 1. Seismic profile (TW : two-way travel time) that runs over the MD07-3117 core location with indication of MTDs and the H2 tephra layer. The top of the core corresponds to the 2007 earthquake. The ages of the main identified MTD are reported close by.

Parution du livre « Paleoclimatology »

Editeurs : G. Ramstein,N. Bouttes, A. Govin, A. Landais, P. Sepulchre

Ce livre en deux volumes offre une compréhension complète et détaillée de la paléoclimatologie, en commençant par décrire les données *« proxy »* à partir desquelles les paramètres climatiques sont reconstruits de manière quantitative et en développant un modèle complet du système terrestre capable de décrire les climats passés de la Terre.

Le premier volume décrit les différentes méthodes techniques géochronologiques utilisées en paléoclimatologie. Différentes techniques de géosciences (stratigraphie, magnétisme, dendrochronologie, sédimentologie, géochimie) sont ensuite présentées qui permettent de reconstruire les anciens climats à partir de données glaciaires, terrestres (spéléothèmes, lacs et végétation) et océaniques.

Le deuxième volume explique la construction de modèles complets de l'évolution climatique passée. Les chapitres sont basés sur la compréhension des processus qui régissent l'évolution de chaque composante du système terrestre (atmosphère, océan, glace). Ce volume fournit à la fois une compréhension analytique de chaque composante en utilisant une hiérarchie de modèles (des modèles conceptuels aux modèles 3D de circulation générale très sophistiqués) et une approche synthétique incorporant toutes ces composantes pour étudier l'évolution de la Terre en tant que système global.

Dans l'ensemble, ce livre offre au lecteur une vue complète de la reconstruction des données et de la modélisation du climat de la Terre depuis les temps les plus anciens jusqu'à nos jours, avec une ouverture sur le climat futur.

https://www.springer.com/gp/book/9783030249816

SOUTENANCES DE THESE

Li/Mg ratio in scleractinian corals: a new and powerful proxy for ocean paleo-temperatures?

Kristan Cuny-Guirriec

PhD thesis, February 27, 2020 – ***Keywords***: Li/Mg, corals, geochemistry, oceanography, paleoclimatology

The geochemical proxy Li/Mg was here revisited in a calibration including 11 species of coral from diverse environments, from tropical surface waters to Antarctic waters, allowing reconstructions of temperatures in a wide range from -1°C to 29°C, with a general uncertainty of ± 0.9°C (***Fig. 1***).

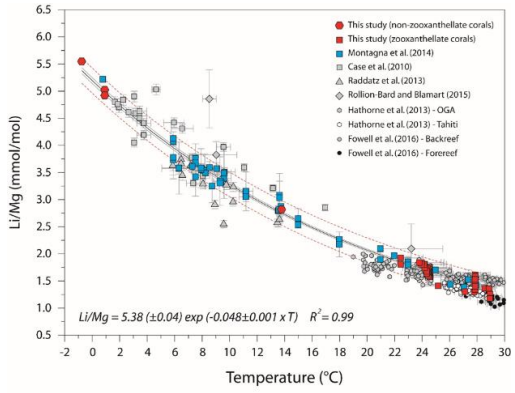

Fig.1. Li/Mg ratios vs. ambient seawater temperature for the chemically-cleaned zooxanthellate and non-zooxanthellate corals analysed in the present study (red symbols), excluding the samples showing detectable traces of calcite and green bands, plotted together with literature data (Case et al., 2010; Raddatz et al., 2013; Hathorne et al., 2013; Montagna et al., 2014; Rollion-Bard and Blamart, 2015; Fowell et al., 2016).

However, this thesis demonstrates that organic matter or diagenesis can bias the proxy. These effects can be corrected by a non-destructive cleaning protocol, and by precise analysis to avoid calcite zones. Furthermore, uncertainties are higher for tropical corals. This is probably linked to a calcification and kinetics effects, related to seasonal variation of environmental parameters. By combining Li/Mg and Sr/Ca ratios in a multi-proxy approach, these uncertainties can be considerably reduced. In this way, two distinct paleo-environments could be reconstructed in temperature. First, the evolution of Sea Surface Temperatures since two-centuries was reconstructed from the aragonite skeleton of a *Siderastrea siderea* colony, and clearly shows the current global warming acting in the Caribbean. Then, the use of Li/Mg on deep water corals from the Mediterranean Sea made possible to provide a first approach of the temperature evolution of intermediate waters of the Mediterranean Sea, since 55.000 years, in response to the glacial/interglacial cycle (***Fig. 2***)

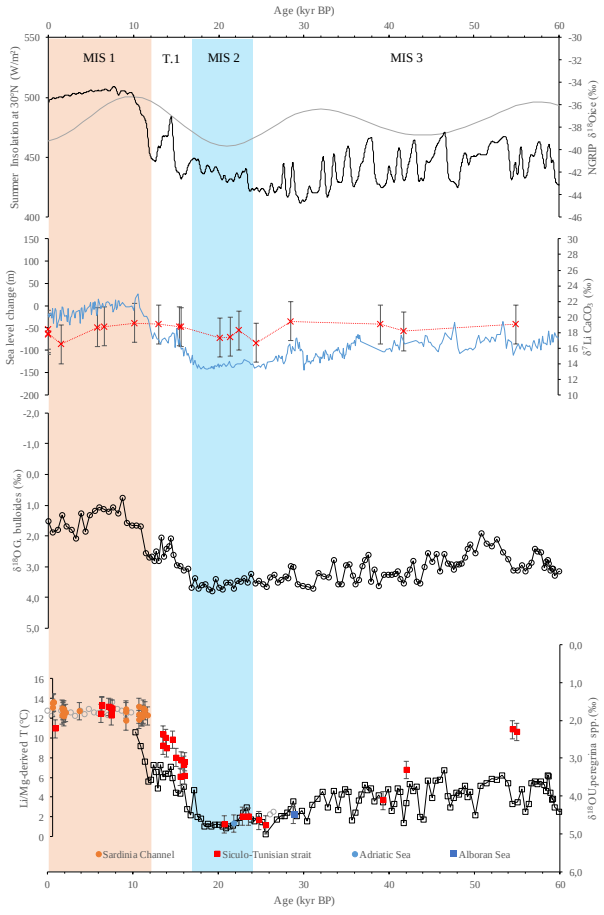

Fig. 2. Time evolution of the Li/Mg-derived temperature since 55 kyr in the Siculo-Tunisian Strait (red squares) and in Sardinia Channel (orange circles), and their comparison with the evolution of the $\delta^{18}O$ of U. peregrina and G. bulloides (from Toucanne et al, 2012), $\delta^{18}O$ recorded on NGRIP ice core, and summer insolation at 30°N. Values of $\delta^{7}Li$ recorded on fossils cold-water corals are also shown with comparison with the sea level change.

Les changements majeurs de la Productivité Biologique au cours du Quaternaire et leurs impacts sur les cycles du carbone et de l'oxygène (thèse 2017 – 2020)

Margaux Brandon encadrée par Stéphanie Duchamp-Alphonse et Amaëlle Landais

Soutenance le 18 Décembre 2020

L'objectif de cette thèse est de reconstruire les changements de productivité biologique et d'estimer leur contribution sur les variations d'O_2 et de CO_2 atmosphérique au cours des derniers 800 ka, avec une attention particulière portée sur la Terminaison V et l'interglaciaire MIS 11. Des mesures de $\Delta^{17}O$ de O_2 dans les bulles de la carotte Epica Dome C (Antarctique) sont réalisées pour remonter au flux d'oxygène biosphérique global entre 400 et 800 ka. Des analyses géochimiques (COT, $CaCO_3$, XRF) et micropaléontologiques (coccolithes) sont effectuées sur une carotte de sédiments marins pour remonter aux variations de l'efficacité de la pompe biologique au long des derniers 800 ka dans le secteur Indien de l'Océan Austral. Le couplage de ces deux approches empiriques permet ainsi d'obtenir une meilleure vision des changements de productivité à l'échelle globale et locale. Les résultats ont montré une productivité exceptionnelle lors du stade isotopique marin 11, un interglaciaire particulièrement long il y a 420 000 ans avant aujourd'hui.

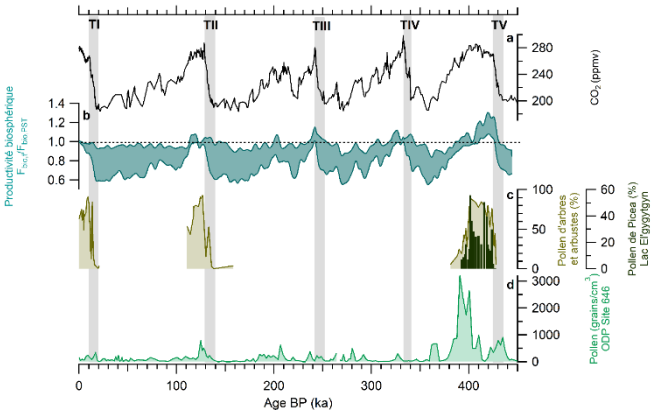

***Figure 3:** Evolution de la productivité biosphérique au cours des 445 derniers milliers d'années. a courbe de CO_2. b reconstitution du ratio de productivité biosphérique entre un temps donné t et la période préindustrielle, calculée à partir des données de $\Delta^{17}O$ de O_2. c Enregistrement de pollen d'arbres, d'arbustes et de Picea dans le lac El'Gygytgyn, Sibérie. d Enregistrement de pollen dans la carotte sédimentaire marine ODP Site 646 au Sud du Groenland*

Dynamique du Phosphore dans les sédiments à l'interface fleuve-mer : couplage modèle-données

Ait Ballagh, F.E.

Thèse de Doctorat de l'Université Paris Saclay (France) et l'Université Cadi Ayyad (Maroc), soutenue le 10 juillet 2020

Le but de cette thèse était de clarifier et à quantifier les processus diagénétiques primaires et secondaires, contrôlant le devenir de la matière organique sédimentaire, la transformation du phosphore et les flux de DIP induits vers l'eau de fond.

Pour cela, nous avons utilisé des données de terrain couplées avec un modèle existant (OMEXDIA), étendu au cycle benthique du phosphore (P), pour étudier la dynamique du P et évaluer la capacité des sédiments à servir de puits ou de sources de P dans les estuaires eutrophes de l'Elorn et de l'Aulne et dans le prodelta du Rhône. Tout d'abord, le modèle OMEXDIA-P a été adapté aux données d'eau interstitielle et de solides de quatre saisons dans les stations amont, milieu et aval des estuaires de l'Elorn et de l'Aulne. Ensuite, le modèle a été ajusté aux mêmes variables d'état pour neuf stations situées dans l'embouchure du Rhône, son prodelta et son plateau continental adjacent, et échantillonnées en Mai 2018. Les deux applications du modèle OMEXDIA-P ont montré une bonne concordance avec la distribution verticale des phases dissoutes et solides dans toutes les stations et toutes les saisons.

L'utilisation combinée de ces deux bases de données avec ce modèle a révélé que les flux de C organique déposés dans l'IES des estuaires de l'Elorn et de l'Aulne et dans le prodelta du Rhône étaient intenses, en particulier à l'embouchure du fleuve. Par conséquent, la minéralisation en P organique a représenté la principale source de DIP produit à l'interne dans les deux estuaires (77 % de la production totale de DIP) et dans le prodelta du Rhône (> 90 %). La contribution des voies de minéralisation a mis en évidence une augmentation de la contribution de la minéralisation anoxique due au gradient salin de l'amont vers l'aval des estuaires. Alors que ces voies de minéralisation ont montré une diminution de l'embouchure du Rhône vers le plateau continental, en fonction de la diminution des apports de matière organique avec la distance. Le calcul du bilan du P sédimentaire effectué par le modèle a également indiqué que le P lié au fer joue un rôle clé dans le cycle du P, en retenant le DIP dans les sédiments depuis la diffusion jusqu'aux eaux sus-jacentes et en favorisant la précipitation de P lié au calcium. De plus, le P lié au fer représente une source supplémentaire de DIP dans les sédiments, particulièrement dans les estuaires de l'Elorn et de l'Aulne. La plus grande proportion du DIP produit a été recyclée dans l'eau de fond de ces sédiments estuariens (85 % de la production totale de DIP) et deltaïques (72 %), tandis que l'enfouissement sous forme de P lié au calcium était une fraction mineure. Dans l'ensemble, les résultats du modèle présentés ici ont également démontré que ces sédiments estuariens et deltaïques jouaient un rôle essentiel dans le cycle benthique du P et constituaient des sources de DIP dans la colonne d'eau. De plus, les apports de DIP produits dans les sédiments de l'Elorn et de l'Aulne étaient plus élevés que les apports fluviaux actuels en DIP.

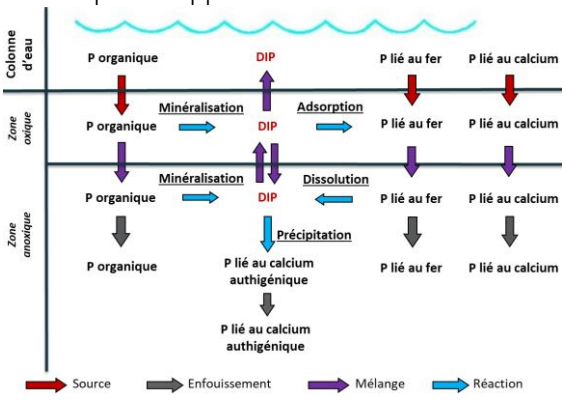

Fig. 1. Cycle du phosphore dans les sédiments marins (d'après Slomp, 1995)

Les stages 2020

Stages 3eme

Guilhem Delpias (en télétravail), Compréhension du signal isotopique de l'eau et les techniques de mesure, encadrant Bénédicte Minster, équipe GLACCIOS

Maxime Durand (en télétravail), préparation du forage de glace européen couvrant 1.5 millions d'années (projet Beyond EPICA); encadrant Amaëlle Landais, équipe GLACCIOS

Rebecca Reichel (en télétravail) « suivi de mesures des isotopes de l'eau dans la vapeur d'eau, la précipitation et la neige de surface dans trois stations australes (île d'Amsterdam, Concordia, Dumont d'Urville) », encadrant Amaëlle Landais, équipe GLACCIOS

Martin Schanne (en télétravail) « Méthodes de reconstruction des températures océaniques dans le passé (régions tropicales) », encadrement Franck Bassinot, équipe PALEOCEAN

Stages Licence et IUT

Alexis Bento Cardadeiro (IUT) : « Mise au point de la mesure de l'azote par un spectromètre de masse couplé à un analyseur élémentaire pour l'analyse de sédiments », Encadrement Christine Hatté & Caroline Gauthier, équipe GEOTRAC

Leoni Janssen (Licence): "Traitement des données isotopique de la vapeur d'eau sur la traverse Est-Antarctique de EAIIST », encadrement Amaëlle Landais, équipe GLACCIOS

Stages M1

Vincent Girard:"Composition isotopique de la vapeur d'eau sur le site de Dome C – comparaison entre plusieurs instruments de spectroscopie optique», encadrement Amaëlle Landais, équipe GLACCIOS

Stages M2

Guillaume Boisrame « Variations hydrologiques au large de la côté sud chilienne au cours du stade isotopique 3, influences respectives de la calotte Patagonienne et de l'Océan Austral. », co-encadrement E. Michel et G. Siani, équipe PALEOCEAN

Bruno Millet : " Abyssal Circulation in the Glacial North Pacific", encadrement W. Gray, équipe PALEOCEAN

Grégoire Tazduck : « Dynamique de la circulation profonde en Atlantique Nord au cours du dernier Interglaciaire », co-encadrement A. Govin, C. Kissel équipe CLIMAG

Cécile Darvinche : « Etude de l'anomalie isotopique de la vapeur lors de l'événement de rivière atmosphérique à Dome C en dec 2018 », co-encadrement C. Agosta et A. Berchet, équipe GLACCIOS et thème 2

Clémence Brochet : « modélisation écoulement de la calotte - datation des carottes de Terre Adélie », encadrement A. Orsi, équipe GLACCIOS

Tanguy Sandre : « What is the environmental story behind data and observations in Ittoqqortoormiit collected since 1932 ? ", encadrement J. Gherardi, équipe GLACCIOS

Nicolas Pasquier : « détermination des coefficients de fractionnement de l'oxygène lors de la respiration et de la photosynthèse », encadrement A. Landais, équipe GLACCIOS

Bibliographie

Article en rouge = Fiche existante

Ai, X., Studer, A., Sigman, D., Martınez-Garcıa, A., Fripiat, F., Thole, L., Michel, E., Gottschalk, J., Arnold, L., Moretti, S., Schmitt, M., Oleynik, S., Jaccard, S., and Haug, G. Southern Ocean upwelling, Earths obliquity, and glacial-interglacial atmospheric CO 2 change. Science, 370(6522) : 1348–1352, December 2020. doi: 10.1126/science.abd2115. https://hal.archives-ouvertes.fr/hal-03053376.

Ait Ballagh, F.E., Rabouille, C., Andrieux-Loyer, F., Soetaert, K., Elkalay, K., Khalil, K. Spatio-temporal dynamics of sedimentary phosphorus along two temperate eutrophic estuaries: A data-modelling approach. Continental Shelf Research, (2020) vol.193, 104037

Barthel, A., Agosta, C., Little, C., Hattermann, T., Jourdain, N., Goelzer, H., Nowicki, S., Seroussi, H., Straneo, F., and Bracegirdle, T. CMIP5 model selection for ISMIP6 ice sheet model forcing: Greenland and Antarctica. The Cryosphere, 14(3):855–879, 2020. doi: 10.5194/tc-14-855-2020. https://hal.archives-ouvertes.fr/hal-02524433.

Baudin, F., Rabouille, C., and Dennielou, B. Routing of terrestrial organic matter from the Congo River to the ultimate sink in the abyss: a mass balance approach. Geologica Belgica, 23(1-2):xx–xx, July 2020. doi: 10.20341/gb.2020.004. https://hal.sorbonne-universite. fr/hal-02945073.

Beny, F., Bout-Roumazeilles, V., Davies, G.R., Waelbroeck, C., Bory, A., Tribovillard, N., Delattre, M., and Abraham, R. Radiogenic isotopic and clay mineralogical signatures of terrigenous particles as water-mass tracers: New insights into South Atlantic deep circulation during the last termination. Quaternary Science Reviews, 228:106089, January 2020. doi: 10.1016/j.quascirev.2019.106089. https://hal.archives-ouvertes.fr/hal-02507062.

Bourges, F., Genty D., Perrier F., Lartiges B., Regnier E., Francois A., Leplat J., Touron S., Bousta F., Massault M., Delmotte M., Dumoulin J.P, Girault F., Ramonet M., Chauveau C., and Rodrigues P. Hydrogeological control on carbon dioxide input into the atmosphere of the Chauvet-Pont dArc cave. Science of the Total Environment, 716:136844, May 2020. doi: 10.1016/j.scitotenv.2020.136844. https://hal-cnrs.archives-ouvertes.fr/hal-03089428.

Bouttes, N., Vazquez Riveiros, N., Govin, A., Swingedouw, D., Sanchez-Goni, M., Crosta, X., and Roche, D. Carbon 13 Isotopes Reveal Limited Ocean Circulation Changes Between Interglacials of the Last 800 ka. Paleoceanography and Paleoclimatology, 35(5): e2019PA003776, May 2020. doi: 10.1029/2019PA003776. https://hal.archives-ouvertes. fr/hal-02844111.

Brandon, M., Landais, A., Duchamp-Alphonse, S., Favre, V., Schmitz, L., Abrial, H., Prie, F., Extier, T., and Blunier, T. Exceptionally high biosphere productivity at the beginning of Marine Isotopic Stage 11. Nature Communications, 11 (1), December 2020. doi: 10.1038/s41467-020-15739-2. https://hal.archives-ouvertes.fr/ hal-02765978.

Briard, J., Puceat, E., Vennin, E., Daeron, M., Chavagnac, V., Jaillet, R., Merle, D., and De Rafélis, M. Seawater paleotemperature and paleosalinity evolution in neritic environments of the Mediterranean margin: insights from isotope analysis of bivalve shells. Palaeogeography, Palaeoclimatology, Palaeoecology, 543:109582, April 2020. doi: 10.1016/j.palaeo.2019.109582. https://hal.archives-ouvertes.fr/hal-02449079. 19 pages.

Capet, A., Cook, P., Garcia-Robledo, E., Hoogakker, B., Paulmier, A., Rabouille, C., and Vaquer-Sunyer, R. Editorial: Facing Marine Deoxygenation. Frontiers in Marine Science, 7:46, 2020. doi: 10.3389/fmars.2020.00046. https://hal. archives-ouvertes.fr/hal-02537804.

Castanet, C., Nondedeo, P., Dussol, L., Teste, M., Purdue, L., Hiquet, J., Lemonnier, E., Garnier, A., Goudiaby, H., Dorison, A., Tomadini, N., Morales-Aguilar, C., Limondin-Lozouet, N., Cavero, J., Develle-Vincent, A-L., Hatte, C., Lanos, P., Mokadem, F., and Sipos, G. Dynamique du socio-ecosysteme maya du territoire de subsistance de la cite de Naachtun (Pet´en, Guatemala) entre 1500 av. et 1000 apr. J.-C. Développements méthodologiques et résultats préliminaires dune approche systémique

multiscalaire. In CIST2020 - Population, temps, territoires, Paris-Aubervilliers, France, November 2020. Centre National de la Recherche Scientifique [CNRS], Ined, Universite Paris 1. URL https://hal.archives-ouvertes.fr/hal-03114089.

Claudet, J., Bopp, L., Cheung, W., , Devillers, R., Escobar-Briones, E., Haugan, P., Heymans, J., Masson-Delmotte, V., Matz-Luck, N., Miloslavich, P., Mullineaux, L., Visbeck, M., Watson, R., Milena Zivian, A., Ansorge, I., Araujo, M., Arico, S., Bailly, D., Barbiere, J., Barnerias, C., Bowler, C., Brun, V., Cazenave, A., Diver, C., Euzen, A., Thierno Gaye, A., Hilmi, N., Menard, F., Moulin, C., Munoz, N.P., Parmentier, R., Pebayle, A., Portner, H.-O., Osvaldina, S., Ricard, P., Serrao Santos, R., Sicre, M.-A., Thiebault, S., Thiele, T., Trouble, R., Turra, A., Uku, J., Gaill., F. A Roadmap for Using the UN Decade of Ocean Science for Sustainable Development in Support of Science, Policy, and Action. one earth, 2(1):34–42, January 2020. doi: 10.1016/j.oneear.2019.10.012. URL https://hal.archives-ouvertes.fr/hal-02365617.

Clauzel, T., Richardin, P., Ricard, J., Le Bechennec, Y., Amiot, R., Fourel, F., Phouybanhdyt, B., Vinçon-Laugier, A., Flandrois, J.P., and L´ecuyer, C. The Gauls experienced the Roman Warm Period: Oxygen isotope study of the Gallic site of Thézy-Glimont, Picardie, France. Journal of Archaeological Science: Reports, 34:102595, December 2020. doi: 10.1016/j.jasrep.2020.102595. https://hal-univ-lyon1.archives-ouvertes.fr/ hal-02998511.

Cushing, M., Hollender, F., Moiriat, D., Guyonnet-Benaize, C., Theodoulidis, N., Pons-Branchu, E., Sepulcre, S., Bard, P.Y., Cornou, C., Dechamp, A., Marsical, A., and Roumelioti, Z. Building a three dimensional model of the active Plio-Quaternary basin of Argostoli (Cephalonia Island, Greece): an integrated geophysical and geological approach. Engineering Geology, 265:105441, February 2020. doi: 10.1016/j.enggeo.2019.105441. https://hal.archives-ouvertes.fr/hal-02404456.

Donat-Magnin, M., Jourdain, N., Gallee, H., Amory, C., Kittel, C., Fettweis, X., Wille, J., Favier, V., Drira, A., and Agosta, C. Interannual variability of summer surface mass balance and surface melting in the Amundsen sector, West Antarctica. The Cryosphere, 14(1):229–249, 2020. doi: 10.5194/tc-14-229-2020. URL https://hal. archives-ouvertes.fr/hal-03001127.

Drysdale, R., Couchoud, I., Zanchetta, G., Isola, I., Regattieri, E., Hellstrom, J., Govin, A., Tzedakis, P., Ireland, T., Corrick, E., Greig, A., Wong, H., Piccini, L., Holden, P., and Woodhead, J. Magnesium in subaqueous speleothems as a potential palaeotemperature proxy. Nature Communications, 11:5027, October 2020. doi: 10.1038/s41467-020-18083-7. https://hal.archives-ouvertes.fr/hal-02965538.

Duhamel, M., Colin, C., Revel, M., Siani, G., Dapoigny, A., Douville, E., Wu, J., Zhao, Y., Liu, Z., and Montagna, P. Variations in eastern Mediterranean hydrology during the last climatic cycle as inferred from neodymium isotopes in foraminifera. Quaternary Science Reviews, 237:106306, June 2020. doi: 10.1016/j.quascirev.2020.106306. URL https://hal.archives-ouvertes.fr/hal-02624107.

Dumont, M., Pichevin, L., Geibert, W., Crosta, X., Michel, E., Moreton, S., Dobby, K., Ganeshram, R. The nature of deep overturning and reconfigurations of the silicon cycle across the last deglaciation. Nature Communications (2020) vol.11 :1534., doi.org/10.1038/s41467-020-15101-6

Evans, D., Gray, W., Rae, J., Greenop, R., Webb, P., Penkman, K., Kroger, R., and Allison, N. Trace and major element incorporation into amorphous calcium carbonate (ACC) precipitated from seawater. Geochimica et Cosmochimica Acta, 290:293– 311, December 2020. doi: 10.1016/j.gca.2020.08.034. https://hal.archives-ouvertes.fr/ hal-02970846.

Fagny A.M., Nkouandou, O.F., Bardintzeff, J.-M., Guillou, H., Iancu, G. O., Njankouo Ndassa, Z. N., and Temdjim, R. Petrology and geochemistry of the Tchabal Mbabo volcano in Cameroon volcanic line (Cameroon, Central Africa): An intra-continental alkaline volcanism. Journal of African Earth Sciences, 170, 2020. doi: 10.1016/j.jafrearsci.2020.103832. https://hal.archives-ouvertes.fr/hal-02876622.

Flores, J.M., Bourdin, G., Altaratz, O., Trainic, M., Lang-Yona, N., Dzimban, E., Steinau, S., Tettich, F., Planes, S., Allemand, D., Agostini, B., Banaigs, S., Boissin, E., Boss, E., Douville, E., Forcioli, D., Furla, P., Galand, P. E., Sullivan, M., Gilson, E., Lombard, F., Moulin, C., Pesant, S., Poulain, J., Reynaud, S., Romac, S., Sunagawa, S., Thomas, O., Troublé, R., De Vargas, C., Vega Thurber, R., Voolstra, C., Wincker, P., Zoccola, D., Bowler, C., Gorsky, G., Rudich, Y., Vardi, A., and Koren I.Tara Pacific Expeditions Atmospheric Measurements of Marine Aerosols across the Atlantic and Pacific Oceans: Overview and Preliminary Results. Bulletin of the American Meteorological Society, 101(5):E536– E554, May 2020. doi: 10.1175/BAMS-D-18-0224.1. https://hal.archives-ouvertes.fr/ hal-02967981.

Fossile E., Nardelli, M.P., Jouini, A., Lansard, B., Pusceddu, A., Moccia, D., Michel, E., Peron, O., Howa, H., and Mojtahid, M. Benthic foraminifera as tracers of brine production in the Storfjorden "sea ice factory". Biogeosciences, 17(7):1933–1953, 2020. doi: 10.5194/bg-17-1933-2020. https://hal.archives-ouvertes.fr/hal-02539484.

Garel, S., Dupuis, C., Quesnel, F., Jacob, J., Yans, J., Magioncalda, R., Flehoc, C., and Schnyder, J. Multiple Early Eocene carbon isotope excursions associated with environmental changes in the Dieppe-Hampshire Basin (NW Europe). BSGF earth sciences bulletin, September 2020. doi: 10.1051/bsgf/2020030. https://hal.archives-ouvertes.fr/ hal-02950486.

Gdaniec, S., Roy-Barman, M., Levier, M., Valk, O., Rutgers van der Loeff, M., Foliot, L., Dapoigny, A., Missiaen, L., Mörth, C.-M., and Andersson, P. ^{231}Pa and ^{230}Th in the Arctic Ocean: Implications for boundary scavenging and 231Pa230Th fractionation in the Eurasian Basin. Chemical Geology, 532:119380, January 2020. doi: 10.1016/j.chemgeo.2019.119380. https://hal.archives-ouvertes.fr/hal-02467573.

Goelzer, H., Nowicki, S., Payne, A., Larour, E., Seroussi, H., Lipscomb, W., Gregory, J., Abe-Ouchi, A., Shepherd, A., Simon, E., Agosta, C., Alexander, P., Aschwanden, A., Barthel, A., Calov, R., Chambers, C., Choi, Y., Cuzzone, J., Dumas, C., Edwards, T., Felikson, D., Fettweis, X., Golledge, NB., Greve, R., Humbert, A., Huybrechts, P., Le Clech, S., Lee, V., Leguy, G., Little, C., Lowry, D., Morlighem, M., Nias, I., Quiquet, A., Rückamp, M., Schlegel, N.-J., Slater, D., Smith, R., Straneo, F., Tarasov, L., Van de Wal, R., van den Broeke, M. The future sea-level contribution of the Greenland ice sheet: a multi-model ensemble study of ISMIP6. The Cryosphere, 14(9):3071–3096, 2020. doi: 10.5194/tc-14-3071-2020. https://hal.archives-ouvertes.fr/hal-02968752.

Gorsky G, Bourdin G, Lombard F, Pedrotti ML, .. Douville, E., … Expanding Tara Oceans protocols for underway, ecosystemic sampling of the Ocean-Atmosphere interface during Tara Pacific expedition (2016-2018).

Gottschalk, J., Skinner, L., Jaccard, S., Menviel, L., Nehrbass-Ahles, C., and Waelbroeck, C. Southern Ocean link between changes in atmospheric CO_2 levels and northern-hemisphere climate anomalies during the last two glacial periods. Quaternary Science Reviews, 230:106067, February 2020. doi: 10.1016/j.quascirev.2019.106067. https://hal. archives-ouvertes.fr/hal-02407224.

Gottschalk, J., Michel, E., Thöle, L. M., Studer, A. S., Hasenfratz, A. P., Schmid, N., Butzin, M., Mazaud, A., Martínez-García, A., Szidat, S., and Jaccard, S. L. (2020). Glacial heterogeneity in Southern Ocean carbon storage abated by fast South Indian deglacial carbon release. *Nature communications*, *11*(1), 1-14.

Gray, W.R., Wills, R.C.J., Rae, J.W.B., Burke, A., Ivanovic, R.F., Roberts, W.H.G., Ferreira, D., and Valdes, P. Wind-Driven Evolution of the North Pacific Subpolar Gyre Over the Last Deglaciation. Geophysical Research Letters, 47(6), March 2020. doi: 10.1029/2019GL086328. https://hal.archives-ouvertes.fr/hal-02968755.

Grellier S., Janeau, J.L., Richard, P., Florsch, N., Ward, D., Bariac, T., and Lorentz, S. Water uptake plasticity of savanna trees in encroached grassland: small trees match the mature trees. African Journal of Range and Forage Science, pages 1–13, December 2020. doi: 10.2989/10220119.2020.1834453. URL https://hal.archives-ouvertes.fr/hal-03086912.

Gutjahr, M., Bordier, L., Douville, E., Farmer, J., Foster, G., Hathorne, E., Hönisch, B., Lemarchand, D., Louvat, P., Mcculloch, M., Noireaux, J., Pallavicini, N., Rae, J., Rodushkin, I., Roux, P., Stewart, J., Thil, F., and You, C.-F. Sub-Permil Interlaboratory Consistency for Solution-Based Boron Isotope Analyses on Marine Carbonates. Geostandards and Geoanalytical Research, October 2020. doi: 10.1111/ggr.12364. https://hal.archives-ouvertes.fr/hal-03026894.

Haddam, N., Michel E., Siani, G., Licari, L., and Dewilde, F. Ventilation and Expansion of Intermediate and Deep Waters in the Southeast Pacific During the Last Termination. Paleoceanography and Paleoclimatology, 35(7), July 2020. doi: 10.1029/2019PA003743. URL https://hal.archives-ouvertes. fr/hal-02916001.

Hatté, C., Zazzo, A., and Selosse, M.-A. The radiocarbon age of mycoheterotrophic plants. New Phytologist, 227(5):1284–1288, September 2020. doi: 10.1111/nph.16637. https: //hal.archives-ouvertes.fr/hal-03114529.

Hongxi, P., Hou, S., Zhang, W., Wu, S., Jenk, T., Schwikowski, M., and Jouzel, J. Temperature Trends in the Northwestern Tibetan Plateau Constrained by Ice Core Water Isotopes Over the Past 7,000 Years. Journal of Geophysical Research: Atmospheres, 125(19), October 2020. doi: 10.1029/2020JD032560. https://hal.archives-ouvertes.fr/hal-02975814.

Jacob, J., Thibault, A., Simonneau, A., Sabatier, P., Le Milbeau, C., Gautret, P., Ardito, L. and Morio, C. High-resolution sedimentary record of anthropogenic deposits accumulated in a sewer decantation tank. Anthropocene, page 100238, March 2020. doi: 10.1016/j.ancene.2020.100238. https://hal-insu.archives-ouvertes.fr/insu-02507329.

Jolly-Saad, M.-C., Pastre, J.-F., and Nomade, S. The Zanclean palaeofloras around the Mont-Dore strato-volcano: A window into upper Neogene vegetation and environments in the Massif Central (Puy de Dome, France). Geobios, 59:29–46, April 2020. doi: 10.1016/j.geobios.2020.01.001. https://hal.archives-ouvertes.fr/hal-02934515.

Jouzel, J. and Michelot, A. Quelle justice climatique pour la France ? Revue de lOFCE, 165(3): 71, 2020. doi: 10.3917/reof.165.0071. https://hal.archives-ouvertes.fr/hal-02971350.

Juillet-Leclerc, A. Could Coral Skeleton Oxygen Isotopic Fractionation be Controlled by Biology? In Isotopes Applications in Earth Sciences. IntechOpen, June 2020. doi: 10.5772/intechopen.89146. URL https://hal.archives-ouvertes.fr/hal-02955549.

Kaufman, D. and the Temperature-12ka consortium, including A. Orsi. A global database of Holocene paleotemperature records. Scientific Data (2020) 7:115 https://doi.org/10.1038/s41597-020-0445-3

Kissel, C., Laj, C., Jian, Z., Wang, P., Wandres, C. and Rebolledo-Vieyra, M. Past environmental and circulation changes in the South China Sea: Input from the magnetic properties of deep-sea sediments. Quaternary Science Reviews, 236:106263, May 2020. doi: 10.1016/j.quascirev.2020.106263. https://hal.archives-ouvertes.fr/hal-02875152.

Kuzucuoglu, C., Gündogdu Atakay, E., Mouralis, D., Atıcı, G., Guillou, H., Turkecan, A., and Pastre, J.-F. Geomorphology and tephrochronology review of the Hasanda˘g volcano (southern Cappadocia, Turkey). Mediterranean Geoscience Reviews, January 2020. doi: 10.1007/s42990-019-00017-1. https://hal.archives-ouvertes.fr/hal-02447753.

Lawrence, C., Beem-Miller, J., May Hoyt, A., Monroe, G., Sierra, C., Stoner, S., Heckman, K., Blankinship, J., Crow, S., McNicol, G., Trumbore, S., Levine, P., Vinduskova, O., Todd-Brown, K., Rasmussen, C., Hicks Pries, C., Schadel, C., McFarlane, K., Doetterl, S., Hatte, C., He, Y., Treat, C., Harden, J., Torn, M., Estop-Aragones, C., Asefaw Berhe, A., Keiluweit, M., Della Rosa Kuhnen, A., Marin-Spiotta, E., Plante, A., Thompson, A., Shi, Z., Schimel, J., Vaughn, L., von Fromm, S., and Wagai, R. An open-source database for the synthesis of soil radiocarbon data: International Soil Radiocarbon Database (ISRaD) version 1.0. Earth System Science Data, 12(1):61–76, 2020. doi: 10.5194/essd-12-61-2020. https://hal.archives-ouvertes.fr/hal-02467677.

Lecuyer, C., Bojar, A.-V., Daux, V., and Legendre, S.. Geographic variations in the slope of the δ 2 H–δ 18 O meteoric water line over Europe: A record of increasing continentality. The Geological Society, London, Special Publications, pages SP507–2020–68, 2020. doi: 10.1144/SP5072020-68. URL https://hal.archives-ouvertes.fr/hal-02897843.

Lemelle, L., Bartolini, A., Simionovici, A., Tucoulou, R., De Nolf, W., Bassinot, F., and de Garidel-Thoron, T. Nanoscale trace metal imprinting of biocalcification of planktic foraminifers by Tobas super-eruption. Scientific Reports, 10:10974, 2020. doi: 10.1038/s41598-020-67481-w. URL https://hal.archives-ouvertes.fr/hal-02867755.

Leroy-Dos Santos, C., Masson-Delmotte, V., Casado, M., Fourré, E., Steen-Larsen, H., Maturilli, M., Orsi, A., Berchet, A., Cattani, O., Minster, B., Gherardi, J., and Landais, A. A 4.5 Year-Long Record of Svalbard Water Vapor Isotopic Composition Documents Winter Air Mass Origin. Journal of Geophysical Research: Atmospheres, 125(23), December 2020. doi: 10.1029/2020JD032681. https://hal.archives-ouvertes.fr/hal-03087623.

Ma, R., Sepulcre, S., Bassinot, F., Haurine, F., Tisnerat-Laborde, N., and Colin, C. North Indian Ocean Circulation Since the Last Deglaciation as Inferred From New Elemental Ratio Records for Benthic Foraminifera Hoeglundina elegans. Paleoceanography and Paleoclimatology, 35(6), June 2020. doi: 10.1029/2019PA003801. URL https://hal. archives-ouvertes.fr/hal-02888271.

Maja, A., Sabatier, P., Rapuc, W., Ogrinc, N., Dolenec, M., Arnaud, F., Von Grafenstein, U., and Smuc, A. 6600 years of human and climate impacts on lake-catchment and vegetation in the Julian Alps (Lake Bohinj, Slovenia). Quaternary Science Reviews, 227:106043, January 2020. doi: 10.1016/j.quascirev.2019.106043. URL https://hal.archives-ouvertes.fr/ hal-02467643.

Marino, M., Girone, A., Gallicchio, S., Herbert, T., Addante, M., Bazzicalupo, P., Quivelli, O., Bassinot, F., Bertini, A., Nomade, S., Ciaranfi, N., and Maiorano, P. Climate variability during MIS 20–18 as recorded by alkenone-SST and calcareous plankton in the

Ionian Basin (central Mediterranean). Palaeogeography, Palaeoclimatology, Palaeoecology, 560:110027, December 2020. doi: 10.1016/j.palaeo.2020.110027. URL https://hal. archives-ouvertes.fr/hal-02970812.

Metcalfe, B., Lougheed, B., Waelbroeck, C., and Roche, D. A proxy modelling approach to assess the potential of extracting ENSO signal from tropical Pacific planktonic foraminifera. Climate of the Past, 16(3):885–910, 2020. doi: 10.5194/cp-16-885-2020. URL https://hal.archives-ouvertes.fr/hal-02766071.

Missiaen, L., Wacker, L., Lougheed, B., Skinner, L., Hajdas, I., Nouet, J., Pichat, S., and Waelbroeck, C. Radiocarbon Dating of Small-sized Foraminifer Samples: Insights into Marine sediment Mixing. Radiocarbon, 62(2):313–333, April 2020a. doi: 10.1017/RDC.2020.13. URL https: //hal.archives-ouvertes.fr/hal-02884300.

Missiaen, L., Bouttes, N., Roche, D., Dutay, J.-C., Quiquet, A., Waelbroeck, C., Pichat, S., and Peterschmitt, J.-Y. Carbon isotopes and Pa/Th response to forced circulation changes: a model perspective. Climate of the Past, 16(3):867–883, 2020b. doi: 10.5194/cp16-867-2020. URL https://hal.archives-ouvertes.fr/hal-02407200.

Mojtahid, M., Michel, E., and De Deckker, P. From "source to sink" – A new perspective on the past dynamics of the Murray Canyon Group from benthic foraminiferal communities. Marine Micropaleontology, page 101877, May 2020. doi: 10.1016/j.marmicro.2020.101877. https://hal.archives-ouvertes.fr/hal-02915999.

Moncel, M.-H., Biddittu, I., Manzi, G., Saracino, B., Pereira, A., Nomade, S., Hertler, C., Voinchet, P., and Bahain, J.-J. Emergence of regional cultural traditions during the Lower Palaeolithic: the case of Frosinone-Ceprano basin (Central Italy) at the MIS 11–10 transition. Archaeological and Anthropological Sciences, 12(8), August 2020. doi: 10.1007/s12520-020-01150-x. https://hal.archives-ouvertes.fr/hal-02950771.

Montagna, P., and Douville, E. Geochemical proxies in marine biogenic carbonates: New developments and applications to global change. Chemical Geology, 533:119411, February 2020. doi: 10.1016/j.chemgeo.2019.119411. https://hal.archives-ouvertes.fr/hal-02467696.

Moreno, E., Caroir, F., Fournier, L., Fauquembergue, K., Zaragosi, S., Joussain, R., Colin, C., Blanc-Valleron, M.-M., Baudin, F., De Garidel-Thoron, T., Valet, J.-P. and Bassinot, F. Magnetic fabric of Bengal fan sediments: Holocene record of sedimentary processes and turbidite activity from the Ganges-Brahmaputra river system. Marine Geology, 430:106347, December 2020. doi: 10.1016/j.margeo.2020.106347. URL https://hal.archives-ouvertes.fr/hal-02970912.

Nikulkina, I., Gordyachkova, O.V., Sukneva, S.A., Romanova, E.V., Gherardi, J., Wardekker, A., and Antonova, M.E. Resilience of Arctic Communities: Socio-Economic Aspect. International Journal of Humanities and Social Science Research, 9:3066–3081, December 2020. doi: 10.6000/1929-4409.2020.09.373. URL https://hal.archives-ouvertes.fr/hal-03116725.

Nowicki, S. Goelzer, H., Seroussi, H., Payne, A.J., Lipscomb, W. H., Abe-Ouchi, A., Agosta, C., Alexander, P.M., Asay-Davis, X.S., Barthel, A., Bracegirdle, T.J., Cullather, R., Felikson, D., Fettweis, X., Gregory, J. M., Hattermann, T., Jourdain, N., Kuipers Munneke, P., Larour, E. Y., Little, C.M., Morlighem, M., Nias, I.J., Shepherd, A.P., Simon, E., Slater, D.A., Smith, R.S., Straneo, F., Luke D. Trusel, L.D., Van Den Broeke, M.R., and Van De Wal, R.S.W. Experimental protocol for sea level projections from ISMIP6 stand-alone ice sheet models. The Cryosphere, 14(7):2331–2368, 2020. doi: 10.5194/tc-14-2331-2020. URL https://hal.archives-ouvertes.fr/hal-02927370.

Oyabu, I., Kawamura, K., Kitamura, K., Dallmayr, R., Kitamura, A., Sawada, C., Severinghaus, J., Beaudette, R., Orsi, A., Sugawara, S., Ishidoya, S., Dahl-Jensen, D., Goto-Azuma, K., Aoki, S., and Nakazawa, T. New technique for high-precision, simultaneous measurements of CH4, N2O and CO2 concentrations; isotopic and elemental ratios of N2/O2, Ar and total air content in ice cores by wet extraction. Atmospheric Measurement Techniques, 13(12):6703–6731, 2020. doi: 10.5194/amt-13-6703-2020. URL https://hal.archives-ouvertes. fr/hal-03099163.

Pace, B., Valentini, A., Ferranti, L., Vasta, M., Vassallo, M., Montagna, P., Colella, A., and Pons-Branchu, E. A Large Paleoearthquake in the Central Apennines, Italy, Recorded by the Collapse of a Cave Speleothem. Tectonics, 39(10), October 2020. doi: 10.1029/2020TC006289. https://hal.archives-ouvertes.fr/hal-03106691.

Pang, X., Bassinot, F. and Sophie Sepulcre, S. Cleaning method impact on the Mg/Ca of three planktonic foraminifer species: A downcore study along a depth transect. Chemical Geology, 549, 2020. doi: 10.1016/j.chemgeo.2020.119690. URL https://hal.archives-ouvertes.fr/ hal-02867474.

Parrenin, F., & Landais, A. (2020). La datation des archives glaciaires. *La Météorologie*, (110), 018.

Paul A., Balesdent J, Hatté C. ^{13}C-^{14}C relations reveal that soil ^{13}C-depth gradient is linked to historical changes in vegetation ^{13}C, Plant Soil (2020), 447, 305-317 – doi: 10.1007/s11104-019-04384-4

Penchenat, T., Vimeux, T., Daux, V., Cattani, O., Viale, M., Villalba, R., Srur, A., and Outrequin, C. Isotopic equilibrium between precipitation and water vapor in Northern Patagonia and its consequences on δ 18 O cellulose estimate. Journal of Geophysical Research: Biogeosciences, February 2020. doi: 10.1029/2019JG005418. URL https://hal.archives-ouvertes.fr/hal-02496691.

Peral, M., Blamart, D., Bassinot, F., Daeron, M., Dewilde, F., Rebaubier, H., Nomade, S., Girone, A., Marino, M., Maiorano, P., and Ciaranfi, N. Changes in temperature and oxygen isotopic composition of Mediterranean water during the MidPleistocene transition in the Montalbano Jonico section (southern Italy) using the clumped-isotope thermometer. Palaeogeography, Palaeoclimatology, Palaeoecology, 544:109603, April 2020. doi: 10.1016/j.palaeo.2020.109603. URL https://hal.archives-ouvertes.fr/hal-02524892.

Pereira, A., Monaco, L., Marra, F., Nomade, S., Gaeta, M., Leicher, N., Palladino, D., Sottili, G., Guillou, H., Scao, V., and Giaccio, B. Tephrochronology of the central Mediterranean MIS 11c interglacial (~425–395 ka): New constraints from the Vico volcano and Tiber delta, central Italy. Quaternary Science Reviews, 243:106470, September 2020. doi: 10.1016/j.quascirev.2020.106470. https://hal.archives-ouvertes.fr/hal-02969561.

Planes S., Allemand D., Agostini S., Banaigs B., Boissin E., Boss E., Bourdin G., Bowler C., Douville E., … & The Tara Pacific Consortium. The Tara Pacific expedition—A pan-ecosystemic approach of the "-omics" complexity of coral reef holobionts across the Pacific Ocean. PLoS Biol 17(9): e3000483. https://doi.org/10.1371/journal.pbio.3000483

Pons-Branchu, E., Sanchidrian, J. L., Fontugne, M., Medina-Alcaide,M. A., Quiles, A., Thil, F. and Valladas, H. U-series dating at Nerja cave reveal open system. Questioning the Neanderthal origin of Spanish rock art. Journal of Archaeological Science, 117: 105120, May 2020. doi: 10.1016/j.jas.2020.105120. URL https://hal.archives-ouvertes.fr/ hal-02514905.

Quivelli, O., Marino, M., Rodrigues, T., Girone, A., Maiorano, P., Abrantes, F., Salgueiro, E., and Bassinot, F. Surface and deep water variability in the Western Mediterranean (ODP Site 975) during insolation cycle 74: High-resolution calcareous plankton and molecular biomarker signals. Palaeogeography, Palaeoclimatology, Palaeoecology, 542:109583, March 2020. doi: 10.1016/j.palaeo.2019.109583. URL https://hal.archives-ouvertes.fr/ hal-02917020.

Rae, J., Gray, W., Wills, R., Eisenman, I., Fitzhugh, B., Fotheringham, M., Littley, E., Rafter, P., ReesOwen, R., Ridgwell, A., Taylor, B., and Burke, A. Overturning circulation, nutrient limitation, and warming in the Glacial North Pacific. Science Advances , 6(50):eabd1654, December 2020. doi: 10.1126/sciadv.abd1654. https://hal.archives-ouvertes.fr/hal-03088627.

Rassmann, J., Eitel, E., Lansard, B., Cathalot, C., Brandily, C., Taillefert, M., and Rabouille, C. Benthic alkalinity and dissolved inorganic carbon fluxes in the Rhˆone River prodelta generated by decoupled aerobic and anaerobic processes. Biogeosciences, 17(1):13–33, 2020. doi: 10.5194/bg-17-13-2020. URLhttps://hal.archives-ouvertes.fr/hal-02524910.

Richard, M., Falgueres, C., Pons-Branchu, E., Richter, D., Beutelspacher, T., Conard, N.J., Kindh, C.-J. The Middle to Upper Palaeolithic transition in Hohlenstein-Stadel cave (Swabian Jura, Germany): A comparison between ESR, U-series and radiocarbon dating. Quaternary International 556, -49-57. doi.org/10.1016/j.quaint.2019.04.009.

Rivera, M., Samaniego, P., Vela, J., Le Pennec, J.L., Guillou, H., Paquette, J.-L., and Liorzou, C. The eruptive chronology of the Yucamane-Calientes compound volcano: A potentially active edifice of the Central Andes (southern Peru). Journal of Volcanology and Geothermal Research, 393:106787, March 2020. doi: 10.1016/j.jvolgeores.2020.106787. URL https://hal.uca.fr/hal-02529338. Co-auteur ´etranger.

Rousseau D.-D., Antoine, P., Boers, N., Lagroix, F., Ghil, M., Lomax, J., Fuchs, M., Debret, M., Hatte, C., Moine, O., Gauthier, C., Jordanova, D., and Jordanova, N. Dansgaard-Oeschger-like events of the penultimate climate cycle: the loess point of view. Climate of the Past, 16(2):713–727, 2020. doi: 10.5194/cp-16-713-2020. URL https: //hal.archives-ouvertes.fr/hal-02537811.

Ryan, S.E., Crowley, Q.G., Snoeck, C., Reynard, L., Bouchaud, C., Zazzo, A., Douville, E., and Tuross, N. Research update: The varied application of strontium isotopes to archaeological questions, from an early medieval Irish population to pre-Islamic cotton in Arabia. In Irish Isotope Research Group Meeting, Dublin, Ireland, February 2020. URL https: //hal.archives-ouvertes.fr/hal-02952525.

Salavert, A., Zazzo, A., Martin, L., Antolin, F., Gauthier, C., Thil, F., Tombret, O., Bouby, L., Manen, C., Mineo, M., Mueller-Bieniek, A., Piqué, R., Rottolli, M., Rovira Buendia, N., Toulemonde,F., and Vostrovska, I. Direct dating reveals the early history of opium poppy in Western Europe. Scientific Reports, 10(20263), November 2020. doi: 10.1038/s41598-020-76924-3. URL https://halshs.archives-ouvertes.fr/ halshs-03021796.

Savard , M., and Daux, V. An overview on isotopic divergences – causes for instability of treering isotopes and climate correlations. Climate of the Past, 16(4):1223–1243, 2020. doi: 10.5194/cp16-1223-2020. URL https://hal.archives-ouvertes.fr/hal-02943381.

Schaen, A., Jicha, B., Hodges, K., Vermeesch, P., Stelten, M., Mercer, C., Phillips, D., Rivera, T., Jourdan, F., Matchan, E., Hemming, S., Morgan, L., Kelley, S., Cassata, W., Heizler, M., Vasconcelos, P., Benowitz, J., Koppers, A.A.P., Mark, D., Niespolo, E., Sprain, C., Hames, W., Kuiper, K., Turrin, B., Renne, P., Ross, J., Nomade, S., Guillou, H., Webb, L., Cohen,B., Calvert, A., Joyce, N., Ganerod, M., Wijbrans, J., Ishizuka, O., He, H., Ramirez, A., Pfander, J., Lopez-Martinez, M., Qiu, H., and Singer, B. Interpreting and reporting $^{40}Ar/^{39}Ar$ geochronologic data. Geological Society of America Bulletin, July 2020. doi: 10.1130/B35560.1. URL https://hal.archives-ouvertes.fr/hal-02903663.

Seroussi, H., Nowicki, S., Payne, A., Goelzer, H., Lipscomb, W., Abe-Ouchi, A., Agosta, C., Albrecht, T., Asay-Davis, X., Barthel, A., Calov, R., Cullather, R., Dumas, C., Galton-Fenzi, B., Gladstone, R., Golledge, N., Gregory, J., Greve, R., Hattermann, T., Hoffman, M., Humbert, A., Huybrechts, P., Jourdain, N., Kleiner, T., Larour, E., Leguy, G., Lowry, D., Little, C., Morlighem, M., Pattyn, F., Pelle, T., Price, S., Quiquet, A., Reese, R., Schlegel, N.-J., Shepherd, A., Simon, E., Smith, R., Straneo, F., Sun, S., Trusel, L., Van Breedam, J., Van de Wal, R., Winkelmann, R., Zhao, C., Zhang, T., Zwinger, T. ISMIP6 Antarctica: a multi-model ensemble of the Antarctic ice sheet evolution over the 21st century. The Cryosphere, 14(9):3033–3070, 2020. doi: 10.5194/tc-143033-2020. URL https://hal.archives-ouvertes.fr/hal-02972030.

Servettaz, A., Orsi, A., Curran, M., Moy, A. D., Landais, A., Agosta, C., Holly L. Winton, V., Touzeau, A., McConnell, J. R., Werner, M., and Baroni, M. Snowfall and Water Stable Isotope Variability in East Antarctica Controlled by Warm Synoptic Events. Journal of Geophysical Research: Atmospheres, 125(17), September 2020. doi: 10.1029/2020JD032863. https://hal.archives-ouvertes.fr/hal-02970942.

Shin, J., Nehrbass-Ahles, C., Grilli, R., Chowdhry Beeman, J., Parrenin, F., Teste, G., Landais, A., Schmidely, L., Silva, L., Schmitt, J., Bereiter, B., Stocker, T.F., Fischer, H., and Chappellaz, J. Millennial-scale atmospheric CO2variations during the Marine Isotope Stage 6 period (190-135 ka). Climate of the Past, 16 (6):2203–2219, 2020. doi: 10.5194/cp-16-2203-2020. URL https://hal.archives-ouvertes.fr/ hal-03032254.

Simon, Q., Thouveny, N., L. Bourlès, D., Valet, J.P., and Bassinot, F. Cosmogenic ^{10}Be production records reveal dynamics of geomagnetic dipole moment (GDM) over the Laschamp excursion (20-60 ka). Earth and Planetary Science Letters, 550:116547, 2020. doi: 10.1016/j.epsl.2020.116547. URL https://hal.archives-ouvertes.fr/hal-02928960.

Solaro, C., Boudon, G., Le Friant, A., Balcone-Boissard, H., Emmanuel, L., Paterne, M., and IODP Expedition Science Party. New insights into the recent eruptive and collapse history of Montagne Pelée (Lesser Antilles Arc) from offshore marine drilling site U1401A (IODP Expedition 340). Journal of Volcanology and Geothermal Research, 403:107001, October 2020. doi: 10.1016/j.jvolgeores.2020.107001. URL https://hal.archives-ouvertes.fr/hal-02915945.

Svensson, A., Dahl-Jensen, D., Steffensen, J. P., Blunier, T., Rasmussen, S. O., Vinther, B. M., Landais, A.... & Bigler, M. (2020). Bipolar volcanic synchronization of abrupt climate change in Greenland and Antarctic ice cores during the last glacial period. *Climate of the Past*, *16*(4), 1565-1580.

Toti , F., Bertini, A., Girone, A., Marino, M., Maiorano, P., Bassinot, F., Combourieu-Nebout, N., Nomade, S., and Buccianti, A. Marine and terrestrial climate variability in the western Mediterranean Sea during marine isotope stages 20 and 19. Quaternary Science Reviews, 243:106486, September 2020. doi: 10.1016/j.quascirev.2020.106486. https://hal.archives-ouvertes.fr/hal-02921315.

Trippanera D., Porreca M., Urbani S., Kissel C., Winkler A., Sagnotti L., Nazzareni S., Acocella V. Interpreting Inverse Magnetic Fabric in Miocene Dikes. Journal of Geophysical Research: Solid Earth, 125, e2020JB020306. https://doi.org/10.1029/2020JB020306

Valet J.P., Thevarasan, A., Bassinot, F., Savranskaia, T., and Haddam N. Two Records of Relative Paleointensity for the Past 4 Myr. Frontiers in Earth Science, 8:148, 2020. doi: 10.3389/feart.2020.00148. URL https://hal.archives-ouvertes.fr/hal-02917019.

Van Vliet-Lanoe, B. , Bergerat, F., Allemand, P., Innocentd, C., Guillou, H., Cavailhes, T., Gumundsson, A., Chazot, G., Schneider, J.L., Grandjean, P., Liorzou, C., and Passot, S. Tectonism and volcanism enhanced by deglaciation events in southern Iceland. Quaternary Research, 94:94–120, March 2020b. doi: 10.1017/qua.2019.68. URL https://hal.archives-ouvertes.fr/hal-02936125.

Van Vliet-Lanoe, B., Knudsen, O., Gumundsson, Guillou, H., Chazot, G., Langlade, J., Liorzou, C., and Nonnotte, P. Volcanoes and climate: the triggering of preboreal Jokulhlaups in Iceland. International Journal of Earth Sciences, 109(3):847–876, April 2020a. doi: 10.1007/s00531-020-01833-9. URL https://hal.archives-ouvertes.fr/hal-02938576.

Voinchet, P., Pereira, A., Nomade, S., Falguères, C., Biddittu, I., Piperno, M., Moncel, M.H., and Bahain, J.-J. ESR dating applied to optically bleached quartz - A comparison with 40Ar/39Ar chronologies on Italian Middle Pleistocene sequences. Quaternary International, 556:113–123, 2020. doi: 10.1016/j.quaint.2020.03.012. URL https://hal.archives-ouvertes.fr/hal-02996718.

Wils, K., Van Daele, M., Kissel, C., Moernaut, J., Schmidt, S., Siani, G., and Lastras, G. Seismo-Turbidites in Aysén Fjord (Southern Chile) Reveal a Complex Pattern of Rupture Modes Along the 1960 Megathrust Earthquake Segment. Journal of Geophysical Research: Solid Earth, 125, e2020JB019405.

Yu, Z., Colin, C., Bassinot, F., Wan, S., and Bayon, G. Climate Driven Weathering Shifts Between Highlands and Floodplains. Geochemistry, Geophysics, Geosystems, 21(7), July 2020. doi: 10.1029/2020GC008936. URL https://hal.archives-ouvertes.fr/hal-02921274.

Zhang, J., Genty, D., Sirieix, C., Michel, S., Minster, B., and Regnier, E. Quantitative assessments of moisture sources and temperature governing rainfall δ18O from 20 years monitoring records in SW-France: Importance for isotopic-based climate reconstructions. Journal of Hydrology, 591:125327, December 2020. doi: 10.1016/j.jhydrol.2020.125327. URL https://hal.archives-ouvertes.fr/hal-02970833.

Livre « Paleoclimatology » Eds : G. Ramstein,N. Bouttes, A. Govin, A. Landais, P. Sepulchre

Table des matières